

## Gravitational lenses

Sjur Refsdal† and Jean Surdej‡§||

† Hamburg Observatory, Gojenbergsweg 112, D-21029 Hamburg-Bergedorf 80, Germany

‡ Institut d'Astrophysique, Avenue de Cointe 5, B-4000 Liège, Belgium

### Abstract

According to Einstein's general theory of relativity, a gravitational field bends electromagnetic waves in much the same way as low atmospheric air layers (subject to a vertical density gradient) curve the trajectory of a propagating light ray. Large mass concentrations in the universe (stars, galaxies, clusters, etc) can thereby act as a type of lens, a gravitational lens. Magnificent cosmic mirages may sometimes result and it is therefore not surprising that gravitational lensing perturbs our view of the distant universe and also affects our physical understanding of various classes of extragalactic objects.

After briefly reviewing the history of gravitational lensing since the early thoughts of Newton in 1704 until the serendipitous discovery of the first gravitational lens system by Walsh, Carswell and Weymann in 1979, we recall the basic principles of atmospheric and gravitational lensing. We then describe a simple optical gravitational lens experiment which has the merit of accounting for all types of image configuration observed among currently known gravitational lens systems. Various types of gravitational lens models (point mass, singular isothermal sphere, uniform disk, spiral galaxy, etc) are described in detail as well as the resulting image properties of a distant source.

An updated list as well as colour illustrations of the best known examples of multiply imaged quasars, radio rings and giant luminous arcs and arclets are presented. Some of these observations are discussed in detail.

Finally, we show how it is possible to use gravitational lensing as a cosmological and astrophysical tool, the most interesting applications being the determination of the Hubble parameter  $H_0$ , the mass of very distant lensing galaxies as well as the distribution of luminous and dark matter in the universe. We also show how to determine the size and structure of distant quasars from observations of micro-lensing effects. Such observations may also be used to probe the nature of dark matter in the universe.

This review was received in its present form in September 1993.

§ Maître de Recherches au FNRS (Belgium) and senior visitor at the European Southern Observatory (Garching bei München, Germany).

|| Member of the Astrophysics Division, Space Science Department of the European Space Agency. Present address: Space Telescope Science Institute, 3700 San Martin Drive, Baltimore, MD 21218, USA.

## Contents

	Page
1. Introduction	119
2. Historical background	120
3. Atmospheric lensing	122
4. Physical basis of gravitational lenses	124
4.1. General remarks	124
4.2. The lens equation	125
4.3. Magnification and amplification	126
4.4. Axially symmetric lenses	126
5. The optical gravitational lens experiment	127
5.1. Shapes of axially symmetric optical lenses	127
5.2. Setup of the optical gravitational lens experiment	130
6. Gravitational lens models	131
6.1. Axially symmetric lens models	131
6.2. Asymmetric lenses	142
6.3. Timescales of gravitational lensing effects	145
7. Optical depth for lensing and some observational results	146
7.1. The point-mass lens model	146
7.2. The amplification bias correction	147
7.3. The SIS lens model	147
7.4. Some observational results on gravitational lensing statistics	148
8. Observations of individual gravitational lens systems	149
8.1. Accepted cases of multiply imaged sources	149
8.2. Additional proposed cases of multiply imaged sources	163
8.3. Radio rings	165
8.4. Giant luminous arcs and arclets	167
9. Cosmological and astrophysical applications	168
9.1. Determination of the Hubble parameter $H_0$	168
9.2. Determination of the mass of the lensing galaxy from a multiply imaged quasar	171
9.3. Determination of the mass of the lensing cluster from arcs and arclets	171
9.4. Micro-lensing	172
10. General conclusions	178
Acknowledgments	179
References	180

**General guidelines.** We recommend that physicists who are not very familiar with the field of gravitational lensing first read sections 1–6 (just subsections 6.1.1, 6.1.2 and 6.2), section 8 (just the first few lines of introduction preceding subsection 8.1.1 and those following subsections 8.3 and 8.4, see also tables 2 and 3 and figure 24) and section 10. At second reading, more details concerning the gravitational lens models, the astrophysical and cosmological use of gravitational lenses and the observations may be found in sections 6–9.

## 1. Introduction

The first example of a gravitational lens system, the doubly imaged quasar Q0957+561 A and B, was serendipitously identified by Walsh, Carswell and Weymann in 1979. Since then, gravitational lensing has become a very 'hot' topic in astronomical research. Several tens of new lens systems have been found and studied during the last decade. Furthermore, theoretical modelling of these enigmatic objects has already provided us with important astrophysical and cosmological information, unattainable by any other standard methods. This article summarizes the history and present status of the observations and of our physical understanding of gravitational lensing effects.

The general layout of our article is organized as follows (see contents): we first briefly review the historical background of gravitational lenses in section 2. The reader will note with some interest that, unlike most other astrophysical discoveries made during this century, the basic physics of gravitational lenses was understood well before the first example was actually found. Then a brief discussion of atmospheric lensing, which presents many analogies with gravitational lensing, follows in section 3.

In section 4, we describe the basic principles of gravitational lensing. We derive there the form of the lens equation and, by making use of the Einstein deflection angle, we determine an expression for the image magnification (or amplification). For didactical purposes, we show in section 5 how to derive the shape of optical lenses in order to simulate and to understand better the image properties of distant sources which are gravitationally lensed by various types of axially symmetric mass distribution. The optical setup of our gravitational lens experiment is presented at the end of that section.

In section 6, we discuss in detail the image properties of a distant source resulting from the gravitational deflection of light rays passing near a black hole, a singular isothermal sphere, a spiral galaxy seen face on, a uniform disk of matter as well as a truncated one. We first establish a sufficient condition for an observer to see multiple images from a distant source. In the case of perfect alignment between an observer, a symmetric deflector and a source, the resulting lensed image consists of a ring (the so-called 'Einstein ring') and we show how the expression for its angular diameter relates to physical parameters. By means of ray-tracing and bending-angle diagrams, the optical gravitational lens experiment and by directly solving the lens equation, we study the image properties associated with the lens models mentioned earlier. The concept of 'caustics' emerges naturally from the ray-tracing diagram associated with the spiral galaxy model and we then show with the help of our optical lens experiment how all image configurations observed in the universe may be simply understood in terms of the relative location of the observer (or equivalently of the source) with respect to the caustics associated with a singular asymmetric lens.

Considering both the point-mass and the singular isothermal-sphere-lens models, we derive in section 7 an expression for the optical depth for multiple imaging. The importance of taking into account a correction factor due to the amplification bias is pointed out. Some observational results on gravitational lensing statistics are then presented.

A detailed description of the best known gravitational lens systems is given in section 8. These include accepted and proposed cases of multiply imaged distant sources, radio rings and giant luminous arcs and arclets.

Some of the most promising cosmological and astrophysical applications of gravitational lensing are addressed in section 9. We first describe the independent determination of the Hubble parameter  $H_0$  via the measurement of the time delay  $\Delta t$  between the observed light curves of multiply imaged extragalactic sources. The possibility of weighing the mass of lensing galaxies and galaxy clusters from the observation of multiply imaged quasars, arcs

and arclets is also briefly described. The great scientific interest of using micro-lensing effects as an astrophysical tool is discussed at length. Finally, general conclusions form the last section.

## 2. Historical background

Do not Bodies act upon Light at a distance, and  
by their action bend its Rays; and is not this action  
strongest at the least distance? (Isaac Newton 1704)

Considering that light may be composed of elementary constituents, as early as 1704 Newton suggested that the gravitational field of a massive object could possibly bend light rays as well as the trajectory of material particles. About 100 years later, the astronomer Soldner (1804) from Munich Observatory found that, in the framework of Newtonian mechanics, a light ray passing near the limb of the Sun should undergo an angular deflection of  $0.875''$ . However, because the wave description of light prevailed during the whole 18th and 19th centuries, neither Newton's conjecture nor Soldner's result were ever taken seriously.

During the elaboration of his theory of general relativity, Einstein predicted that a massive object would curve the spacetime in its vicinity and that any particle, massive or not (cf the photons), will move along the geodesics of this curved space. He predicted in 1915 that a light ray passing near the solar limb would be deflected by an angle equal to

$$\hat{\alpha} = \frac{4GM_{\odot}}{c^2R_{\odot}} = 1.75'' \quad (2.1)$$

where  $G$  stands for the gravitational constant,  $c$  for the velocity of light and  $M_{\odot}$ ,  $R_{\odot}$  for the mass and radius of the Sun, respectively. As we may note, this deflection angle turns out to be exactly twice the value derived by Soldner.

Using photographs of a stellar field taken during the solar eclipse in May 1919 and six months later, Eddington and his collaborators (see Dyson *et al* 1920) were able to confirm, within a 20–30% uncertainty, the deflection angle predicted by Einstein. This was not only a triumph for general relativity but also a marvelous confirmation of the concept that light rays may undergo deflections in gravitational fields. Let us note that this uncertainty has been presently reduced to less than 1% thanks to radio interferometric observations of quasi-stellar sources (Fomalont and Sramek 1975a, b, Robertson *et al* 1991).

It seems that Eddington (1920) was the first to propose the possible formation of multiple images of a background star by the gravitational lensing effect of a foreground one. Let us note, however, that Lodge (1919) had already characterized massive objects like the Sun to be imperfect focusing lenses since they had no real focal length; the light from a background object being mainly concentrated along a focal line of 'infinite' length. In 1923, Frost, then director of the Yerkes Observatory, initiated a programme to search for multiply imaged stars in the galaxy but it seems that these observations never really took place.

Chwolson (1924) suggested that, in the case of a perfect alignment between an observer and two stars located at different distances, the former should see a ring-shaped image of the background star around the foreground one. Furthermore, following Etherington who demonstrated in 1933 that gravitational lensing preserves the specific intensity (or surface brightness) of electromagnetic waves, it is then straightforward to establish that the amplification of a source is just equal to the 'magnification' ratio of its image size (cf the solid angle subtended by the 'Chwolson' ring) to that it would have if no lensing was taking place (i.e. the solid angle subtended by the real stellar disk). Independently, Einstein (1936)

rediscovered the major characteristics (double images, the 'Chwolson' ring usually referred to as the 'Einstein' ring, etc) of a star lensed by another one but he was very sceptical as to the possibility of observing this phenomenon among stars.

Zwicky (1937a, b) was the first to realize the very high probability of identifying a gravitational lens mirage, i.e. one made of several distinct images resolvable from the ground, among extragalactic objects (see figure 1). He even proposed using galaxies as natural cosmic telescopes to observe otherwise too faint and distant background objects. He also emphasized the possibility of weighing the mass of distant galaxies by simply applying gravitational lens optometry and, in addition, of testing the theory of general relativity. Link (1937) has thoroughly discussed the effects of gravitational lensing expected from such galaxies. In 1937, Zwicky stated that 'the probability that galactic nebulae which act as gravitational lenses will be found becomes practically a certainty'; and he was therefore very much surprised to note some 20 years later that no such lensing effects had yet been found with the 200-in Palomar telescope (Zwicky 1957).

#### GRAVITATIONAL BENDING OF LIGHT RAYS

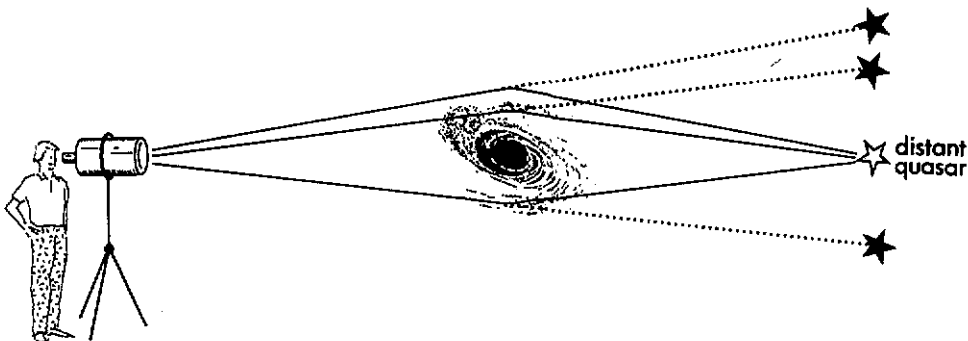


Figure 1. An observer sees the lensed images of a distant quasar along the directions of light rays deflected by a massive intervening galaxy.

After an inter-regnum of nearly a quarter of a century, interest in the theory of gravitational lenses was revived by Klimov (1963; galaxy-galaxy lensing), Liebes (1964; star-star lensing) and Zel'dovich (1964) and Refsdal (1964a, b, 1966a; cosmological applications of gravitational lensing). Some of these proposed applications were particularly promising because of the recent discovery of quasars by Schmidt (1963). It would indeed be much easier to prove the lensing origin of multiple quasi-stellar object (QSO) images rather than that of extended and diffuse galaxy images, since the former consist of very distant, luminous and star-like objects. Based on the great similarity between the spectra of quasars and nuclei of Seyfert 1 galaxies, Barnothy (1965) even proposed that high redshift quasars could actually be the lensed images of distant Seyfert 1 galaxy nuclei.

Theoretical work continued on a low level of activity throughout the 1970s. Refsdal (1965, 1970) and Press and Gunn (1973) discussed problems on lens statistics, Bourassa and Kantowski (1975) considered extended non-symmetric lenses (see also Sanitt 1971, Bourassa *et al.* 1973) and Dyer and Roeder (1972) derived a distance-redshift relation for the case of inhomogeneous universes. In spite of clear theoretical predictions, the interest from observers was low and no systematic search for lenses was initiated.

Forty-two years after Zwicky's prediction, the dream of some astronomers finally became reality: Walsh, Carswell and Weymann serendipitously discovered in 1979 the

first example of a distant quasar (0957+561), multiply imaged by a foreground massive lensing galaxy. Following this pioneering detection, the levels of observational as well as theoretical activities have increased dramatically: up to now, more than 1000 scientific publications have been written on the subject of gravitational lensing (cf the non-exhaustive bibliography on gravitational lensing by Pospieszalska-Surdej *et al* (1993)). As shown in this article, gravitational lensing does constitute a new and very important branch of extragalactic astronomy. We refer to Schneider *et al* (1992) for a more detailed account of the history of gravitational lensing, as well as for a more complete and general presentation of this subject.

Before studying the bending of light rays in the gravitational field of massive objects, let us first describe a better known and somewhat related phenomenon, i.e. the bending of light rays by atmospheric lensing.

### 3. Atmospheric lensing

It is interesting to note that gravitational fields in the universe deflect light rays in a way that is very similar to the refraction properties of the lower atmospheric air layers: because of significant temperature and density gradients near the ground, light rays often undergo significant bendings (figures 2(a)–(d)). Figure 3 gives a schematic representation of the light ray paths when the ground is somewhat hotter than the ambient air. As air refraction always bends light rays towards regions of colder air, the formation of one lower, inverted and somewhat deformed image of a distant source may result (see the distant truck in figure 2(b)). Similarly, upper mirages may form when the temperature gradient is reversed (see figures 2(c)–(d)).

In order to understand in more detail light propagation across a plane parallel atmosphere whose refractive index is affected by a vertical gradient  $dn/dz$ , we may apply Fermat's principle according to which the path(s) followed by light between two given points is that (or those) which correspond(s) to an extremum in the propagation time, i.e.

$$\delta \left( \int_0^s \frac{1}{v} ds \right) = 0 \quad (3.1)$$

where  $ds = \sqrt{dx^2 + dz^2}$  represents an infinitesimal element along the light trajectory and  $v = c/n$ , the velocity of light in the medium with a refractive index  $n(z)$  (see figure 3). It is easy to show, by means of the Euler–Lagrange equation, that the variational equation (3.1) simply reduces to Descartes's law

$$n(z) \cos(i(z)) = K \quad (3.2)$$

where  $K$  is a constant and  $i(z)$  represents the angle between the tangent to the light ray and the horizontal direction. It is then straightforward to derive the expression for the small angle increment  $\delta i$  of the ray between two neighbouring points whose abscissae are  $x$  and  $x + dx$ . For a small but finite value of  $dx$ , we find with a good approximation that

$$\delta i = \frac{(dn/dz)dx}{n(z) + (dn/dz) \tan(i)dx}. \quad (3.3)$$

This relation is very useful in order to construct numerically the trajectory of light rays across an atmosphere characterized by a refractive index distribution  $n(z)$  (Claeskens *et al* 1994). In doing so, one finds that under special circumstances (cf specific refractive index distributions  $n(z)$ , source distance, etc) there may exist several geodesics between

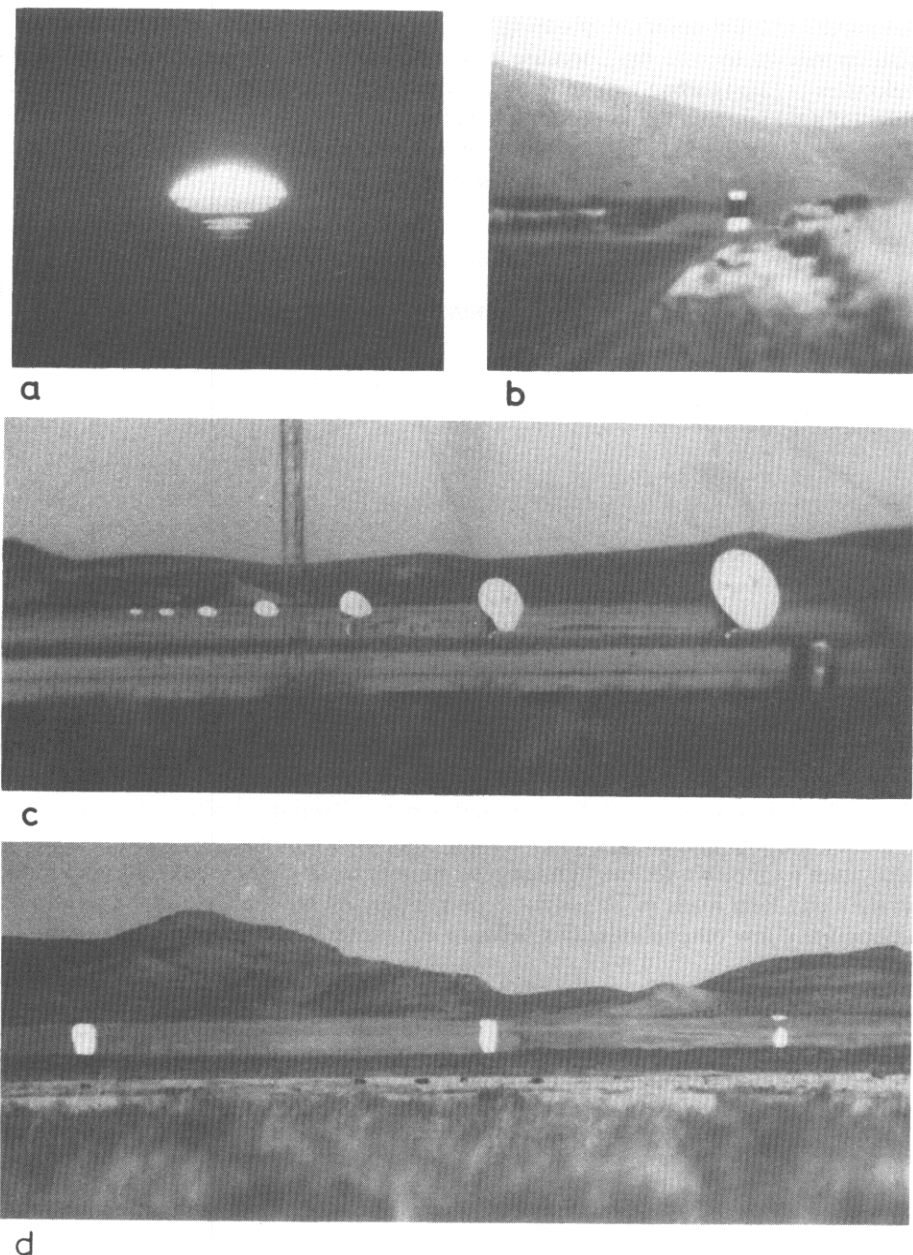


**Figure 2.** Atmospheric lensing: (a) represents a sunset as photographed at the European Southern Observatory (hereafter ESO, La Silla) in Chile on 25 November 1987; (b) illustrates the double image of a distant truck along the North Panamericana highway between the towns of Pichidangui and La Serena (Chile, 2 December 1987); (c) and (d) correspond to two different views of the north-south arm of the Very Large Array (VLA) at the National Radio Astronomical Observatory (Socorro, New Mexico) as seen in the early morning of 17 January 1989. All photographs are from the authors.

the source and the observer, resulting in the possible formation of multiple images. It is also interesting to note that, because of the difference in the geometric lengths and light velocities ( $c/n(z)$ ) along two geodesics, there will generally be a delay between the arrival times of a signal from the source (cf a hypothetical light flash) as seen by a distant observer. This time delay depends on the refractive index distribution  $n(z)$  and also on the absolute distance between the source and the observer.

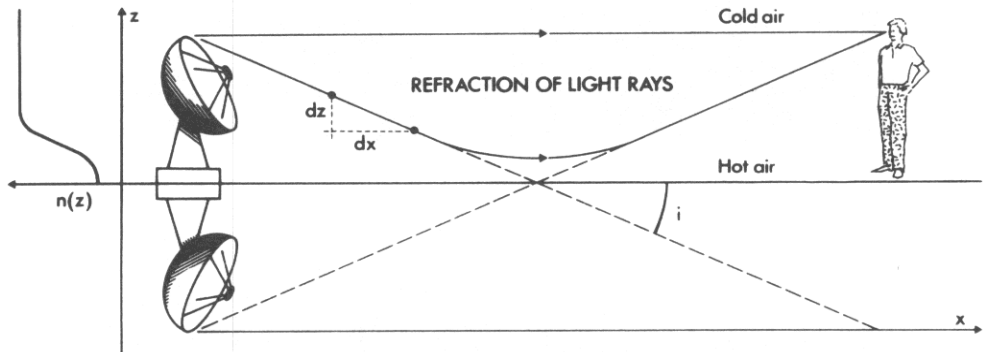


**Figure 3.** Formation of atmospheric mirages across an atmosphere characterized by a refractive index distribution  $n(z)$ , as shown along the left horizontal axis.

Finally, let us remark that because atmospheric lensing preserves surface brightness, just as in the case of gravitational lensing, the amplification of a mirage's luminosity is simply given by the ratio of the solid angle of the observed (lensed) image to that of the (unlensed) source. Therefore, in addition to affecting significantly our view (image deformation, multiplication, etc) of distant resolved Earth sources, atmospheric lensing is also often responsible for the light amplification of distant unresolved objects located along straight and long roads or across flat countrysides. As we shall see in the remainder, there exist quite a few other similarities between atmospheric and gravitational lensing.

#### 4. Physical basis of gravitational lenses

##### 4.1. General remarks

The physical basis of gravitational lensing essentially consists in the deflection of light, and electromagnetic waves in general, in gravitational fields as predicted by Einstein's theory of general relativity. In the regime of small deflection angles and weak gravitational fields, which are of practical interest to us here, the so-called Einstein deflection of a light ray passing near a compact mass at a distance  $\xi$  is

$$\hat{\alpha}(\xi) = \frac{4GM}{c^2\xi} = \frac{2R_{sc}}{\xi} \ll 1 \quad (4.1)$$

where  $G$  and  $c$  stand for the constant of gravitation and the velocity of light, respectively, and where  $R_{sc}$  represents the Schwarzschild radius associated with the mass  $M$  (see figure 4). For an extended mass, it is easy to calculate the deflection angle by just summing (integrating) the individual deflections due to all the mass elements constituting the lens. Since there is usually just one mass concentration which acts as a lens, and which has a small size relative to the distances involved, the thin lens approximation is usually justified. We therefore

introduce a lens plane ( $\zeta = (\xi, \eta)$ ) through the centre of mass of the lens and perpendicular to the deflector–observer line (see figure 4). All the mass can then be considered to be located in the lens plane and the deflection to take place where the ray crosses the lens plane. The deflection can therefore be expressed as a two-dimensional vector,

$$\hat{\alpha}(\zeta) = \frac{4G}{c^2} \iint \frac{\Sigma(\zeta') (\zeta' - \zeta)}{|\zeta - \zeta'|^2} d\xi' d\eta' \quad (4.2)$$

where  $\Sigma(\zeta)$  represents the surface mass density of the lens at the location  $\zeta$ . In Newtonian terms, the Einstein deflection also follows if one assumes a refractive index  $n$  which depends on the Newtonian gravitational potential  $U$  of the lens via the relation  $n = 1 - 2U/c^2$ . We see here once more some analogy with atmospheric lensing.

Since the Einstein deflection is independent of wavelength, gravitational lenses are *achromatic* (indirect chromatic effects may, however, be induced by micro-lensing, see section 9.4). Furthermore, *geometrical optics* can be used since the physical optical effects are negligible in realistic situations.

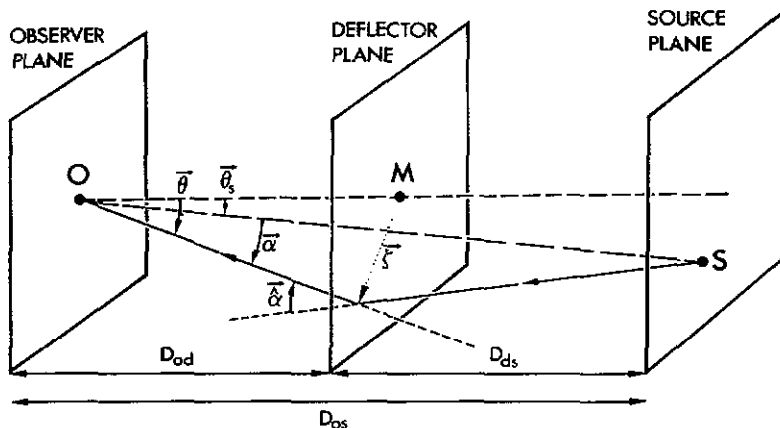


Figure 4. Geometrical quantities characterizing the deflection of a light ray by a point-mass lens (M).

#### 4.2. The lens equation

Let the true position of the source S on the sky now be defined by the angle  $\theta_s$  and the image position(s) by  $\theta_i$  ( $i = 1, 2, \dots$ ). These correspond to the solutions of the *lens equation*

$$\theta - \theta_s = \alpha(\theta) = -(D_{ds}/D_{os})\hat{\alpha}(\theta) \quad (4.3)$$

where  $D_{ds}$  and  $D_{os}$  represent respectively the ‘deflector–source’ and ‘observer–source’ angular size distances and where  $\alpha$  is the displacement angle,  $\alpha = -(D_{ds}/D_{os})\hat{\alpha}$  (see figures 4 and 5). We note that a given image position always corresponds to a specific source position whereas a given source position may sometimes correspond to several distinct image positions. Such cases of multiply imaged sources constitute the most spectacular and interesting aspects of gravitational lensing.

A typical lens situation is shown in figure 5, where source and image positions (one image in this case) are seen projected on the sky. We see again that the image position is shifted by  $\alpha$  relative to the source position; note, however, that  $\alpha$  is usually not constant over the source and this results in possible (de-)magnification and deformation of extended sources.

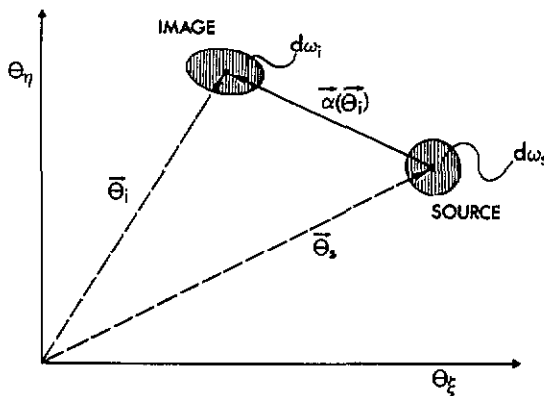


Figure 5. Image of a lensed source as seen projected on the sky.

#### 4.3. Magnification and amplification

Since gravitational lensing preserves the surface brightness of a source, the ratio (magnification) between the solid angle  $d\omega_i$  covered by the lensed image and that of the unlensed source  $d\omega_s$  immediately gives the flux amplification  $\mu_i$  due to lensing. More formally, this is given for an infinitesimally small source by the inverse Jacobian of the transformation matrix between the source and the image(s):

$$\mu_i = d\omega_i/d\omega_s = |\det(\partial\theta_s/\partial\theta_i)|^{-1}. \quad (4.4)$$

If there are several images of a given source, the total magnification (amplification) is given by the sum of all individual image magnifications (amplifications). We suggest hereafter using the term ‘magnification’ whenever the lensed images (e.g. luminous arcs, radio rings, etc) are resolved by the observer, thus emphasizing the change in angular size, and the term ‘amplification’ otherwise (cf when referring to micro-lensing effects or to the integrated flux of resolved macro-lensed images).

#### 4.4. Axially symmetric lenses

Considering a thin gravitational lens that is axially symmetric with respect to the line-of-sight, we can, by virtue of Gauss’ law applied to the two-dimensional case, rewrite the deflection given in equation (4.2) as the scalar angle

$$\hat{\alpha}(\xi) = \frac{4G}{c^2} \frac{M(\xi)}{\xi}. \quad (4.5)$$

It is as if only the mass  $M(\xi)$  located inside the cylinder defined by the impact parameter  $\xi$  was contributing to the light deflection and may be thought of as acting like a single point mass located at the centre (compare with equation (4.1)). The deflection caused by the matter distributed outside this cylinder exactly cancels out. All this reminds us of gravitational (or Coulomb) forces caused by spherically symmetric mass (or electric charge) distributions.

Since light deflection by an axially symmetric lens reduces to a one-dimensional problem, it is also straightforward to simplify expression (4.4) for the magnification  $\mu_i$  of the lensed images as follows

$$\mu_i = \frac{\theta_i d\theta_i}{\theta_s d\theta_s}. \quad (4.6)$$

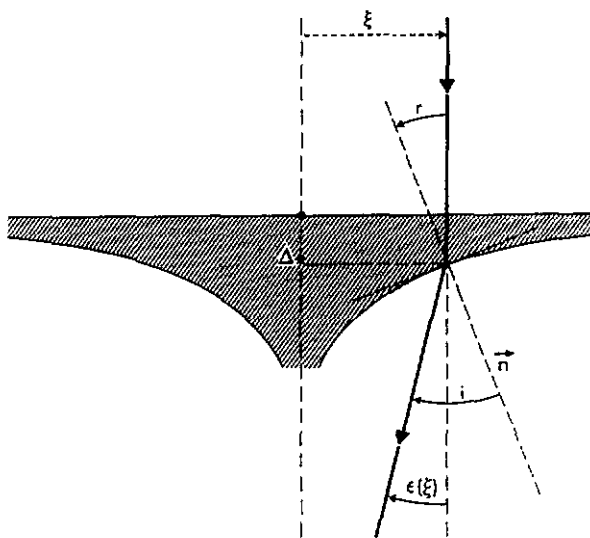


Figure 6. Deflection of a light ray passing through an axially symmetric optical lens.

## 5. The optical gravitational lens experiment

For didactical purposes (see the applications in section 6), it is very useful to construct and use optical lenses that mimic the deflection of light rays as derived in equation (4.5) for the case of axially symmetric gravitational lenses. Such optical lenses should be rotationally symmetric, flat on one side (for simplicity) and have, on the other side, a surface determined in such a way that rays characterized by an impact parameter  $\xi$  are deflected by the angle  $\epsilon(\xi) = \hat{\alpha}(\xi)$  (see equation (4.5) and figure 6).

### 5.1. Shapes of axially symmetric optical lenses

Applying Descartes' law (cf equation (3.2)) to the ray depicted in figure 6 and assuming that the angles ( $r$  and  $i$ ) between the normal  $n$  to the optical surface and the incident and refracted rays are very small, we may write the relation

$$n = \frac{\sin(i)}{\sin(r)} \simeq \frac{i}{r} \quad (5.1)$$

where  $n$  represents here the refractive index of the lens with respect to the air. Furthermore, since we have

$$i = \epsilon(\xi) + r = \frac{4GM(\xi)}{c^2\xi} + r \quad (5.2)$$

and that the tangent to the optical surface at the point  $(\xi, \Delta)$  is merely given by (see figure 6)

$$d\Delta/d\xi = -r \quad (5.3)$$

it is straightforward to derive the shape of a lens by means of the following differential equation

$$\frac{d\Delta}{d\xi} = \frac{-4GM(\xi)}{(n-1)c^2\xi}. \quad (5.4)$$

*5.1.1. The optical point-mass lens.* By definition, the mass  $M$  of a point lens model is concentrated at one point such that we have  $M(\xi) = M$ . It is then simple to solve equation (5.4) and derive the thickness  $\Delta(\xi)$  of the corresponding optical lens as a function of the impact parameter  $\xi$ . We find that

$$\Delta(\xi) = \Delta(\xi_0) + \frac{2R_{sc}}{n-1} \ln\left(\frac{\xi_0}{\xi}\right) \quad (5.5)$$

where  $R_{sc}$  represents the Schwarzschild radius of the compact lens (cf equation (4.1)). In practice, the point  $(\xi_0, \Delta(\xi_0))$  is chosen in order to specify a given thickness (e.g.  $\Delta(\xi_0) = 1$  cm) for the optical lens at a selected radius (e.g.  $\xi_0 = 14$  cm). The resulting shape of such an optical 'point-mass' lens is illustrated in figure 7(a). It looks very much like the foot of some glasses of wine which, therefore, have been commonly used in the past by well known astronomers to simulate lensing effects. A realistic 'point-mass' lens, made of plexiglas-like material (refractive index  $n = 1.49$ ; diameter of 28 cm), was manufactured in 1979 at the Hamburg Observatory for the particular value of  $R_{sc} = 0.3$  cm. This corresponds in fact to the Schwarzschild radius of one-third of the Earth mass (see figure 8).

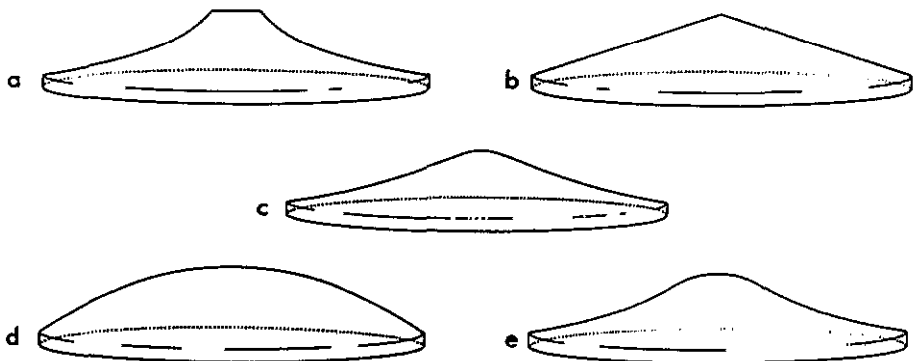


Figure 7. Several examples of axially symmetric optical lenses simulating the light deflection properties due to a point mass (a), an SIS galaxy (b), a spiral galaxy (c), a uniform disk (d) and a truncated uniform disk of matter (e).

*5.1.2. The SIS optical lens.* For the case of a singular isothermal sphere (hereafter SIS) lens model, it is well known that the mass of such a galaxy increases linearly with the impact parameter  $\xi$ , i.e.  $M(\xi) \propto \xi$ . We may thus rewrite equation (5.4) in the form

$$d\Delta/d\xi = -K \quad (5.6)$$

where  $K$  represents a positive constant. Integration of this equation leads to the solution

$$\Delta(\xi) = \Delta(\xi_0) + K(\xi_0 - \xi). \quad (5.7)$$

The shape of the resulting SIS lens is thus merely an axially symmetric cone as illustrated in figure 7(b).

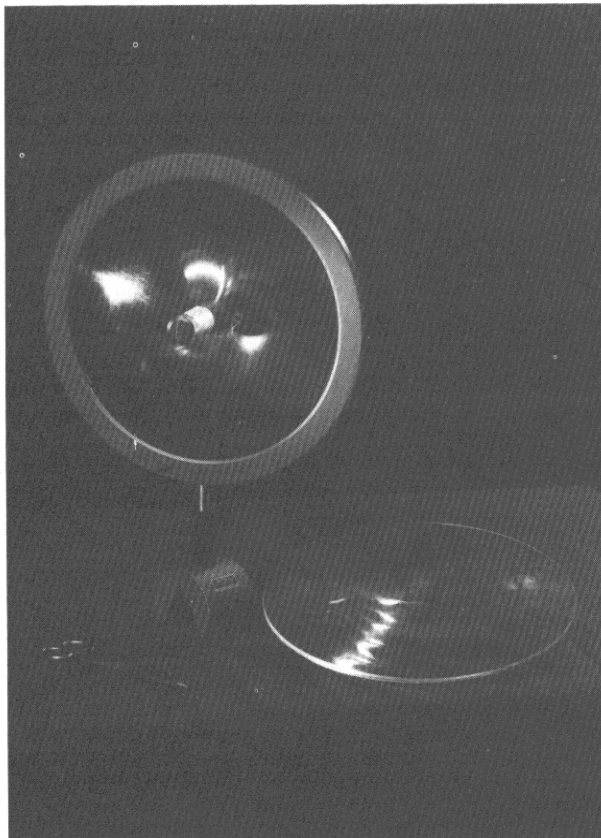


**Figure 8.** Examples of (left-hand side) a ‘point-mass’ lens (28 cm in diameter) manufactured at the Hamburg Observatory and of (right-hand side) a ‘spiral galaxy’ optical lens (30 cm in diameter) produced by the authors at ESO (Garching bei München). We have used these particular lenses, made of plexiglas-like material ( $n = 1.49$ ), to simulate the formation of multiple images of a distant source (see section 6). Our optical gravitational lens experiment is described in section 5.2.

### 5.1.3. The ‘spiral galaxy’ optical lens.

Given the exponential surface mass density

$$\Sigma(\xi) = \Sigma_0 \exp(-\xi/\xi_c) \quad (5.8)$$

which describes reasonably well the mass distribution of a spiral galaxy disk having a characteristic size  $\xi_c$ , we may derive the mass distribution  $M(\xi)$  of such a deflector by means of the relation

$$M(\xi) = 2\pi \int_0^\xi \Sigma(\xi') \xi' d\xi'. \quad (5.9)$$

Integration of this last expression leads immediately to the result

$$M(\xi) = 2\pi \xi_c^2 \Sigma_0 [1 - \exp(-\xi/\xi_c)(\xi/\xi_c + 1)]. \quad (5.10)$$

Inserting this result into equation (5.4) and performing the integration, we find that

$$\Delta(\xi) = \Delta(\xi_0) + \frac{8\pi G \xi_c^2 \Sigma_0}{(n-1)c^2} \left[ \ln\left(\frac{\xi_0}{\xi}\right) - \exp\left(\frac{-\xi}{\xi_c}\right) + \exp\left(\frac{-\xi_0}{\xi_c}\right) + \int_{\xi_0/\xi_c}^{\xi/\xi_c} \frac{\exp(-z)}{z} dz \right]. \quad (5.11)$$

The general shape of a 'spiral galaxy' optical lens is illustrated in figure 7(c). A 30-cm diameter 'spiral galaxy' lens, produced by the authors at the European Southern Observatory (ESO, Garching bei München, Germany) is shown in figure 8. This lens is characterized by the following physical parameters: an equivalent Schwarzschild radius of one-third of the Earth mass, i.e.  $R_{sc} = 2GM(\xi \rightarrow \infty)/c^2 = 4\pi G\xi_c^2\Sigma_0/c^2 = 0.3$  cm (see equation (5.10)),  $\xi_c = 2.0$  cm,  $\xi_0 = 15$  cm and  $\Delta(\xi_0) = 0.7$  cm. We should also like to mention that Vanderriest (1985) has manufactured a similar type of lens ( $\approx 20$  cm in diameter) directly from a piece of glass, at the Meudon Observatory.

**5.1.4. The uniform disk optical lens.** As we shall see in section 6.1.5, a uniform circular disk of matter leads to a perfect convergence of all incoming light rays from a distant source into a single 'focal' point, assuming that the line-of-sight is perpendicular to the disk. We conclude that a classical converging optical lens constitutes the natural counterpart of such a deflector (see figure 7(d)).

**5.1.5. The truncated uniform disk optical lens.** For the case of a truncated uniform disk of matter, let us assume that the surface mass density  $\Sigma(\xi)$  is constant ( $= \Sigma_0$ ) for values of the impact parameter  $\xi$  in the range  $[0, \xi_c]$  and that it is zero outside. We then get

$$M(\xi) = \pi \Sigma_0 \xi^2 \quad \text{if } \xi \leq \xi_c \quad (5.12a)$$

and

$$M(\xi) = \pi \Sigma_0 \xi_c^2 \quad \text{if } \xi > \xi_c. \quad (5.12b)$$

Inserting these results into equation (5.4), a simple integration leads to the solutions for the thickness  $\Delta(\xi)$  of the optical lens as a function of the impact parameter  $\xi$

$$\Delta(\xi) = \Delta(\xi_0) + \frac{4\pi G \Sigma_0}{(n-1)c^2} \xi_c^2 \ln\left(\frac{\xi_0}{\xi}\right) \quad \text{if } \xi_c \leq \xi \leq \xi_0 \quad (5.13a)$$

from which we may derive

$$\Delta(\xi_c) = \Delta(\xi_0) + \frac{4\pi G \Sigma_0}{(n-1)c^2} \xi_c^2 \ln\left(\frac{\xi_0}{\xi_c}\right) \quad (5.13b)$$

and

$$\Delta(\xi) = \Delta(\xi_c) + \frac{2\pi G \Sigma_0}{(n-1)c^2} (\xi_c^2 - \xi^2) \quad \text{if } \xi \leq \xi_c. \quad (5.13c)$$

We have illustrated in figure 7(e) the shape of such an optical lens that simulates the gravitational lensing effects due to a truncated uniform disk of matter.

## 5.2. Setup of the optical gravitational lens experiment

In order to simulate the formation of lensed images by a given mass distribution (point mass, etc), we have used the optical setup that is shown in figure 9. A compact light source is located on the left-hand side (not clearly seen), then comes the point-mass optical lens (see figure 8) that deflects the light rays very nearly as a black hole having one-third of the Earth mass ( $R_{sc} \approx 0.3$  cm). Behind the lens, we find a white screen with a small hole at the centre (pinhole lens). Further behind, there is a large screen on which is projected the lensed image(s) of the source (the Einstein ring, in this case) as it would have been seen if our eye were located at the position of the pinhole. In the example illustrated here, the pinhole is set very precisely on the optical axis of the gravitational lens so that the source, the lens and the pinhole (observer) are perfectly aligned. Considering other relative positions between the source, the lens and the observer, and also for the additional case of an asymmetric lens, we shall illustrate in section 6 the resulting lensed images as a function of the pinhole position in the observer plane. Note that the bright regions seen on the lens in figure 9 are caused by scattered light.

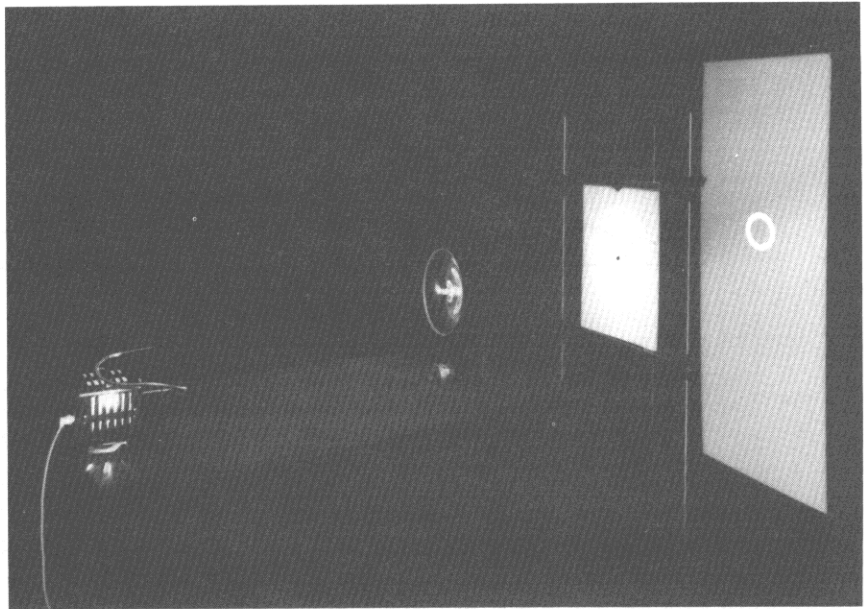


Figure 9. Setup of the optical gravitational lens experiment.

## 6. Gravitational lens models

### 6.1. Axially symmetric lens models

**6.1.1. Generalities.** In the case of perfect alignment between a source (S), an axially symmetric deflector (D) and an observer (O) (see figure 10), we easily see that, with the exception of the direct ray propagating from the source to the observer, the condition for any other light ray to reach the observer is

$$\theta/D_{ds} \simeq \hat{\alpha}_0/D_{os} \quad (6.1)$$

as obtained from the direct application of the sine rule to the triangle SXO and assuming that the angles  $\theta$  and  $\hat{\alpha}_0$  remain very small. This will also be true if the real deflection angle  $\hat{\alpha} \geq \hat{\alpha}_0$  since it will then be always possible to find a light ray with a greater impact parameter  $\xi$  such that equation (6.1) is fulfilled. Expressing the angle  $\theta$  between the direct ray and the incoming deflected ray as

$$\theta \simeq \xi/D_{od} \quad (6.2)$$

and making use of equations (4.5) and (6.1), we may thus rewrite this condition as follows

$$\Sigma(<\xi) \geq \Sigma_c \quad (6.3)$$

i.e. the average surface mass density of the lens

$$\Sigma(<\xi) = M(\xi)/\pi\xi^2 \quad (6.4)$$

evaluated within the impact parameter  $\xi$ , must simply exceed the critical surface mass density  $\Sigma_c$ , defined by

$$\Sigma_c = \frac{c^2 D_{os}}{4\pi G D_{od} D_{ds}}. \quad (6.5)$$

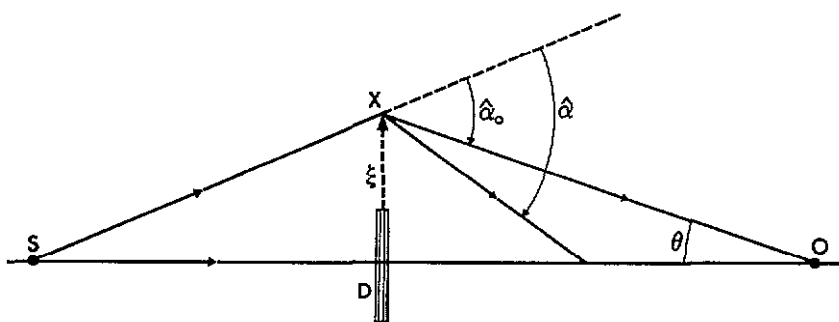


**Figure 10.** On the condition for an observer O to see a light ray from a distant source S, deviated by a deflector D so that more than one image can be seen. Note that O, D and S are co-aligned and that axial symmetry is assumed. No scale is respected in this and all subsequent diagrams.

Let us note that the latter quantity is essentially determined by the distances between the source, the deflector and the observer. As we shall see in section 6.1.5, a circular disk with uniform surface mass density  $\Sigma$  acts as a perfect converging lens, and we have  $\Sigma = \Sigma_c$  for the particular case when the observer is precisely located at its focal point.

Although this reasoning essentially applies to a static Euclidean space, Refsdal (1966b) has shown that it also remains valid for Friedmann-Lemaître-Robertson-Walker (FLRW) expanding universe models, provided that  $D_{os}$ ,  $D_{od}$  and  $D_{ds}$  represent angular size distances. Adopting typical cosmological distances for the deflector (redshift  $z_d \simeq 0.5$ ) and the source ( $z_s \simeq 2$ ), we find that  $\Sigma_c \simeq 1 \text{ g cm}^{-2}$ .

Substituting  $M(\xi)$  and  $\xi$  in equation (6.4) with a typical mass  $M$  and a radius  $R$  for the deflector, we have listed in table 1 values for the ratio  $\Sigma(< R)/\Sigma_c$  considering a star, a galaxy and a cluster of galaxies located at various distances.

**Table 1.** Ratio of the average  $\Sigma(< R)$  and critical  $\Sigma_c$  surface mass densities, angular ( $\theta_E$ ) and linear ( $\xi_E$ ) radii of the Einstein ring for different values of the mass  $M$ , distance  $D_{od}$  and radius  $R$  of the deflector, assuming that  $D_{os} = 2 \times D_{od}$  (1 parsec = 1 pc = 3.262 light years =  $3.086 \times 10^{18}$  cm).

Deflector	$M(M_\odot)$	$D_{od}(\text{pc})$	$R(\text{pc})$	$\Sigma(< R)/\Sigma_c$	$\theta_E$	$\xi_E = \theta_E D_{od}(\text{pc})$
Star	1	$10^4$	$2 \times 10^{-8}$	$2 \times 10^6$	$6 \times 10^{-4''}$	$3 \times 10^{-5}$
Star	1	$10^9$	$2 \times 10^{-8}$	$2 \times 10^{11}$	$2 \times 10^{-6''}$	$10^{-2}$
Galaxy core	$10^{12}$	$10^9$	$5 \times 10^3$	4	$2''$	$10^4$
Cluster core	$10^{14}$	$10^9$	$10^5$	1	$20''$	$10^5$

We see that only stars and very compact, massive galaxies and galaxy clusters, for which  $\Sigma(< R)/\Sigma_c \geq 1$ , constitute promising ‘multiple imaging’ deflectors.

In the case of axial symmetry, it is clear that in the presence of an efficient deflector, an observer located on the symmetry axis will actually see a ring (the so-called ‘Einstein ring’, see figure 9) of light from a distant source. Combining equations (4.5), (6.1) and (6.2), the angular radius of this ring may be conveniently expressed as

$$\theta_E = \sqrt{\frac{4GM(\leq D_{od}\theta_E)D_{ds}}{c^2 D_{od} D_{os}}} \quad (6.6)$$

We have also listed in table 1 typical values of  $\theta_E$  for different types of deflector located at various distances.

As we shall see in the next sections, the value of  $\theta_E$  derived here is very important because it can usually be used to estimate the angular separation between multiple lensed images in more general cases where the condition of perfect alignment between the source, deflector and observer is not fulfilled or even for lens mass distributions which significantly depart from the axial symmetry. Observed image separations ( $\simeq 2\theta_E$ ) can therefore lead to the value of  $M/D_{od}$  or to the value of  $M$  times the Hubble constant, if the redshifts  $z_d$  and  $z_s$  are known. This is the simplest and most direct astrophysical application of gravitational lensing. We see from table 1 that for a source and a lens located at cosmological distances ( $z_d \simeq 0.5$  and  $z_s \simeq 2$ ), the angle  $\theta_E$  can vary from micro-arcsec (stellar deflection) to arcsec (galaxy lensing), and up to some tens of arcsec in the case of cluster lenses. Let us also finally note that condition (6.3) for a deflector to produce multiple images of a lensed source turns out to be usually applicable, even when there is no axial symmetry. We shall now describe in more detail some of the best known lens models.

**6.1.2. The point-mass lens model.** We first consider the classical model consisting of a single point mass (cf a black hole or a very compact object, see figure 4). Due to the axial symmetry, the propagation of light rays essentially reduces to a one-dimensional problem. Given the deflection angle in equation (4.1), the lens equation (4.3) may thus be rewritten as

$$\alpha = \frac{2R_{sc}D_{ds}}{\theta D_{od}D_{os}} = \theta - \theta_s. \quad (6.7)$$

We have used this result to illustrate in figure 11 a typical ray-tracing diagram for the model of a point-mass lens. In the case of perfect alignment between the source, the lens and the observer, the latter ( $O_1$  in figure 11) sees a ring of light due to the symmetry (cf the Einstein ring in the gravitational lens experiment shown in figure 9). As the observer moves away from the symmetry axis (cf  $O_2$  in figures 11 and 12(b)), the Einstein ring breaks into two images that are located in the direction of the deflected rays, on opposite sides of the deflector (cf figures 11 and 12(c)).

The solutions of the lens equation may be obtained in a simple way from a bending-angle diagram (see figure 13(b)) where  $\alpha$  and  $\theta - \theta_s$  are plotted as a function of  $\theta$  and where the intersections between the hyperbola (i.e.  $\alpha(\theta)$ ) and the straight line (i.e.  $\theta - \theta_s$ ) passing through the point  $(\theta_s, 0)$  correspond to the desired solutions. For a given circular source S, it is then straightforward to construct geometrically the resulting images projected on the sky, as seen by an observer for the two cases of perfect and non-perfect alignments (see figures 13(a) and (c), respectively). Finally, an alternative way to solve the lens equation (6.7) is to make use of the results (4.1) and (6.6) and to rewrite the former equation as follows

$$\theta^2 - \theta_s\theta - \theta_E^2 = 0 \quad (6.8)$$

so that the two solutions may be simply expressed as

$$\theta_{A,B} = \frac{1}{2}\theta_s \pm \sqrt{\left(\frac{1}{2}\theta_s\right)^2 + \theta_E^2}. \quad (6.9)$$

For  $\theta_s = 0$ , we find that the angular radius of the Einstein ring is given by  $\theta_{A,B} = \pm\theta_E$  and by means of equation (4.6) that the magnification of this ring is

$$\mu_E = 2\theta_E/d\theta_s \quad (6.10)$$

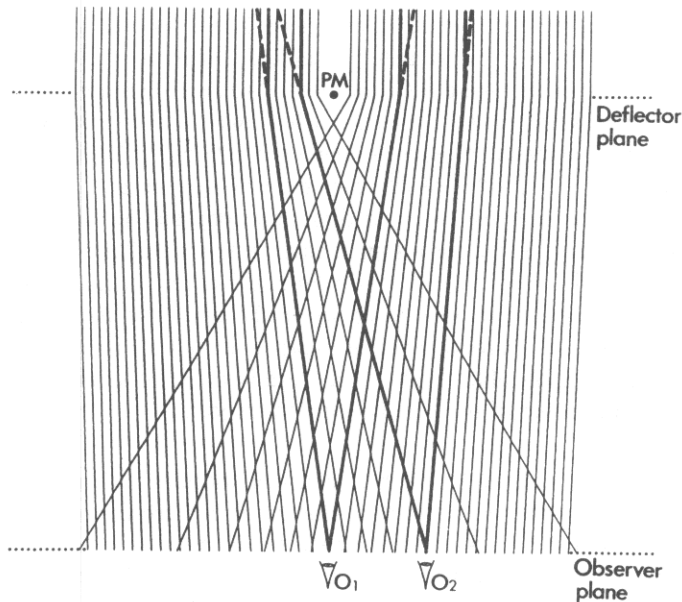


**Figure 11.** Ray-tracing diagram for the point-mass (PM) lens model. This diagram, as well as all subsequent ray-tracing diagrams, represent a set of parallel light rays, originating from a very distant point source, that deviate from their path as they cross the deflector plane. Different observer positions are represented in the 'observer' plane from where multiple lensed images may usually be seen.

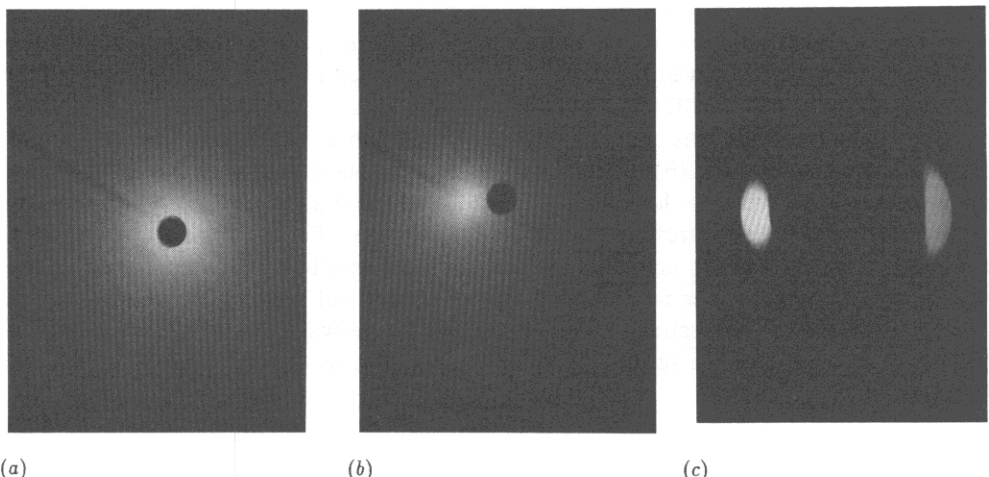


**Figure 12.** Optical gravitational lens experiment: in this first experiment used to simulate the gravitational deflection of light rays by a point-mass lens model (see section 5.2), the pinhole (observer) is set very precisely on the optical axis of the gravitational lens so that the source, the lens and the observer are perfectly aligned (a). The resulting image is an Einstein ring (see figure 9). As the pinhole is moved slightly away from the symmetry axis (b), the Einstein ring breaks up in two images (c).

where  $d\theta_s (\ll \theta_E)$  represents the true angular radius of the source. As we depart from perfect

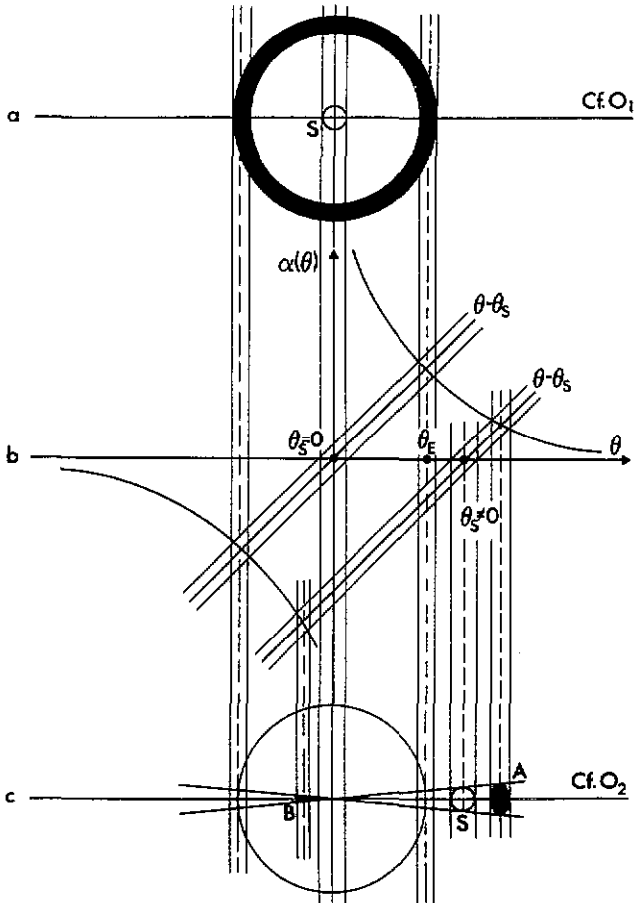


**Figure 13.** Combined bending-angle diagram (*b*) and resulting lensed images ((*a*) and (*c*)) produced for the circular source  $S$  by a point-mass lens model. In this and all subsequent bending-angle diagrams, the solutions ( $\theta$ ) of the lens equation (see equation (4.3)) are obtained from the geometric intersections between the bending curve  $\alpha(\theta)$  and the straight line  $\theta - \theta_s$ , for the case of a circular source  $S$  whose centre is located at a true angular distance  $\theta_s$  from the deflector. The resulting lensed images are then constructed from simple geometric projections. For the particular case  $\theta_s = 0$ , the circular source  $S$  is lensed into an Einstein ring whose angular radius is  $\theta_E$ .

alignment (i.e.  $\theta_s \neq 0$ ), it is easy to show (see equations (6.9) and (4.6)) that the angular separation between the two lensed images is

$$\Delta\theta = \sqrt{\theta_s^2 + 4\theta_E^2} \quad (6.11)$$

and that their magnification is given by

$$\mu_{A,B} = \frac{1}{4} \left( \frac{\Delta\theta}{\theta_s} + \frac{\theta_s}{\Delta\theta} \pm 2 \right). \quad (6.12)$$

The total magnification of the two images is thus

$$\mu_T = \frac{1}{2} \left( \frac{\Delta\theta}{\theta_s} + \frac{\theta_s}{\Delta\theta} \right). \quad (6.13)$$

We can then easily deduce that for great misalignment between the source and the lens and the observer, one of the two images approaches its true luminosity whereas the second one gets very close to the position of the deflector and becomes extremely faint.

When the true position of the source lies inside the imaginary Einstein ring (i.e.  $\theta_s \leq \theta_E$ ), the net magnification of the two images amounts to  $\mu_T \geq 1.34$ . This means that the cross section for significant lensing (by convention  $\mu_T \geq 1.34$ ) is equal to  $\pi \theta_E^2$ , which is proportional to  $M$  (see equation (6.6)). We shall make use of this result when discussing the optical depth for lensing in section 7 and when using the observed frequency of multiply imaged sources within a sample of highly luminous quasars to set an upper limit on the cosmological density of compact objects in the universe (cf subsection 7.4).

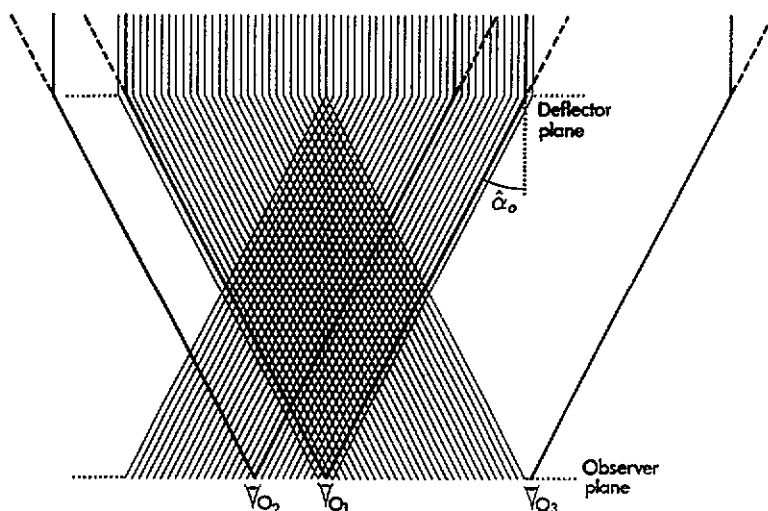


Figure 14. Ray-tracing diagram for the SIS lens model.

**6.1.3. The SIS lens model.** The SIS provides us with a reasonable approximation to account for the lensing properties of a real galaxy. Since the mass  $M(\xi)$  of an SIS galaxy is proportional to the impact parameter  $\xi$ , the value of the deflection angle  $\hat{\alpha}(\xi)$  is constant, irrespective of the value of  $\xi$  (see equation (4.5), the ray-tracing diagram in figure 14 and the bending-angle diagram in figure 15(b)). From galaxy modelling, it can be shown that the value of the deflection angle is given by

$$\hat{\alpha}(\xi) = \hat{\alpha}_0 = 4\pi\sigma^2/c^2 \quad (6.14)$$

where  $\sigma$  represents the one-component (observable) velocity dispersion of the galaxy. For  $|\theta_s| \leq \alpha_0 = \hat{\alpha}_0(D_{ds}/D_{os})$ , the solutions of the one-dimensional SIS lens equation are then found to be

$$\theta_{A,B} = \theta_s \pm \alpha_0 \quad (6.15)$$

in accordance with equation (4.3). From these equations, we may directly infer that an observer located on the symmetry axis (i.e. for  $\theta_s = 0$ ; see  $O_1$  in figure 14) will also see in this case an Einstein ring, the latter one being characterized by the angular radius

$$\theta_E = \alpha_0 \quad (6.16)$$

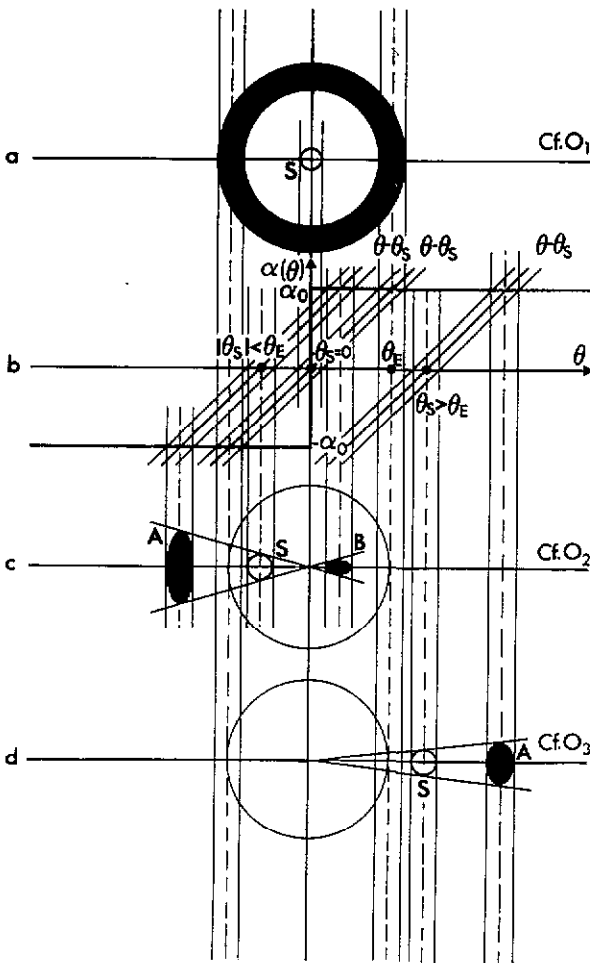


**Figure 15.** Combined bending-angle diagram (*b*) and resulting lensed images produced for the circular source *S* by a sis lens model ((*a*), (*c*) and (*d*); see text).

and that the magnification of this ring amounts to

$$\mu_E = 4\theta_E/d\theta_s. \quad (6.17)$$

This last value for the magnification is found to be twice as large as that for the point-mass lens; the reason being that the angular thickness of the SIS Einstein ring is  $2d\theta_s$  (see figure 15(*a*)), i.e. it is twice as large as that in the point-mass case. As the observer moves away from the symmetry axis (cf *O*<sub>2</sub> in figure 14), the Einstein ring also breaks here into two images with an angular separation  $\Delta\theta = 2\theta_E$  (see figure 15(*c*)). As long as  $\theta_s \leq \theta_E$ , we easily find by means of equations (4.6) and (6.15) that the magnification of the two images is

$$\mu_A = \theta_E/\theta_s + 1 \quad (6.18a)$$

and

$$\mu_B = \theta_E/\theta_s - 1. \quad (6.18b)$$

The net total magnification affecting the two images is thus

$$\mu_T = \mu_A + \mu_B = 2\theta_E/\theta_s. \quad (6.19)$$

For  $\theta_s > \theta_E$ , the observer only sees one image (cf  $O_3$  in figure 14, see also figure 15(d)) and its magnification is given by

$$\mu_A = \theta_E/\theta_s + 1. \quad (6.20)$$

We see that  $\mu_A \rightarrow 1$  when  $\theta_s$  increases to large values. We recall that the SIS lens model constitutes a good first approximation with which to simulate the lensing properties of real galaxies over a large range of impact parameters and that it is therefore often used to estimate lensing probabilities (see section 7). The most serious shortcoming of this model is that for light rays passing near to the centre of the galaxy the deflection is too large. However, for statistical purposes, this is not too serious since small values of the impact parameter  $\xi$  occur very seldomly. Since for real (finite) galaxies, the deflection angle obviously tends to zero as the impact parameter increases, one may naturally introduce truncated SIS models or even more complex ones, as shown in the next section.

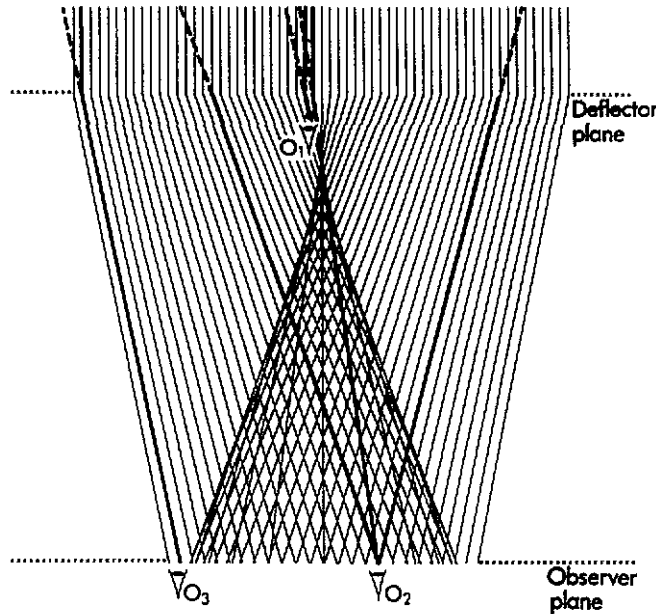


Figure 16. Ray-tracing diagram for the spiral galaxy lens model.

**6.1.4. The spiral galaxy lens model.** If we combine equation (4.5) with equation (5.10) that characterizes the mass distribution of the disk of a spiral galaxy, seen face on, we may easily construct the resulting ray-tracing diagram (figure 16) and the combined bending-angle diagrams (figures 17(b) and (c)) in order to understand the formation of multiple lensed images due to this somewhat more complex deflector model. From these diagrams, we directly see that whenever the observer is located between the lens and the focal point caused by the inner part of the disk (cf  $O_1$  in figure 16, see also figure 17(a)), we have  $\Sigma_c > \Sigma_0$ , where  $\Sigma_c$  represents the critical surface density defined by equation (6.5) and  $\Sigma_0$

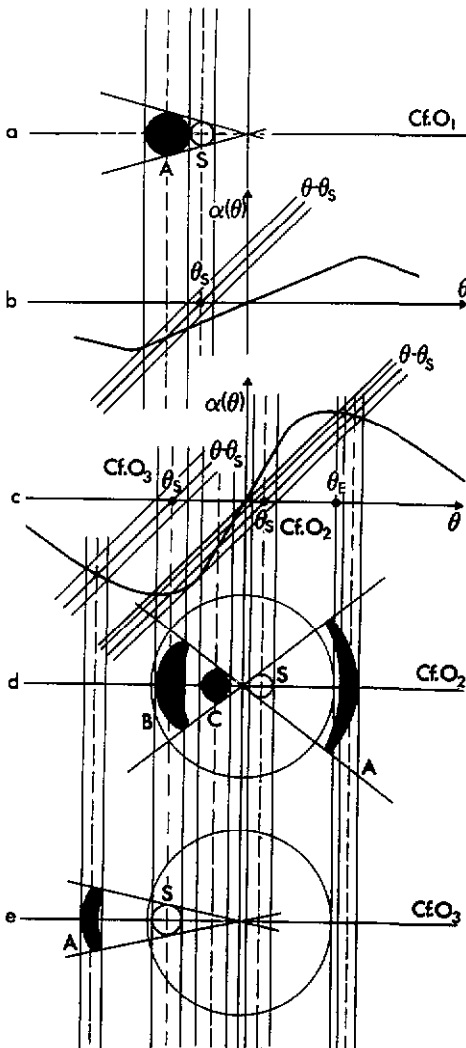


Figure 17. Combined bending-angle diagrams ((b) and (c)) and resulting lensed images produced for the circular source  $S$  by a spiral galaxy lens model ((a), (d) and (e)); see text).

the central surface mass density of the spiral galaxy (cf equation (5.8)). In this case, the observer only sees one single image of the distant source. However, when the observer is located behind the focal point ( $\Sigma_c < \Sigma_0$ ), he may see either three images (cf  $O_2$  in figure 16, see figure 17(d)) or one single image (see  $O_3$  in figure 16, see figure 17(e)), depending on whether he is located within, or outside, the caustic line. This caustic is very well seen in the ray-tracing diagram as the envelope curve formed by the deflected light rays originating from a very distant point source. Mathematically, the caustic corresponds to the solution of equation (4.6) for the case when the magnification of one of the lensed images becomes infinitely large (i.e.  $\mu_i \rightarrow \infty$ ). We will see in subsection 6.2 that caustics constitute generic features characterizing realistic lens models and that, very generally speaking, an observer crossing a caustic (i.e. going from the positions  $O_2$  to  $O_3$  in figure 16) always sees two of

the lensed images approaching each other, becoming very bright while they merge and then totally vanishing when the observer reaches the other side of the caustic. For the case of the spiral galaxy lens model, this sequence of events may easily be understood while changing the position of the source in the bending-angle diagram illustrated in figure 17(c).

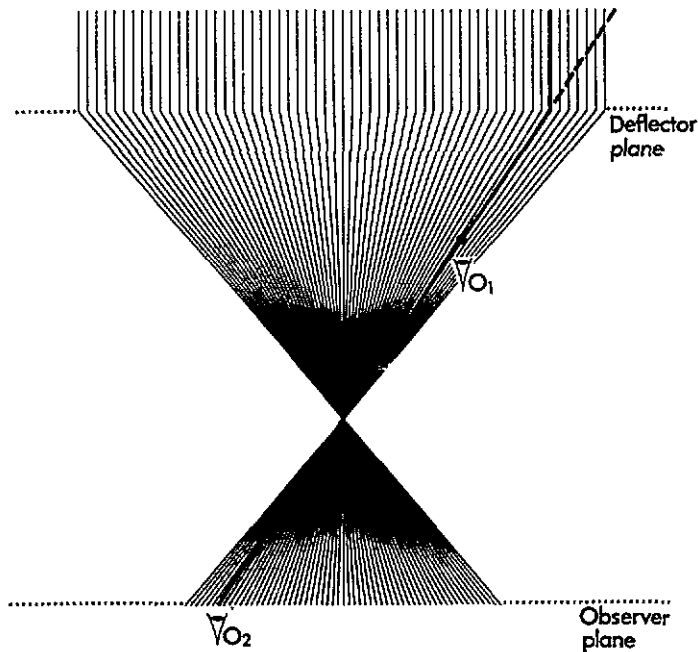


Figure 18. Ray-tracing diagram for the uniform disk lens model.

**6.1.5. The uniform disk lens model.** A transparent circular disk of matter, seen face on, characterized by a uniform surface mass density  $\Sigma_0$  has an effective deflecting mass equal to  $\pi \xi^2 \Sigma_0$ , where  $\xi$  represents the impact parameter of a chosen light ray. The deflection angle is thus (see equation (4.5)) given by

$$\hat{\alpha}(\xi) = 4\pi G \Sigma_0 \xi / c^2. \quad (6.21)$$

The disk is therefore acting as a normal converging lens (see the ray-tracing diagram in figure 18), whose focal length is

$$f = c^2 / 4\pi G \Sigma_0. \quad (6.22)$$

It is then easy to show that the lens equation (4.3) leads to the solution

$$\theta = \theta_s / (1 - \kappa) \quad (6.23)$$

where  $\kappa = \Sigma_0 / \Sigma_c$ ,  $\Sigma_c$  being the critical surface mass density defined in equation (6.5). With the exception of a hypothetical observer that would be precisely located at the focal point ( $\kappa = 1$ , the perceived image would then be a fully illuminated disk of light!), the observer just sees one single image of the distant source, somewhat displaced and (de)magnified (see

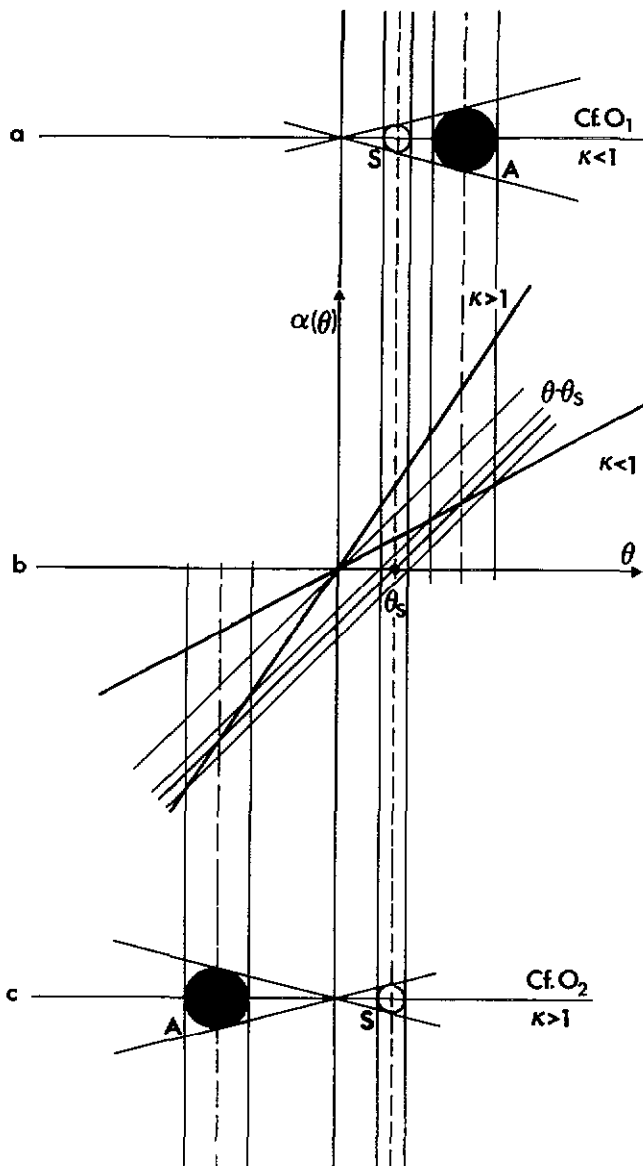


**Figure 19.** Combined bending-angle diagram (b) and resulting lensed images produced for the circular source S by two different uniform disk lens models ( $\kappa < 1$  in (a) and  $\kappa > 1$  in (c); see text).

the combined bending-angle diagram in figure 19). The magnification of this lensed image is directly found to be

$$\mu_A = 1/(1 - \kappa)^2. \quad (6.24)$$

Let us note that for an observer located between the lens and the focal point we have  $\kappa < 1$  (see O<sub>1</sub> in figure 18, see also figure 19(a)), whereas we have  $\kappa > 1$  when the observer is located behind the focal point (see O<sub>2</sub> in figure 18, see also figure 19(c)).

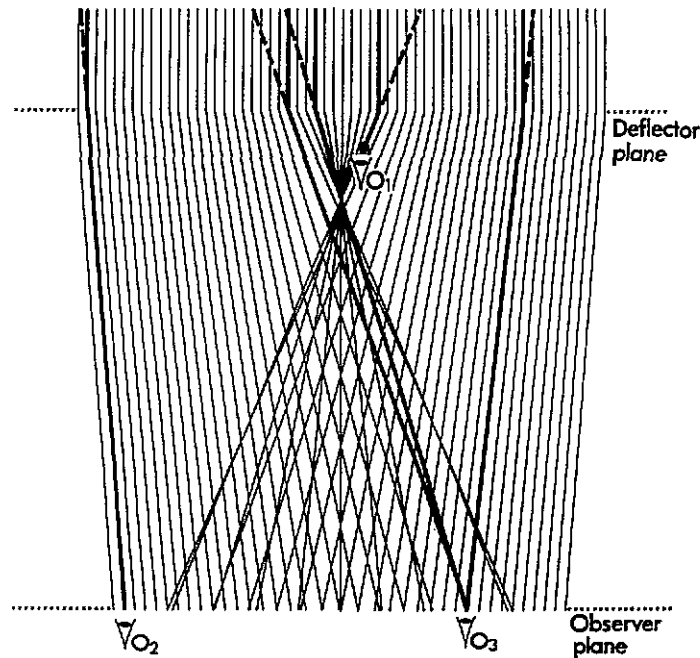


Figure 20. Ray-tracing diagram for the truncated uniform disk lens model.

**6.1.6. The truncated uniform disk lens model.** Let us finally consider the case of a truncated uniform disk, i.e. such that we may possibly have  $\xi > R$ . For those external rays, the disk effectively acts as a point mass and the lens equation leads to a combination of the solutions (6.9) and/or (6.23), depending on whether the condition  $\theta > R/D_{\text{od}}$  or  $\theta < R/D_{\text{od}}$  is fulfilled. From the ray-tracing diagram depicted in figure 20 and the combined bending-angle diagrams represented in figures 21(b) and (c), we see that only one image can be formed for  $\kappa < 1$  (see  $O_1$  in figure 20, see also figure 21(a)), whereas for  $\kappa > 1$ , there may result the formation of one or three images (see  $O_2$  and  $O_3$  in figure 20, see also figures 21(d) and (e)).

## 6.2. Asymmetric lenses

Let us first summarize some of the important results that have been obtained in the previous subsection when considering the formation of multiple images by an axially symmetric lens model. For the case of the point-mass and SIS deflectors that are singular in their centre, the maximum number of lensed images has been found to be equal to two. For non-singular deflectors such as the spiral galaxy or the truncated uniform disk, we have seen that there were one or, at most, three lensed images, one of these being often very faint and located very near to the centre of the lens.

As we may expect, symmetric lenses are very seldomly realized in nature; usually the main lens itself is asymmetric or some asymmetric disturbances may also be induced by the presence of neighbouring masses. In an important paper, Burke (1981) has demonstrated that a non-singular, transparent (symmetric or asymmetric) lens always produces an odd number of images for a given point source (except when located on the caustics). However, for the case of a singular lens, as in our optical lens experiment, one may obtain an even number of images.

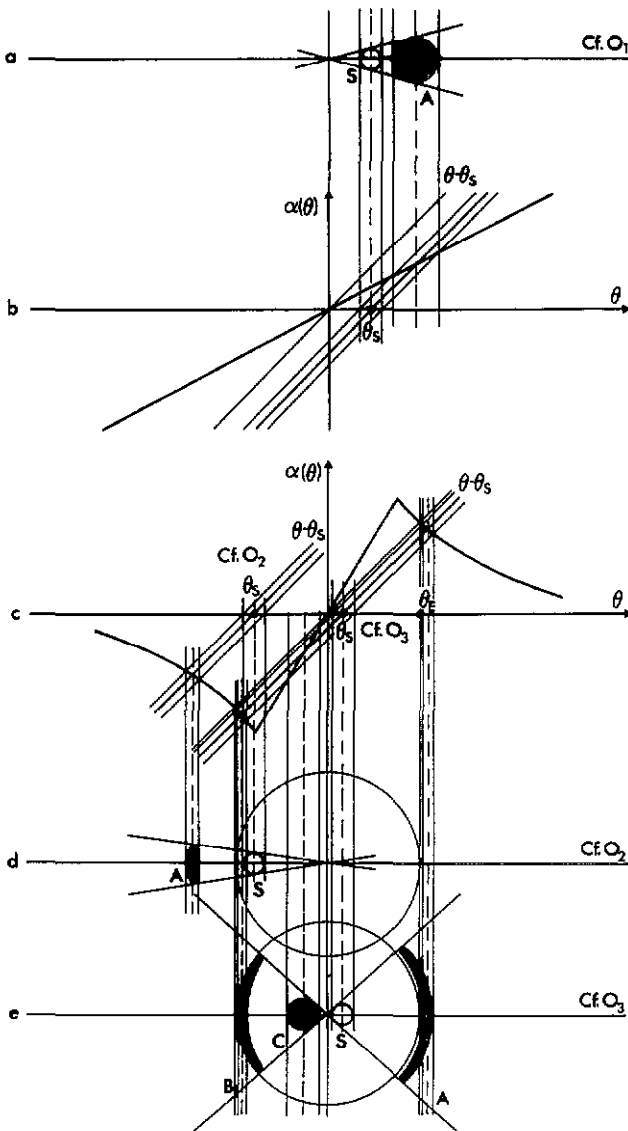
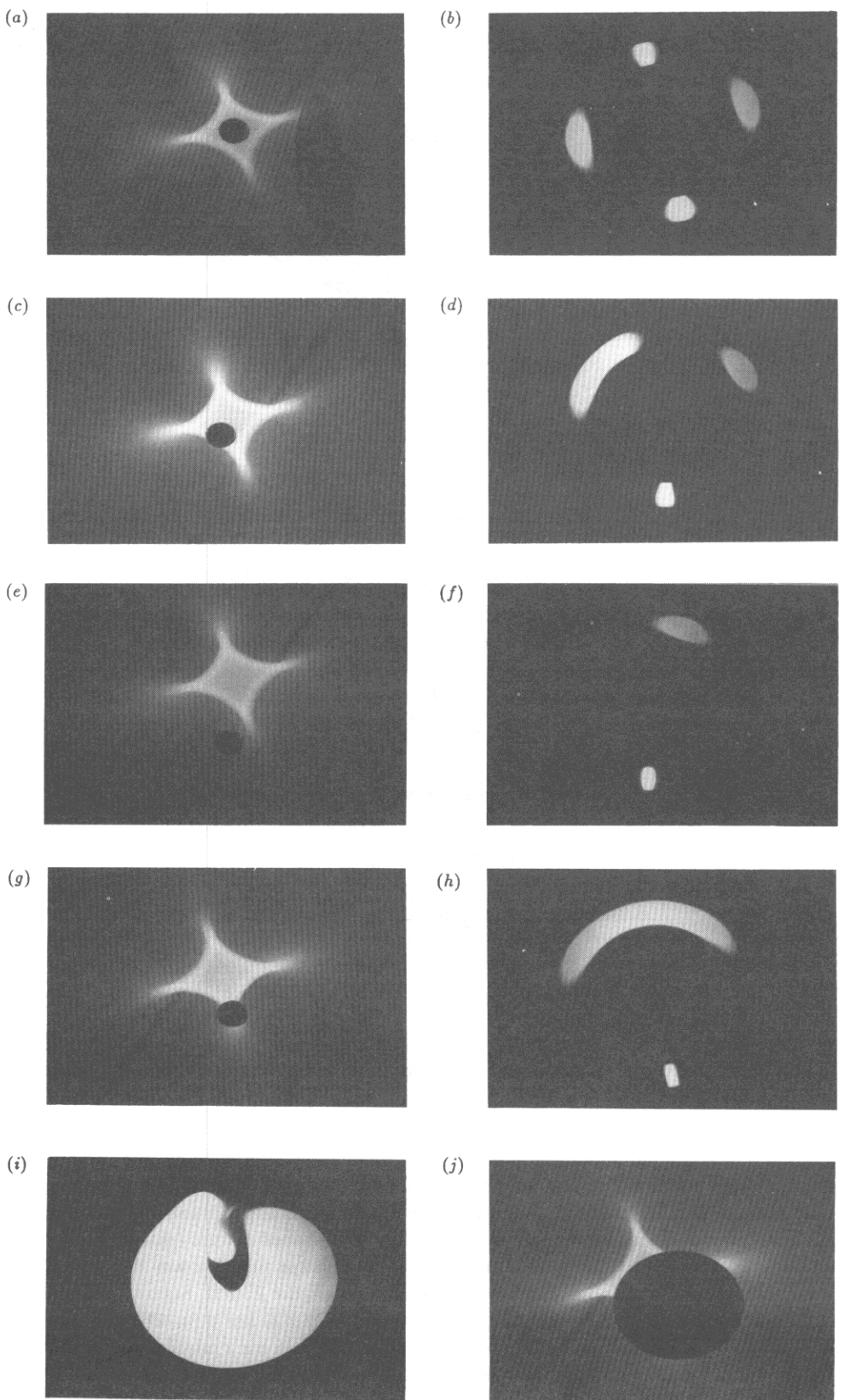


Figure 21. Combined bending-angle diagrams ((b) and (c)) and resulting lensed images produced for the circular source  $S$  by a truncated uniform disk lens model ((a), (d) and (e); see text).

In our optical gravitational lens experiment (cf section 5.2), the effects of a typical non-symmetric (singular) gravitational lens may be simulated by simply tilting the optical lens. In this case (see figure 22(a)), the bright (focal) line along the optical axis which existed in the symmetric configuration (cf figures 9 and 12(a)) has changed into a two-dimensional caustic surface, a section of which is seen as a diamond-shaped caustic (made of four folds and four cusps) in the pinhole plane. As a result, the Einstein ring that was observed in the symmetric case has now split up into four lensed images (figure 22(b)). Such a configuration ( $D_{od} \approx 10$  kpc), we find  $t_E$  to be just a few months ( $V \approx 200$  km s $^{-1}$ ). The timescale for the merging and disappearance of lensed images, as shown in our optical gravitational lens experiment, can be much shorter than the timescales given here; this will be discussed later.



of four lensed images always arises when the pinhole (observer) lies inside the diamond formed by the caustic. Let us immediately note that such caustics constitute a generic property of gravitational lensing, the focal line in the symmetric configuration being just a degenerate case. Figure 22(d) shows the merging of two of the four images into one, single, bright image when the pinhole approaches one of the fold caustics (figure 22(c)). Just after the pinhole has passed the fold caustic (see figure 22(e)), the two merging images have totally disappeared (figure 22(f)). A particularly interesting case occurs when the pinhole (observer) is located very close to one of the cusps (cf figure 22(g)). Three of the four previous images have then merged into one luminous arc, whereas the fourth one appears as a faint counterimage (figure 22(h)). For large sources that cover most of the diamond-shaped caustic (figure 22(i)), an almost complete Einstein ring is observed (figure 22(j)), although the source, lens and observer are not perfectly aligned and the lens is still being tilted. In this last experiment, the increase of the source size has been simulated by enlarging the pinhole radius by a factor  $\approx 4$ . In order to show that this is a correct simulation, one may consider the pinhole and the screen behind it as a camera. It is then clear that an increase in the size of the pinhole leads to a larger and less well focused image of the compact source, corresponding indeed to an increase in the source size. A more detailed and rigorous analysis does confirm this result. The image configurations illustrated in figures 22(a)–(j) are all found among the observed gravitational lens systems which will be discussed in section 8. It is obvious that if our optical lens were to have been non-singular in the centre (cf the ‘spiral galaxy’ optical lens shown in figure 8), we would have seen an additional image formed in the central part of the lens. For the known lenses with an even number of observed images, it may well be that a black hole resides in the centre of the lens. The presence of a compact core could also account for the ‘missing’ image since then the very faint image expected to be seen close to, or through the core, would be well below the detection limits that are presently achievable (cf the third faint lensed image (c) in figures 17(d) and 21(e)). Let us finally note that whereas the formation of multiple lensed images by asymmetric gravitational lenses is mathematically well understood (cf the pioneering work by Bourassa *et al* (1973)), the theoretical developments turn out to be very technical and rather tedious. The main results, however, reduce to the conclusions obtained in the above optical gravitational lens experiment.

### 6.3. Timescales of gravitational lensing effects

Since for asymmetric lenses the size of the diamond-shaped caustic is usually comparable with the radius  $\xi_E$  of the Einstein ring associated with a compact object of similar mass, a characteristic timescale  $t_E$  for a gravitational lens system should be the time it would take for an observer (the pinhole) to cross the radius  $x_E = \xi_E D_{\text{os}}/D_{\text{ds}}$  of the Einstein ring projected onto the observer’s plane. The relative motion between the observer and the caustic arises because of relative velocities between the observer, the lens and the source. If  $V$  represents the effective transverse velocity of the observer, then  $t_E$  is given by

$$t_E \approx x_E/V. \quad (6.25)$$

Referring to table 1 and assuming  $V \approx 600 \text{ km s}^{-1}$ , we see that, for typical cosmological distances and for the case of a massive galaxy lens, we obtain  $t_E \approx 2 \times 10^7 \text{ y}$ , whereas for one solar mass star acting as a lens, we get  $t_E \approx 20 \text{ y}$ . If the star is in our galaxy

---

Figure 22. The optical gravitational lens experiment for the case of an asymmetric, singular deflector (see text in section 6.2).

## 7. Optical depth for lensing and some observational results

### 7.1. The point-mass lens model

For randomly distributed point-mass lenses (e.g. stars, a putative cosmological population of black holes, etc), let us now estimate the frequency of significant gravitational lensing from observations of distant compact sources, i.e. objects and lenses whose angular sizes are definitely smaller than  $\theta_E$  (see equation (6.6)).

Since the total amplification  $\mu_T$  of a compact source lensed by a point-mass lens exceeds 1.34 whenever the true source position lies inside the imaginary Einstein ring associated with the deflector (i.e. for  $\theta_s < \theta_E$ , see section 6.1.2), the probability  $P$  to have significant lensing (by convention,  $\mu_T > 1.34$ ) for a randomly located compact source at a distance  $D_{os}$  is simply given by

$$P = \frac{\pi \theta_E^2}{4\pi} = \frac{D_{ds} GM}{c^2 D_{os} D_{od}} = -\frac{D_{ds} U}{D_{os} c^2} \quad (7.1)$$

where  $U (< 0)$  represents the Newtonian gravitational potential of the deflector as measured at the observer. We see that the probability  $P$  is linear in  $U$  so that equation (7.1) is also valid when several deflectors are acting independently of each other, irrespective of their individual masses. Considering a constant density of deflectors in a static universe, we may take an appropriate average of  $D_{ds}$  ( $D_{os}$  being fixed) and derive the expression for the total probability  $P$  (or optical depth  $\tau$  for lensing)

$$P = \tau = -\left(\frac{D_{ds}}{D_{os}}\right) \frac{U_L}{c^2} = -\frac{U_L}{3c^2} \quad (7.2)$$

where  $U_L$  is the gravitational potential at the observer due to all possible lenses at distances  $D_{od} < D_{os}$ . We note that  $\tau$  is equal to the fraction of the sky being covered by the corresponding Einstein rings. From this simple result, it is clear that stars in our galaxy have an extremely small optical depth for lensing ( $|U_L^*/c^2| \simeq 10^{-6}$ ). The situation, however, looks much more promising for distant sources. Following Refsdal (1965, 1970) and Press and Gunn (1973), it can be shown that for small source redshifts (typically  $z_s \leq 0.5$ )

$$\tau = \frac{1}{4} \Omega_L z_s^2 \quad (7.3)$$

where  $\Omega_L$  is the cosmological density parameter of compact lenses. For  $z_s > 0.5$ ,  $\tau$  still increases with  $z_s$  but not as fast as indicated by equation (7.3). For a more detailed discussion on lensing optical depth, see Canizares (1982) and Turner *et al* (1984). We see that values of  $\tau$  near unity may be reached for  $z_s \geq 1$ , if  $\Omega_L$  is close to one, and that very distant cosmic sources constitute the best candidates for being lensed. Therefore, even before the discovery of the first gravitational lens in 1979, it was natural to consider quasars as the best candidates to search for gravitational lensing effects. Since an upper value on  $\tau$  may be directly derived from the most optimistic estimated frequency of multiply imaged compact sources in a given sample (e.g. quasars), we may generalize equation (7.3)—including cosmological corrections—to infer an upper limit on  $\Omega_L$ . However, because of instrumental limitations (e.g. restricted ranges in accessible angular separations, etc), the derived upper limit on  $\Omega_L$  will essentially concern a specific mass range  $M_L$  for the point-mass lenses.

Let us remark here that, in this reasoning, we have assumed that our quasar sample is volume-limited in space. However, in practice, only flux-limited samples of sources are available such that a correction due to an amplification bias must be taken into account before using equations such as equation (7.3). As we shall see later, the amplification bias correction may turn out to be very substantial.

## 7.2. The amplification bias correction

Indeed, because multiple imaging is intimately connected with large amplifications of the selected sources, a strong bias effect arises if the intrinsic luminosity function of the latter objects is very steep since then an appreciable number of multiply imaged sources which were originally fainter than the flux threshold of the sample are boosted into it. The net effect is that the frequency of multiple imaging appears much greater in flux-limited samples of quasars than in volume-limited ones (Turner *et al* 1984). Following Fukugita and Turner (1991), amplification bias correction factors amounting to approximately 15, 25, 40 and 50 must be applied to estimates of the frequency of multiply imaged quasars when considering samples limited in flux down to blue apparent magnitudes  $B = 18, 17, 16$  and 15, respectively.

Another direct consequence of the amplification bias is that one would naturally expect to find an excess of foreground (amplifying) galaxies near distant and bright quasars selected from a flux-limited sample (see Narayan (1989) and Schneider (1987a, b)). Van Drom *et al* (1993) have recently reported the detection of a significant excess ( $\simeq 2.5$ ) of moderately bright galaxies ( $R \leq 21$ ) located in the neighbourhood ( $\leq 3''$ ) of a sample of 185 highly luminous quasars ( $M_V \leq -27$ ), in good agreement with current expectations.

## 7.3. The SIS lens model

As already discussed in section 6.1.3, the SIS lens model has been successfully used in the past to represent as a first approximation the lensing properties of galaxies in the universe. In accordance with this model, an observer sees two lensed images of a distant source provided that  $\theta_s \ll \theta_E$ , which means that the cross section for an SIS deflector to produce double lensed images is  $\pi\theta_E^2$ , just like the cross section for a point-mass lens to produce a total amplification  $\mu_T \geq 1.34$ . If, because of the limited dynamical range of existing imaging instruments, a condition is imposed on the maximum detectable brightness ratio of two lensed images (e.g. only systems for which the magnitude difference does not exceed four magnitudes), one can easily show that the real cross section is only reduced very slightly (smaller than 5% in our example), so that we can effectively use a cross section equal to  $\pi\theta_E^2$  when evaluating the frequency of multiply imaged sources (e.g. quasars). Given the dependence of the angular Einstein radius on the one-component velocity dispersion  $\sigma$  of a SIS galaxy (i.e.  $\theta_E \propto \sigma^2$ , see equations (6.14)–(6.16)), it is straightforward to establish that, for a given cosmological distribution of SIS galaxies, the optical depth for producing multiply imaged quasars will be directly proportional to the efficiency parameter  $F(\propto n_0\sigma_{\text{eff}}^4)$ , where  $n_0$  represents the local number density of the different known types of galaxies (elliptical, S0, spiral) and  $\sigma_{\text{eff}}$  an effective value for their one-component velocity dispersion. Of course, if one wishes to determine the value of the  $F$  parameter from the frequency of quasars which are multiply imaged by galaxies, here we must also take into account an amplification bias correction factor, as described in the previous section.

Finally, it is important to note that only the mass ‘inside’ the imaginary Einstein ring in fact contributes to the cross section  $\pi\theta_E^2$  (cf equation (6.6)), so that for an extended deflector, there is no way from the observed frequency of multiply imaged sources to trace the mass located outside the Einstein ring. In the case of non-symmetric and/or non-singular lenses, more than two images may be seen, but for such more realistic types of deflectors, the probabilities depend unfortunately on many uncertain parameters (ellipticity, core radius, etc) and are therefore more difficult to evaluate. Let us finally note that in most statistical estimates of the lensing effects, it is assumed that the unlensed population of the sources is the one that is actually observed and that these same sources consist of point-like objects.

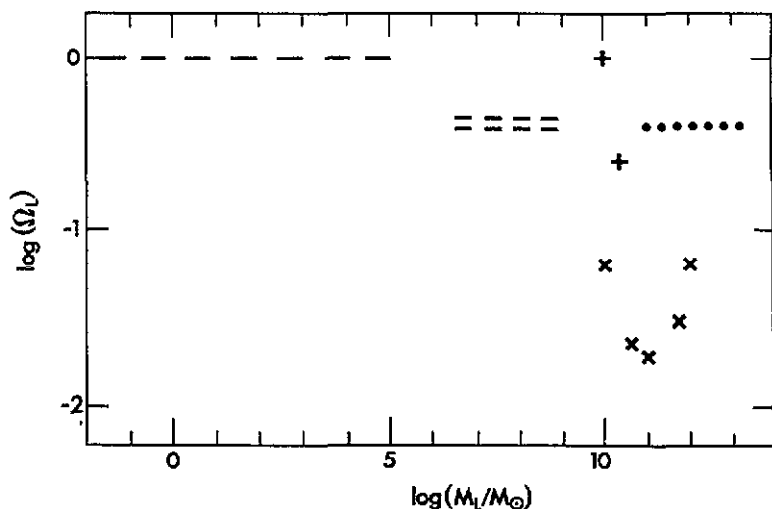


**Figure 23.** Adopting  $H_0 = 50 \text{ km s}^{-1} \text{ Mpc}^{-1}$ ,  $\Omega_0 = 1$  and  $\Lambda = 0$ , we have illustrated in this diagram the various upper bounds derived for the density parameter  $\Omega_L$  of compact lenses, with mass  $M_L$ , capable of producing multiple images of distant sources. The various determinations are: —, Canizares (1982); ●, Hewitt (1986); +, Nemiroff (1991); =, Kassiola *et al* (1991); and ×, Surdej *et al* (1993a). Figure reproduced courtesy of the *Astron. J.*

#### 7.4. Some observational results on gravitational lensing statistics

Given the dependence of the optical depth for lensing on the redshift (cf equation (7.3)) and on the apparent magnitude of the sources (via the amplification bias correction factor, see section 7.2), it was natural to expect that high angular resolution (typically better than  $0.3''$ ) direct observations of a large sample of bright and distant quasars would constitute the best approach to searching for new gravitational lens systems, and also to setting limits on the parameters  $\Omega_L$  and  $F$ , previously described. The possibility of using statistical gravitational lens studies as an astrophysical and cosmological tool has led a group of observers to obtain direct images for 469 highly luminous quasars (i.e. characterized by an absolute visual magnitude  $M_V < -27$ ), either from the ground at the ESO (La Silla) and with the Canada-Franco-Hawaii telescope under optimal seeing conditions or using the Hubble Space Telescope (HST) (see Surdej *et al* (1993a) for a more detailed account of these observations). These authors have reported the identification of three certain gravitational lenses (see the description of PG1115+080, UM673 and H1413+117 in section 8) and of ten additional possible candidates. From these numbers, it is straightforward to estimate realistic values for the effectiveness parameter  $F$  of galaxies to produce multiply imaged quasars (i.e.  $0.005 < F < 0.5$ , at the 99.7% confidence level) and an upper limit for the cosmological density  $\Omega_L$  ( $\leq 0.02$ , at the 99.7% confidence level) of uniformly distributed compact objects in the mass range  $5 \times 10^{10} - 7 \times 10^{11} M_\odot$ . The range of values derived for the efficiency parameter  $F$  essentially overlaps previous estimates that have been made by Fukugita and Turner (1991) on the basis of direct observations of local galaxies. In a more elaborate study, Kochanek (1993) shows that the statistics of multiply imaged quasars are in agreement with our standard knowledge of the distribution and luminosity function of galaxies, on the relation between luminosity and velocity dispersion, on the quasar apparent magnitude number counts, etc. Finally, we have summarized in figure 23 all previous upper limits quoted for  $\Omega_L$  over a wide range of deflector masses. It is striking that the

cosmological density of compact objects in the mass range  $5 \times 10^{10} - 7 \times 10^{11} M_\odot$  already appears to be lower than that of known galaxies!

## 8. Observations of individual gravitational lens systems

By now, more than twenty proposed cases of multiply imaged distant sources, five radio rings and several tens of giant luminous arcs and arclets have been identified (see tables 2–5 for an updated list). Because of space limitation, we shall only describe some of these gravitational lens systems.

### 8.1. Accepted cases of multiply imaged sources

We shall first have a look at some examples of distant sources lensed by an intervening galaxy and which belong to the two major classes of image configurations (i.e. two or four images, see section 6.2). In the two-image configuration (cf figures 12(c) and 22(f)), the lensing galaxy is usually located between the two images. In the four-image configuration (cf figure 22(b)), the lensed images lie roughly on a circle; the deflector being located near its centre.

#### 8.1.1. The two-image configuration.

**0957+561:** The first reported example of a multiply imaged quasar (0957+561) consists of two components (A and B) at a redshift  $z = 1.41$ , separated by  $6.1''$ , accompanied by an extended radio source (Walsh *et al* 1979; see figure 24(a) and table 2). The principal lensing galaxy at  $z = 0.36$  is found to lie very near ( $\simeq 1''$ ) the southern component (cf the fuzz seen near this image in figure 24(a)). This galaxy is a member of a rich cluster whose mass also contributes to the lensing.

0957+561 has turned out to be important from the point of view of cosmological application (determination of the Hubble parameter by means of the measurement of the time delay). Indeed, not only does the light coming from the source along the northern image travel along a different geometric path from that associated with the southern image but the photons travelling along this second path do encounter stronger gravitational potential effects due to the galaxy. These are therefore more slowed down and, at the end, one can show that light from the northern component should reach a terrestrial observer approximately one year ahead. As explained in section 9.1, the measurement of such a time delay can be used to determine the value of the Hubble parameter  $H_0$ .

The most extensive optical and radio photometric monitoring ever carried out for a gravitational lens system over more than ten years has been made for this famous double quasar (Vanderriest *et al* 1989, Schild 1990, Lehár *et al* 1992, Conner *et al* 1992, see also a table summarizing the available data sets in Vanderriest *et al* 1992).

Although a value close to 1.45 y had been previously derived from both the optical and radio light curves (Press *et al* 1992a, b, Beskin and Oknynanskij 1992), a value of 1.14 y is preferred today (Vanderriest *et al* 1992, Kayser 1993, Schild and Thompson 1993). Based upon VLA data recorded at  $\lambda$  6 cm, Conner *et al* (1992) have derived an amplification ratio ( $B/A$ ) of  $0.697 \pm 0.003$  between the two images of the radio core and VLBI jet and  $B/A = 0.75 \pm 0.03$  for the core alone, in agreement with the value directly inferred from optical photometry.

Following the measurement of the line-of-sight velocity dispersion of the primary lensing galaxy ( $303 \pm 50 \text{ km s}^{-1}$ ), Rhee (1991), Narayan (1991), Roberts *et al* (1991) and others have published independent determinations for the value of the Hubble parameter. The values

range between 37 ( $\pm 15$ ) and 69 ( $\pm 20$ )  $\text{km s}^{-1} \text{Mpc}^{-1}$ . However, due to large uncertainties remaining in the lensing model, Falco *et al* (1990, 1991a) and Kochanek (1991a) have cast some doubts on the possibility of deriving a reliable value for  $H_0$  from this system (see also Falco (1992) and Refsdal (1992)). The recent discovery of an additional foreground cluster of galaxies at a redshift  $z = 0.5$  still adds more free parameters to the modelling of the lens (Garret *et al* 1992a, Angonin and Soucail 1992) and strengthens this conclusion. Two giant blue luminous arcs have been discovered at some  $20''$  from the centre of this gravitational lens system by Bernstein *et al* (1993) and these authors have discussed the constraints that these new images impose on the deflector models. Schild and Smith (1991) and Falco *et al* (1991b) have also discussed the possible role played by micro-lensing effects in the light curve of component B. A spectrophotometric monitoring of the two image components of 0957+561 would certainly help in disentangling the effects due to intrinsic variability and/or micro-lensing.

Based on x-ray images of 0957+561 obtained with the high-resolution imager onboard the Einstein satellite, Jones *et al* (1993) have reported the detection of an arc of radiation forming an approximate semi-circle that extends from the northern quasar image (A) to the southern one (B). In addition to this, they find unresolved x-ray emission associated with B, while the A image lies in a region affected by the x-ray arc. They interpret these results as due to the gravitational lensing of an extended source of x-ray emission, slightly offset from the unresolved x-ray source associated with the quasar itself. They suggest that the origin of the extended x-ray emission could arise from radiative cooling of hot gas surrounding the quasar.

Whereas the estimate of the mass of the lensing galaxy comprised between the two images is fairly secure assuming that the time delay is correct (cf Borgeest 1986), it is to be hoped that in addition to the ongoing optical spectroscopy obtained for the lensing clusters associated with this gravitational lens system (Garrett *et al* 1992a, b, Angonin and Soucail 1992), the high angular resolution radio observations of images A and B made at several epochs (cf Wilkinson 1990, Garrett *et al* 1993a) as well as subsequent searches for luminous arcs and arclets will help in constraining more efficiently the mass distribution in the lens(es).

Due to the rather complex nature of the lens for 0957+561, it is probable that observational studies of other systems with a more simple lens (cf 0142-100, 0218+357, 1104-1805, 1115+080) will lead to a more accurate value of  $H_0$ .

**0142-100 = UM673:** This is the first gravitational lens system that has been discovered at the ESO (La Silla) in a systematic survey among highly luminous quasars (HLQs) (Surdej *et al* 1987). The two QSO images ( $z = 2.72$ ) are separated by  $2.2''$  (see figure 24(b)) and their spectra turn out to be strikingly similar. After subtracting a double point spread function (PSF) from the observed QSO images, the lens of this system is seen and it appears to be made of a single isolated galaxy at a redshift  $z = 0.49$  (cf figure 24(c)). The mass of this deflector (within an angular radius of  $1.1''$ ) has been estimated to  $\simeq 2.4 \times 10^{11} h_{50}^{-1} M_\odot (h_{50} = H_0/50 \text{ km s}^{-1} \text{Mpc}^{-1})$ . Because no trace of a galaxy cluster has been detected around the lensing galaxy, this system constitutes a clean and good candidate to attempt an independent determination of  $H_0$ . The expected time delay is of the order of 7 weeks. A photometric monitoring of this system is under way at ESO and with the Nordic Optical Telescope. However, because of scheduling constraints, uncertain weather and seeing conditions, it has been difficult so far to obtain sufficiently well sampled light curves. Preliminary results have been recently reported by Daulie *et al* (1993); no significant light variation could be detected between the two lensed QSO images. A plea for a 2-3-m class optical telescope, fully dedicated to the monitoring of known gravitational

lens systems, has been presented by Refsdal and Surdej (1992) in order to alleviate such a frustrating problem. It is very probable that continuous observations of a few selected multiply imaged quasars would bring, after only a few years, major contributions in the fields of cosmology and the physics of quasars.

Speckle interferometry (i.e. speckle masking reconstruction) of UM673 (Weigelt *et al* 1994) shows that the lensed A and B images are unresolved down to angular separations near  $0.1''$  and magnitude differences near 2 for the A component.

Smette *et al* (1992) have reported a study of the Ly $\alpha$  forest on the basis of high-resolution spectra of this gravitational lens system. Making use of the number of coincidences and anti-coincidences for the Ly $\alpha$  absorption lines detected in the spectra of the two lensed images and by means of Monte Carlo simulations, these authors have derived a value of  $12h_{50}^{-1}$  kpc ( $q_0 = 0$ ) for the  $2\sigma$  lower limit of the diameter of spherical Ly $\alpha$  clouds. Smette *et al* have also suggested how to make use of their present results and those reported for the number of Ly $\alpha$  anti-coincidences in the spectra of 2345+007 A and B (Foltz *et al* (1984) and see section 8.2) in order to assess the physical nature (binary quasar or dark gravitational lens) of the latter system.

Let us finally mention that UM673 A and B were not detected at radio wavelengths ( $< 0.3$  mJy RMS noise), despite serious observational efforts made with the VLA at  $\lambda 6$  cm (National Radio Astronomical Observatory, New Mexico).

**1208+1011:** Magain *et al* (1992a, b) have reported convincing observational evidence that this very high redshift ( $z = 3.803$ ) and luminous quasar ( $M_V = -28.9$ , Hazard *et al* 1986, Sargent *et al* 1986) consists of two lensed images, with a record angular separation of only  $0.45''$  and a brightness ratio of 3.5, in red light (see figure 24(d)).

It is to be stressed that sophisticated data reduction methods (PSF subtraction, deconvolution, etc) had to be used in order to disentangle blended images with such a small angular separation (Magain *et al* 1992b). Q1208+1011 has independently been discovered in the gravitational lens snapshot survey performed with HST (Maoz *et al* 1992, Pirenne *et al* 1992). Additional imagery and spectroscopy obtained with HST essentially confirm the gravitational lens hypothesis for this very interesting system (Bahcall *et al* 1992a, b).

**1009 – 025:** This quasar ( $R = 17.6$ ,  $z = 2.74$ ) is the fourth gravitational lens system that has been discovered at ESO (La Silla) in the context of the ESO Key Programme ‘Gravitational Lensing’ (Surdej *et al* 1993b). This system consists of two lensed QSO images with an angular separation of  $1.55''$  and a magnitude difference of 2.4 in red light (see figure 24(e)). The image of the lens has not yet been identified. Quite unexpectedly, a quasar with a redshift  $z = 1.62$  and a magnitude  $R = 18.9$  has been found at  $4.6''$  from this multiply imaged quasar. Furthermore, during the course of this imaging survey of highly luminous quasars ( $M_V \leq -27$  calculated for  $H_0 = 50 \text{ km s}^{-1} \text{ Mpc}^{-1}$  and  $q_0 = 0.5$ ; see section 7.4), another pair of quasars (1148+055 A and B) with quite different redshifts ( $z_A = 1.89$  and  $z_B = 1.41$ ) has been discovered. The magnitudes of these two quasars are  $R = 17.9$  and  $R = 20.7$ , their angular separation being only  $3.9''$ . The probability of randomly identifying two such tight ( $\leq 5''$ ) associations of quasars with discordant redshifts within a sample of less than 500 highly luminous quasars turns out to be very small. It is very suggestive that a preferential amplification due to gravitational lensing along the line-of-sight to 1009 – 025, and probably also towards 1148+055 is responsible for this excess of apparent quasar associations. For completeness, we should still like to mention that Wampler *et al* (1973) twenty years ago reported the discovery of another interesting close pair ( $\Delta\theta = 4.8''$ ) of quasars 1548+115 A ( $R = 18.1$ ) and B ( $R = 18.8$ ) having very different redshifts ( $z_A = 0.44$  and  $z_B = 1.90$ ).

Table 2. Updated list of currently accepted cases of multiply imaged sources. Explanations G (Galaxy), ML (micro-lensing), R/O (radio and optical detection), C (cluster).

Source name (QSO/AGN)	Number of images	Image brightness/ Abs. Mag.	Separation/ Time delay	$z_s$	Lens type	Lens brightness	$z_l$	$M_l(M_\odot)$	Detection (O/R)	Reference
0957+561 A-B (QSO)	2	$B = 17.5$ (A) $B = 17.7$ (B) $M_B = -27.8$	$6.1''$ (A-B) $1.45$ y	1.41	G/Cs	$R = 18.5$	0.36	$1.1(12)$ $3.1''$ ML	O/R	Walsh <i>et al</i> 1979
1115+080 A1D-C (QSO)	4 5?	$B = 17.2$ (A1) $B = 17.2$ (A2) $B = 18.7$ (B) $B = 18.2$ (C) $M_B = -29.0$	$0.5''$ (A1-2) $1.8''$ (A-B) $2.3''$ (A-C) days months	1.72	G	$R = 19.8$	0.29	ML	O	Weymann <i>et al</i> 1980
2016+112 A-C' (AGN)	3	$i = 22.9$ (A) $i = 23.2$ (B) $i = 24$ (C')	$3.4''$ (A-B) $3.8''$ (A-C') $0.5-1$ y	3.27	2Gs	$i = 21.9$	1.01?	$\geq 2?$ ML?	R/O	Lawrence <i>et al</i> 1984
2237+0305 A-D (QSO)	4	$r = 17.6$ (A) $r = 17.8$ (B) $r = 18.1$ (C) $r = 18.4$ (D) $M_r = -28.7$	$1.8''$ (A-B) $1.4''$ (A-C) $1.7''$ (A-D) days	1.69	G	$r = 14.5$	0.04	$2.0(10)$ $0.9''$ ML	O	Huchra <i>et al</i> 1985
0142-100 A-B (QSO)	2	$B = 17.0$ (A) $B = 19.1$ (B) $M_B = -29.0$	$2.2''$ (A-B) $\simeq 7$ weeks	2.72	G	$R = 19.0$	0.49	$2.4(11)$ $1.1''$	O	Surdej <i>et al</i> 1987
3C324 A-C (AGN)	3	$R = 22.7$ (A) $R = 23.3$ (B)	$2''$ (A-B)	1.206	G	$R = 22.5$	0.84	$1.0(12)$	R/O	Le Feuvre <i>et al</i> 1987
1413+117 A-D (QSO)	4	$R = 18.3$ (A) $R = 18.5$ (B) $R = 18.6$ (C) $R = 18.7$ (D) $M_R = -28.7$	$0.8''$ (A-B) $0.9''$ (A-C) $1.1''$ (A-D) $\leq 1$ month	2.55	G?		1.4? $1.7?$ ML?	O/R	Magain <i>et al</i> 1988	

Table 2. Continued.

Source name (QSO/LCN)	Number of images	Image brightness/ Abs. Mag.	Separation/ Time delay	$z_s$	Lens type	$R = 22.4$	$1.0''$	$M_l(M_\odot)$ Radius/ Mic. lens	Detection (O/R)	Reference
0414+0534 A-D (Radio galaxy)	4	$R = 23$ (A-D)	$3''$ (A-D)	2.63?	G?				R/O	Hewitt <i>et al</i> 1989
1208+1011 A-B (QSO)	2	$V = 17.5$ (A) $V = 19.0$ (B) $M_V = -28.9$	$0.45''$ (A-B)	3.80				O	Magain <i>et al</i> 1992b	
1422+231 A-D (QSO)	4	$R = 16.5$ (A-D) $M_R = -29.5$	$1.3''$ (A-C)	3.62	G?			R/O	Pattnaik <i>et al</i> 1992a	
1009 - 025 A-B (QSO)	2	$R = 17.6$ (A) $R = 20.0$ (B) $M_R = -28.5$	$1.55''$ (A-B)	2.74	G?			O	Surdej <i>et al</i> 1993	
0952 - 01 A-B (QSO)	2	$\Delta I = 1.35$ (A/B)	$0.9''$ (A-B)	4.5				O	McMahon <i>et al</i> 1992	
1938+666 A-D (Radio galaxy?)	4+ mini-arc	$r = 23$ (A-D)		$\leq 1.0''$				R/O?	Pattnaik <i>et al</i> 1993	

Table 3. Additional proposed cases of multiply imaged sources (see table 2 for notation).

Source name (QSO/AGN)	Number of images	Image brightness/ Abs. Mag.	Separation/ Time delay	$z_s$	Lens type	Lens brightness	$z_l$	$M_l(M_\odot)$	Radius/ Mic. lens	Detection (C/R)	Reference
2345+007 A-B (QSO)	2	$B = 19.5$ (A) $B = 20.1$ (B) $M_B = -26.4$	$7.3''$ (A-B)	2.15		$J > 25.5$			0		Weedman <i>et al</i> 1982
1624+267 A-B (QSO)	2	$B = 19.2$ (A) $B = 20.8$ (B) $M_B = -26.4$	$3.8''$ (A-B)	1.96	G?	$R = 20.0?$	0.57?	$1.0(12)?$	0		Djorgovski and Spinrad 1984
0023+171 AB-C (AGN)	2	$r = 22.8$ (AB) $r = 23.4$ (C)	$4.8''$ (AB-C)	0.95					RO		Hewitt <i>et al</i> 1987
3C194 (AGN)	2	$R = 21.5$	$3.5''$	1.18	G	$R = 19.0$	0.31	$1.0(12)$	RO		Le Févre and Hammer 1988
1429-008 A-B (QSO)	2	$R = 17.7$ (A) $R = 20.8$ (B) $M_R = -27.9$	$5.1''$ (A-B)	2.08			1.6?		0		Hewitt <i>et al</i> 1989
1120+019 A-B (QSO)	2	$V = 16.2$ (A) $V = 20.8$ (B) $M_V = -28.6$	$6.5''$ (A-B)	1.46	G? C?	$R = 22.5$	0.6?		0		Meylan and Djorgovski 1989
3C297 (AGN)	2	$R = 21.0$	$2.4''$	1.4	G				RO		Hammer and Le Févre 1990
1104-1805 A-B (QSO)	2	$B = 16.2$ (A) $B = 18.0$ (B) $M_B = -29.7$ $M_B = -29.7$	$3''$ (A-B)	2.303			1.66?		0		Wisotzki <i>et al</i> 1993

Table 4. Radio rings (see table 2 for notation).

Source name	Number of images	Source type	Separation/ Diameter	$z_s$	Lens type	Lens brightness	$z_l$	$M_l(M_\odot)$ / Radius	Detection (O/R)	Reference
1131+0456 A-B	2+ring	radio lobe	2.1''(diam.)	1.13?	G	$R = 22$	0.85?		R/O	Hewitt <i>et al</i> 1988
1654+1346	ring	radio lobe	2.1''(diam.)	1.74	G	$r = 18.7$	0.25	3.0(11) 1.1''	R/O	Langston <i>et al</i> 1989
1830 - 211	2+ring	radio jet	1.0''			$V \simeq 23.0$			R	Rao and Subrah- manyam 1988
1549+3047	ring	radio lobe	2.0''(diam.)	$\geq 0.37$	G	$V = 16$	0.111		R/O	Lehár <i>et al</i> 1993
0218+357 A-B	2+ring	radio lobe	0.33''(diam.)	0.94?	G	$r \simeq 20.0$	0.68		R/O	Pataiak <i>et al</i> 1992b

Table 5. Giant luminous arcs and arclets.

Cluster name	Arc magnitude	$z_s$	$z_l$	Reference
Abell 370	$R = 19.4$	0.725	0.374	Soucail <i>et al</i> 1987
	$R = 22.3$	1.3?		Lynds and Petrosian 1989
Cl 2244 - 02	$R = 20.4$	2.237	0.336	Lynds and Petrosian 1989 Mellier <i>et al</i> 1991
Abell 963	$R = 23.1$	0.771	0.206	Lavery and Henry 1988
Cl 0024+1654	$R = 22.3$	1.39?	0.391	Koo 1987 Mellier <i>et al</i> 1991
Cl 0500 - 24	$R = 19.8$	0.91?	0.316	Giraud 1988
Abell 2218	$r = 21.4$	0.702	0.176	Pello-Descayre <i>et al</i> 1988
	$r = 21.7$	1.034		Pello <i>et al</i> 1992
Abell 1689				Tyson <i>et al</i> 1990
Cl 1409+52				Tyson <i>et al</i> 1990
Abell 2390	$R = 20.0$	0.913	0.231	Pello <i>et al</i> 1991
AC 114				Smail <i>et al</i> 1991
Abell 2163	$R = 21.2$	0.728	0.203	Soucail <i>et al</i> 1993
	$R = 21.8$	0.742		
Abell 1942			0.23	Smail <i>et al</i> 1991
Abell 222			0.213	Smail <i>et al</i> 1991
Abell 2397				Smail <i>et al</i> 1991
MS 2137 - 23	$R = 21.6$		0.32	Fort <i>et al</i> 1992
	$B = 23.3$			Mellier <i>et al</i> 1993
Cl 0302+1658	$R = 22.4$		0.42	Mathez <i>et al</i> 1992
	$R = 22.6$			
MS 1621.5+2640	$V = 23.9$		0.426	Luppino and Gioia 1992
MS 2053.7 - 0449	$V = 22.9$		0.583	Luppino and Gioia 1992
CL 2236 - 04	$R = 19.1$	1.116	0.56	Melnick <i>et al</i> 1993
0957+561	$R = 23.5$		0.5	Bernstein <i>et al</i> 1993
	$R = 23.7$		0.36	

**0952 - 01:** McMahon *et al* (1992) have recently reported the optical discovery of the most distant multiply imaged quasar BRI0952 - 01, with a redshift  $z = 4.5$  (see figure 24(f)). This new gravitational lens system consists of two unresolved lensed images, separated by  $0.95''$ , with a magnitude difference  $\Delta M = 1.35$ . No trace of the lens has yet been found.

### 8.1.2. The four-image configuration.

**1115+080:** By means of the pupil segmentation technique used with the Canada-Franco-Hawaii (CFH; Lelièvre *et al* 1988) telescope, high angular resolution observations of PG1115+080 ( $z = 1.72$ ) have been obtained in the past (see figure 24(g)). This so-called ‘triple quasar’, discovered serendipitously by Weymann and his collaborators in 1980, consists of four images (A, B and C); the brightest component A being a nearly merged double image (hereafter A1 and A2) whose separation is just  $0.5''$  (cf the analogy with figure 22(d) in the optical gravitational lens experiment).

Angonin-Willame *et al* (1993b) have recently measured the redshift  $z_g = 0.294(\pm 0.005)$  of the prime lensing galaxy (catalogued as G5; see Shaklan and Hege (1986) and Christian *et al* (1987)) located between the A and B images. From this, one may easily estimate that the time delays between the different pairs of four images range from some days to several months.

Following the photometric variability study reported by Vanderriest *et al* (1986), it is likely that micro-lensing effects are responsible for the brightness variations observed between the A1 and A2 images. Spectrophotometry of the whole system at various epochs should provide us with a definite answer as to the reality of these effects (cf Saust 1991). Note that in addition to the main galaxy G5, Henry and Heasley (1986) found that there was also a galaxy (G4) centred approximately between the two A components. If real, this would lend support to the micro-lensing-induced variability suspected for the A twin components.

By means of speckle interferometric observations, Foy *et al* (1985) have reported the possible detection of a fifth image (A3), located at  $0.04''$  from A2.

From all these observational results, it seems very clear that further high angular resolution imaging of PG1115+080 is mandatory in order to confirm the reported detections of the A3 and G4 components and that measurements of the velocity dispersion of the prime G5 galaxy are highly desirable to better constrain the lensing model.

**2016+112:** The MIT-Green Bank radio source MG2016+112 was the first lens system actually discovered through a systematic VLA search (Lawrence *et al* 1984; see figure 24(h)). This gravitational lens system appears to be very complex because it consists of at least three lensed images A, B and C' at a redshift  $z_s = 3.27$ , two foreground lensing galaxies C and D, with a measured redshift  $z_d = 1.01$  for the latter one, and two diffuse narrow line emission regions that appear to be physically distinct, and located near images A and B (see Schneider *et al* 1986). Observational evidence for the possible occurrence of micro-lensing effects has also been reported for this system.

Heflin *et al* (1991) have reported on first epoch  $\lambda 18$  cm VLBI observations for this gravitational lens system, indicating that the A and B images show milli-arcsec structures. These should turn out to be very useful in order to set tight constraints on the possible lens models. Garrett *et al* (1993b) have recently obtained  $\lambda 6$  cm MERLIN images of this system, with a 50 milli-arcsec angular resolution. They find that the C' component is extended (east-west) on a scale of  $\simeq 150$  milli-arcsec.

Langston *et al* (1991) have obtained K-band observations of 2016+112 from which they propose a model consisting of a single lens component (galaxy D). However, Lawrence *et al* (1993) have also obtained, under somewhat better seeing conditions, K-band images of MG2016+112 showing very clearly the presence of the two foreground lensing galaxies. From the r-K colour of galaxy C, they suggest that its redshift is probably substantially higher ( $> 2$ ) than that of D and that this may have important consequences for models of this system.

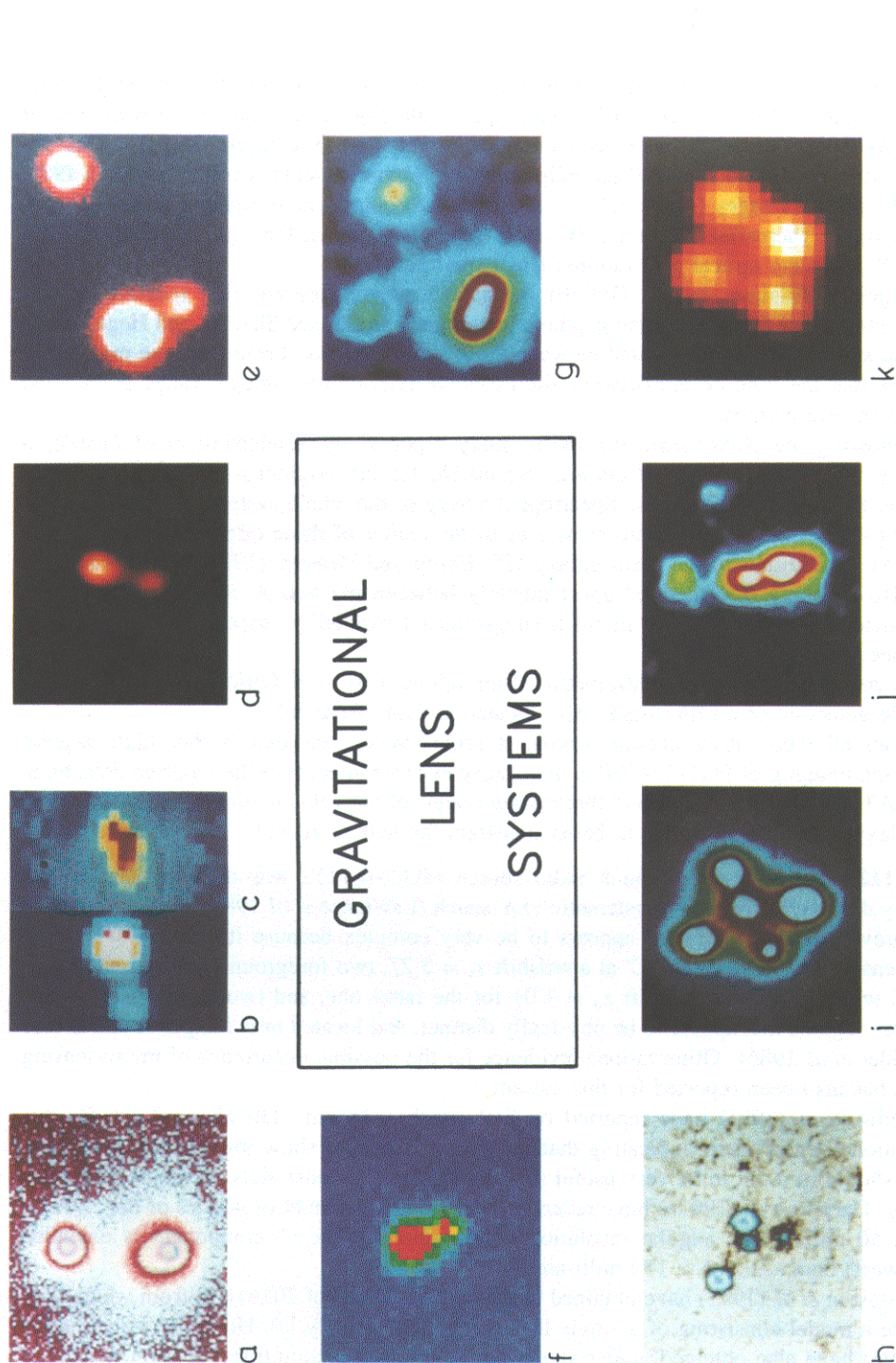


Figure 24. Some examples of known gravitational lens systems ((a)-(u); see caption in table 6).

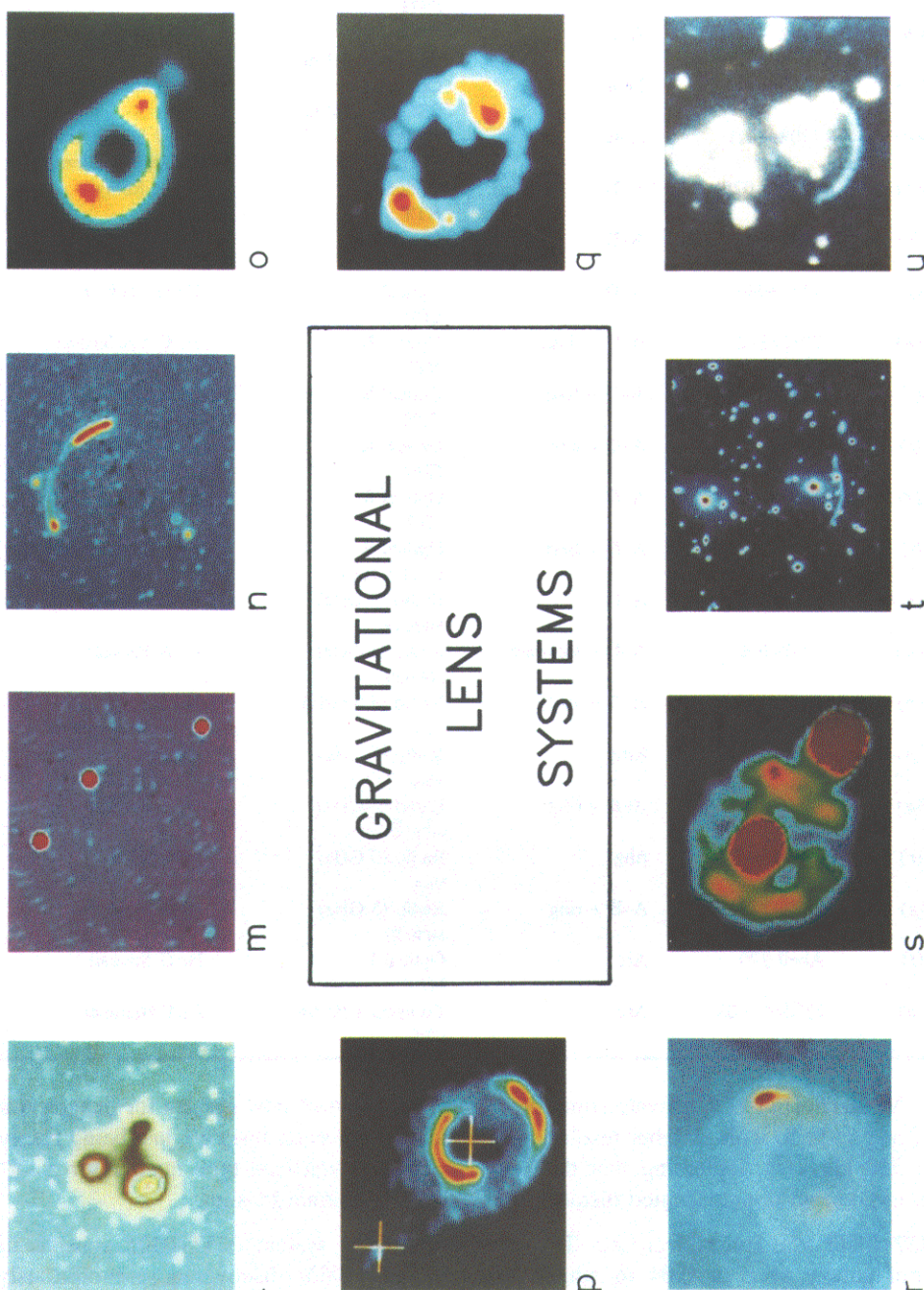


Figure 24. Continued.

Table 6. Observational information relevant to figure 24.

Figure	Source name	Image(s)	Waveband/Telescope	Courtesy of
24(a)	0957+561	A-B + lens	Optical R CFH	Dr C Vanderriest
24(b)	0142 - 100	A-B	Optical R ESO/MPI 2.2 m	Dr P Magain
24(c)	0142 - 100	Lens	Optical R ESO/MPI 2.2 m	Dr P Magain
24(d)	1208+1011	A-B	Optical R NOT	Drs J Hjorth and F. Grundahl Jensen
24(e)	1009 - 025	A-B	Optical R NTT	Dr M Remy
24(f)	0952 - 01	A-B	Optical I CFH	Dr R McMahon
24(g)	1115+080	A-D	Optical R CFH	Dr G Lelièvre
24(h)	2016+112	A-C' + lens	Optical R NTT	Dr C Vanderriest
24(i)	2237+0305	A-D + lens	Optical R CFH	Dr G Lelièvre
24(j)	3C324	A-C + lens	Optical R CFH	Dr F Hammer
24(k)	1413+117	A-D	Optical R NTT	Dr A Smette
24(l)	0414+0534	A-D + lens	Optical R CFH + NTT	Dr C Vanderriest
24(m)	1422+231	A-D	Radio (5 GHz) MERLIN	Dr A Patnaik
24(n)	1938+666	A-D + mini-arc	Radio (5 GHz) MERLIN	Dr A Patnaik
24(o)	1131+0456	A-B + ring	Radio (8.6 GHz) VLA	NRAO
24(p)	1654+1346	Ring	Radio (5 GHz) VLA	NRAO
24(q)	1830 - 211	A-B + ring	Radio (5 GHz) MERLIN	Dr A Patnaik
24(r)	1549+3047	ring	Radio (5 GHz) VLA	Dr J Lehár
24(s)	0218+357	A-B + ring	Radio (5 GHz) MERLIN	Dr A Patnaik
24(t)	Abell 370	Arc	Optical I NTT	Dr G Soucail
24(u)	Cl2244 - 02	Arc	Composite B/V/R CFH	Dr F Hammer

Vanderriest (1992a, private communication) has obtained new spectra for images A and B (mag  $\simeq 22.5$ ) with a higher resolution in which the emission lines are just being resolved ( $\simeq 300 \text{ km s}^{-1}$ ), indicating that they correspond to a starburst-type nucleus or a LINER observed at an unprecedented distance thanks to gravitational lensing.

**2237+0305** (the Einstein cross): The gravitational lens system 2237+0305 consists of a spiral galaxy at  $z \simeq 0.04$  in which Huchra *et al* (1985) discovered serendipitously a high redshift ( $z = 1.69$ ) quasar coincident with the galaxy nucleus. The denomination 'Einstein cross' comes from the fact that high angular resolution imagery (Yee 1988, Schneider *et al* 1988) and spectroscopy (De Robertis and Yee 1988, Adam *et al* 1989) have convincingly demonstrated that Q2237+0305 consists of four lensed quasar images

with angular separations between  $1.4''$  and  $1.8''$ , in addition to the central galaxy nucleus (see figure 24(i)). The mass of the deflector inside the four lensed images has been estimated to about  $2 \times 10^{10} h_{50}^{-1} M_\odot$  and the total quasar image amplification to  $\simeq 18.5$  (Rix *et al* 1992).

This system is unique for displaying micro-lensing effects (Kayser and Refsdal 1989). Indeed, because the expected time delays are so short (at most a few days), intrinsic variability should show up almost simultaneously in the four images so that any brightness variation affecting just some of the four single images may be attributed to micro-lensing. Also, due to the large distance ratio between the source and the lens, micro-lensing should lead to more frequent and rapid high amplification events (HAEs, see section 9.4.2) and the expected number of HAEs should be large (about 0.3 events per year and per image). It was therefore not a surprise when Irwin *et al* (1989, see also Corrigan *et al* 1991) announced the first detection of a micro-lensing event for the A component during the summer 1988. Analysis of CCD frames obtained at ESO (La Silla) by Remy *et al* (1994) in the framework of the ESO key-programme ‘Gravitational Lensing’ and with the Nordic Optical Telescope reveals that at least three (A, C, D) of the four lensed components of the ‘Einstein cross’ display appreciable light variations (see the preliminary light curves of the A, C and D images normalized to that of B in Surdej *et al* (1992)). In particular, the visual brightness ratio  $A/B$  has recently been observed to vary from about 1.3 to 0.8 in less than one year. During this event, Racine (1992) has reported a significant variation in the continuum of image B relative to the flux in the [CIII] emission-line. Re-analysing the HAE of image A that took place between 1988 and 1989, Racine finds that, under the assumption of a transverse velocity for the micro-lens of  $600 \text{ km s}^{-1}$ , the continuum region of the quasar must be  $\leq 10^{15} \text{ cm}$  in radius and that the broad-line region responsible for the observed [CIII] emission line is probably at least ten times larger. Theoretical analysis of these data favours relatively small masses for the micro-lenses; it is, however, not necessary to invoke masses below  $0.1 M_\odot$  (Wambsganss *et al* 1990b), although masses as small as  $10^{-5} M_\odot$  cannot be excluded at the moment (Refsdal and Stabell 1993). Let us still mention that a small difference in the Mg II emission line profile between images A and B, possibly caused by micro-lensing, has been reported by Filippenko (1989).

Nadeau *et al* (1991) have obtained infrared and additional visible photometry of the Einstein cross, allowing them to characterize the extinction in the deflector.

Simulations of micro-lensing effects for 2237+0305 by Wambsganss *et al* (1990a) predict that the shape of HAE light curves should not only depend on the source size and the relative transverse velocity between the source, the lens and the observer but that, due to the very strong effect of the shear by the galaxy, it should also depend on the direction of this velocity. Theoretical work related to the interpretation of the high amplification micro-lensing event reported by Irwin *et al* (1989) has been published by Wambsganss *et al* (1990b), Wambsganss and Paczyński (1991), Witt *et al* (1993) and by Rauch and Blandford (1991). The latter authors examine the constraints that one may place on the quasar source (accretion disk around a black hole, etc) assuming that the relative motions of the source with respect to the caustics network are caused, not by the proper motion of the micro-lens, but by that associated with different moving source regions (cf large Keplerian orbital velocities). Wambsganss (1992) also discusses the expected colour variations in some of the micro-lensed images of 2237+0305 as a tool for the determination of the quasar size.

Crane *et al* (1991) have reported images of the gravitational lens system 2237+0305 obtained with the HST faint object camera. They did not find evidence for a fifth component down to  $1/20$ – $1/30$ th the brightness of image B. Racine (1991) has obtained CCD frames in the R and I bands with the direct camera HRCam at the CFH telescope in  $0.4''$  (FWHM) seeing with very high signal-to-noise ratio ( $\geq 500$ ) and he claims to have detected a fifth image,

4.5 mag fainter than component A, at  $0.07'' \pm 0.035''$  SSE from the lensing galaxy centre. Confirmation of his finding as well as obtaining a spectrum of this putative component would be of great interest. Yee and De Robertis (1991) have reported the possible detection of a compact star-forming region between the A and B images that is possibly associated with either the host galaxy or a companion galaxy at  $z \simeq 1.7$ . We refer to De Robertis and Yee (1992) for a more detailed account of these observations.

Finally, Foltz *et al* (1992) have recently measured the projected central velocity dispersion ( $\sigma_p \simeq 215 \pm 30 \text{ km s}^{-1}$ ) of the galaxy nucleus. Although these authors find some good agreement between their measurements and the predictions of published lensing models, they point out that the velocity dispersion of the galaxy bulge could be affected by some degree of anisotropy.

**3C324:** With this object, Le Fèvre *et al* (1987) have reported the first example of gravitational multiple imaging of a giant radiogalaxy at a redshift  $z = 1.206$  by a foreground (spiral?) galaxy at  $z = 0.84$ . The optical source 3C324 is composed of at least three lensed images within an area having an angular extent less than  $3''$  (see figure 24(j)). Such gravitational lens systems should be monitored photometrically for the possible detection of a supernova event in the different images. This could lead to a very original determination of the Hubble parameter  $H_0$  (cf subsection 9.1).

**1413+117** (the Clover Leaf): H1413+117 is the second example of a multiply imaged QSO ( $z = 2.55$ ) that has been identified at ESO, within a systematic search for lenses among HLQs (Magain *et al* 1988, cf figure 24(k)). This quadruply imaged quasar has also been resolved at  $\lambda 3.6 \text{ cm}$  with the VLA in the A configuration. A detailed modelling of these observations has been made by Kayser *et al* (1990) and nicely supports the optical observations. The estimated time delays between image pairs range from a few days to less than a month. High angular resolution ( $\text{FWHM} = 0.6''$ ) integral field spectroscopy of this system obtained with the bidimensional spectrograph SILFID at the CFH telescope has enabled the spectra of the four individual images to be resolved. The spectra, which show characteristic broad absorption line and emission line profiles, turn out to be very similar, except for narrow absorption line systems at  $z_a = 1.44$  and  $z_a = 1.66$  (probably related to the lens(es)) seen in images A and B and also for small but significant differences in the spectrum of image D which are probably caused by micro-lensing effects (Angonin *et al* 1990).

On the basis of direct CCD images obtained with the ESO/MPI 2.2-m telescope, Altieri and Giraud (1991) have described new interesting data obtained on 17 February 1991 for the 'Clover Leaf'. Their CCD frames reveal a dramatic increase in the relative brightness of B when compared with observations taken earlier. These authors state that the luminosity of B is about 1.5 that of A, whereas it was 0.85 that of A in March 1988. As also suspected independently by Lindblad (1991, private communication), doubt may be cast on this interpretation. Indeed, analysis of the figure published by Altieri and Giraud seems to indicate that there may have been an inversion in their component labels (i.e. A with C and B with D, respectively). If this is the case, it would mean that it is the D component that has been subject to micro-lensing effects, as already suspected earlier (Angonin *et al* 1990, Kayser *et al* 1990). Preliminary photometric lightcurves of H1413+117 A-D have been recently reported by Arnould *et al* (1993).

**0414+0534:** In their presentation of preliminary results of the VLA gravitational lens survey, Hewitt *et al* (1989) have reported the detection of a new lens candidate for the radio source MG0414+0534 (see figure 24(l)). It consists of four radio components with angular separations between  $0.4''$  and  $2''$ , showing rather similar flux ratios at  $\lambda 2$  and  $6 \text{ cm}$  (see also Katz and Hewitt (1993) for a presentation of more recent VLA data). Furthermore,

Hewitt *et al* (1992) have obtained direct multi-colour CCD frames, showing very clearly that the optical morphology of this faint object is reminiscent of that seen at radio wavelengths. These authors have also obtained a spectrum of the whole object indicating that its light is unusually red, with no trace of emission lines and being very distinct from any conventional spectrum of known active galactic nuclei (AGN). Furthermore, the four components of this system have been detected with VLBI to show compact flux at  $\lambda$  18 cm (Hewitt 1989, private communication). Garrett *et al* (1993b) have recently obtained very interesting  $\lambda$  6 cm MERLIN images of this system with a 50 milli-arcsec angular resolution. They find that MG0414+0534 exhibits extended emission in the A and B images which appears to form an unusual 'S-shape' structure.

Recent optical studies of this system by Schechter and Moore (1993) and by Angonin-Willame *et al* (1993a) have led to the identification of a fifth image (very probably resolved) on I and R band CCD frames, lying very near to the centre of the four compact images, within 0.1" of the predicted position of the lensing galaxy (Kochanek 1991b). Schechter and Moore also report the possible detection of a sixth image and they mention the fact that Elston and Lawrence (see their private communication in Blandford and Narayan (1992)) have obtained an IR spectrum indicating that the source redshift is possibly  $z = 2.63$ . It would be very important to confirm this proposed redshift as well as measuring that of the lens. Annis and Lupino (1993) have obtained K-band imaging for this system and they conclude in their study that MG0414+0534 merely represents a member of the expected population of distant radio galaxies.

This gravitational lens system, observable at both radio and optical wavelengths, may also turn out to be useful in the context of an independent determination of  $H_0$  from the measurement of time delays (see section 9.1).

**1422+231:** Patnaik *et al* (1992a) have discovered B1422+231 to be a new gravitationally lensed source at a redshift  $z = 3.62$ . They first identified this object as a multiply imaged radio source, consisting of three (and very probably four) unresolved components whose measured spectral index between 8.4 and 5 GHz, fractional polarization and direction of the polarization position angle are identical, within the measurement errors (see figure 24(m)). The largest angular separation between the lensed images amounts to 1.3". Therefore, they were only able to obtain an optical spectrum covering the whole system. It turns out to be that of a very bright quasar ( $R = 16.5$ ) showing a prominent emission line component due to Ly $\alpha$ +NV. Direct infrared (K band at 2.2  $\mu\text{m}$ ) and optical (V, R and I) imaging of this system by Lawrence *et al* (1992) and by Remy *et al* (1993), respectively, fully corroborates the above interpretation: four unresolved images were detected. These coincide with the radio ones and they are characterized by similar brightness ratios. Individual optical spectra of these components are needed to better understand the physical model of this interesting and very bright gravitational lens system.

**1938+666:** By means of  $\lambda$  6 cm MERLIN radio observations, the source B1938+666 has been imaged by Patnaik *et al* (1993) with an equivalent 35 milli-arcsec angular resolution and found to be a very fascinating gravitational lens system (see figure 24(n)). It consists of four compact components having a similar radio flat spectrum, a jet-like feature connecting one of the compact sources and a well developed but unresolved arc-like structure, reminiscent of the giant optical arcs seen around rich galaxy clusters (see subsection 8.4). The entire structure lies within a diameter of 0.95 arcsec. The source is associated with a faint object ( $r = 23$  mag) of unknown redshift.

### 8.2. Additional proposed cases of multiply imaged sources

**2345+007:** This system constitutes the most controversial gravitational lens candidate. It

was identified by Weedman *et al* (1982) as a pair of QSO images (A and B), separated by  $7.3''$  at a redshift  $z \simeq 2.15$ . The fact that all the arguments used in the past (e.g. the suspected double image structure for component B (Nieto *et al* 1988), the peculiar redshift distribution for the narrow Ly $\alpha$  absorption lines (Foltz *et al* 1984, Duncan 1991)) to support or to dismiss the gravitational lens hypothesis for 2345+007 (cf the unexpected orientation derived for the double image B (Weir and Djorgovski 1991a, b), the absence of photometric light variations between images A and B and also their slightly different emission line characteristics (Steidel and Sargent 1990)) have turned out to be wrong is very surprising. To summarize, let us mention the following: the emission-line redshift difference ( $15 \pm 20 \text{ km s}^{-1}$ ) between the spectra of 2345+007 A and B is found to be non-significant and because of the similarity between the emission line profiles observed in the spectrum of 2345+007 A and B, Steidel and Sargent (1991) conclude that this system is indeed a gravitational lens; contrary to past claims (Nieto *et al* 1988, Weir and Djorgovski 1991a, b), there does not seem to be any evidence for image B to be multiple or elongated (Shaya 1991, private communication), although it could be somewhat redder than image A. Furthermore, flux variations have been reported between the two components of this system (Sol *et al* 1984, Weir and Djorgovski 1991a, b). Heavy absorption line systems have been identified at  $z = 1.491$  (Steidel and Sargent 1990) and possibly at  $z = 0.7545$  (Steidel and Sargent 1991). Because of the important astrophysical consequences implied by the exact nature of this complex system (size of the Ly $\alpha$  forest clouds in the range 5–25 or 100 kpc; type of dark matter for the lens, etc), more observations should be obtained in the near future (spectrophotometric monitoring, high-resolution direct imaging of component B and search for arclets and/or for the lens in the K band, Ly $\alpha$  forest studies of other known gravitational lens systems (cf UM673) or binary quasars (1429-008?), etc). This would help in finally closing the longstanding debate of whether 2345+007 A and B consist of a physical pair of quasars or are the gravitationally lensed images of a distant QSO.

**1634+267:** The pair of QSOs 1634+267 A and B, separated by  $3.8''$  and identified in a slitless spectroscopic quasar survey by Sramek and Weedman (1978), was first proposed to be a gravitational lens system by Djorgovski and Spinrad (1984). Their conclusion was based upon the analysis of better quality spectra from which they could derive a similar redshift ( $z \simeq 1.96$ ) for the two images. Furthermore, the detailed spectroscopic study of 1634+267 A and B by Turner *et al* (1988) has reinforced the conviction that this double quasar constitutes a good case of gravitational lensing. Indeed, not only were they able to show that, after a proper scaling and to within measurement errors, the wavelengths, strengths, widths and profiles of different emission lines were the same in the two image spectra, they also found that the excess of red light in the bright component resembles the continuum emission of a  $z \simeq 0.57$  galaxy. Independently, the modelling of this system by Narasimha and Chitre (1989) also led to the prediction that a lensing galaxy should be located at  $0.75''$  from component A. However, neither the galaxy predicted at  $z = 0.57$  (Turner *et al* 1988) near image A nor the expected multiplicity of this latter component ( $0.75''$ , Narasimha and Chitre 1989) have been seen on direct images obtained recently with HST (Turner 1992, private communication).

Nevertheless, the similarity observed between the detailed emission line profiles and between the continuum shapes in the spectra of 1634+267 A and B has also led Steidel and Sargent (1991) to conclude that this system is caused by a gravitational lens. Note that as for the case of 2345+007 A and B (see earlier), these authors assign the slight differences in velocity between some of the observed emission lines to temporal changes in the structure of the QSO broad emission line region.

Vanderriest (1992b, private communication) has reported variations for the brightness ratio  $A/B = 3.7 \pm 0.1$  as measured in 1985, compared with the value 2.83 derived by Turner *et al* (1988).

**1429-008:** This is a pair of QSOs (redshift 2.08) separated by  $5.1''$  and having a brightness difference of  $\simeq 3.1$  mag (Hewett *et al* 1989). Because of the slight, although significant, differences in the spectra of the two components, higher signal-to-noise spectra remain mandatory in order to confirm or reject the lensing hypothesis for this system.

**1120+019 = UM425:** To our knowledge, little work has been done recently, i.e. since the discovery paper by Meylan and Djorgovski (1989) on this pair of quasi stellar images ( $z = 1.46$ ) separated by 6.5 arcsec, and whose brightness differs by  $\Delta m = 4.7$  mag. Except for images A and B, no spectra have been obtained for the many other objects in the field; the redshift of the lens remains uncertain ( $z \simeq 0.6?$ ). Let us note that it is very unlikely to observe a mirage with two such unequally bright images (but see Kassiola and Kovner 1992).

For completeness, several additional cases of multiply imaged distant sources (0023+171, 3C194, 3C297) that have been proposed in the past are also listed in table 3. New observations of these systems are mandatory in order to assess their real physical nature.

### 8.3. Radio rings

This new class of lensing phenomena, first discovered with the VLA, occurs when some part of the extended radio source covers most of the diamond-shaped caustic associated with the lensing object (see figure 22(i)). The resulting lensed image then consists of a slightly elliptical ring of radio emission (see figure 22(j)).

**1131+0456:** Maps of the radio source MG1131+0456 in Leo have revealed such an elliptical ring of emission with two compact sources lying on opposite sides of the ring (angular separation  $\simeq 2\alpha_0 \simeq 2.1''$ , see figure 24(o)). It was found by Hewitt and her collaborators in 1988. A very sophisticated modelling of this lensed radio source has been reported by Kochanek *et al* (1989). Their numerical inversion of the observed mirage leads to a normal galaxy-like elliptical potential for the lens and an ordinary double-lobed structure for the background radio source. In this model, the two compact images correspond to the lensing of the central core of the source while the ring is associated with a radio jet which covers most of the diamond-shaped caustic in the source plane.

Hammer *et al* (1991) have obtained deep optical CCD frames for this object with the ESO-NTT telescope. They have detected a red excess emission at the exact location of the radio Einstein ring. Subtraction of the lensing object, assumed to be a massive elliptical galaxy, results in the detection of an optical ring that is very similar to the radio ring. They have also obtained a spectrum of the whole optical source and derived tentative redshifts for the background source ( $z = 1.13$ ) and the lens ( $z = 0.85$ ). Annis (1992) has described the unusual K-band characteristics of this gravitational lens system. He also suggests that the infrared image of this object is reminiscent of the structure seen at radio wavelengths. Annis proposes that a likely candidate for the source object could be a very red radio galaxy, in agreement with the optical observations of Hammer *et al* (1991).

Chen and Hewitt (1993) have obtained new multi-frequency VLA maps of MG1131+0456. Their 8 GHz image reveals one additional unresolved image near the centre of the ring. It is likely that this new image represents radio emission from the lensing galaxy. However, it could also be due to an additional lensed image of the source.

**1654+1346:** A second ring was found in Hercules by Langston *et al* in 1989. A deep red optical CCD frame of MG1654+1346 shows only an elliptical galaxy ( $z = 0.25$ ) and a quasar ( $z = 1.74$ ) located  $2.5''$  away (see the two crosses in figure 24(*p*)). However, VLA radio maps at  $\lambda 3.6$  cm reveal that the foreground galaxy lenses one of the quasar's radio lobes into a ring having an angular diameter of  $2.1''$  (see the ring in figure 24(*p*)). From the angular size of the radio ring, it is easy to show (cf equation (6.6)) that the mass of the deflecting galaxy (projected inside the ring) is about  $3 \times 10^{11} h_{50}^{-1} M_\odot$ .

**1830-211:** Following the suggestion by Rao and Subrahmanyan (1988), the very bright radio source PKS1830-211 has been confirmed to be a doubly lensed flat-spectrum radio core surrounded by a partial, elliptical, Einstein ring whose diameter is roughly  $1''$  (Subrahmanyan *et al* 1990, Jauncey *et al* 1991; see figure 24(*q*)). Radio VLBI observations of this system at 2.3 GHz reveal that the two compact images remain unresolved at  $\simeq 20$  milli-arcsec angular scales (Jauncey *et al* 1992). As far as optical observations are concerned, the location of the source close to the galactic plane ( $l = 12.2$ ,  $b = -5.7$ ) makes optical imaging or spectroscopy (i.e. source and lens redshift measurements) very difficult. Even searches for an optical or IR counterpart of the radio object have been unsuccessful (Djorgovski *et al* 1992). Deep direct CCD imaging (I band) only reveals a  $\simeq 20\text{--}22$  mag object ( $m_V \simeq 23$ ). Subrahmanyan *et al* (1992) have observed the HI emission and absorption spectra due to galactic neutral hydrogen towards this source and conclude that it is indeed located at extragalactic distance. The high angular resolution radio maps described in these papers as well as theoretical modelling of this source convincingly show that the observed double flat-spectrum compact images surrounded by a fainter but steeper radio spectrum Einstein ring may be naturally accounted for by the gravitational lensing due to a foreground galaxy of a flat-spectrum radio source having a core-jet-knot structure (see Nair *et al* (1993) and Kochanek and Narayan (1992)). This radio source figures among the six brightest known flat-spectrum radio sources in the sky and, given the very low geometrical probability for lensing a randomly located radio source, the chance of observing such a system turns out to be extremely small (Jauncey *et al* 1991). Amplification bias effects certainly play here also a very important role in order to account for the discovery of this system (cf subsection 7.2).

**1549+3047:** Lehár *et al* (1993) have reported the discovery of a new radio Einstein ring for the source MG1549+3047 within their VLA search for gravitational lenses (see figure 24(*r*)). Their original 4-min VLA map showed a lobed radio source with a core and two lobes. One of these lobes has been resolved as an Einstein ring, somewhat elliptical in shape. Comparison of these observations with an optical finder chart immediately revealed that a bright, 16th magnitude galaxy, that is probably elliptical, is superposed over the brighter radio lobe. The angular diameter of this ring is approximately  $2''$ , which is comparable with the diameters of the three previous Einstein rings. The bright galaxy appears in the CfA Redshift survey with  $z = 0.111$ . Although the source redshift has not yet been measured, Lehár and his collaborators have derived a lower limit of 8 for the value of the mass-to-light ratio of that part of the galaxy which falls within the observed Einstein radio ring. This lower limit is found to be entirely reasonable with typical mass-to-light ratios of about 20 that have been derived for elliptical galaxies. There is thus no need to invoke dark matter in the inner parts of this lensing galaxy to reconcile its observed luminosity with the measured angular diameter of the Einstein ring.

**0218+357:** On the basis of multi-wavelength radio observations obtained with the VLA and MERLIN interferometers and with the Very Long Baseline Interferometry (VLBI) European Network, Patnaik *et al* (1992b,c) have reported the discovery of a new gravitationally lensed system, B0218+357, which consists of two bright flat-spectrum radio components

separated by 335 milli-arcsec, one of which is located near the centre of an Einstein ring (see figure 24(s)). The diameter of this ring is comparable with the separation between the bright components but it is characterized by a much steeper radio spectrum. This is so far the smallest Einstein ring that has been detected. Because the two bright radio components show variability, Patnaik *et al* (1992b,c) point out that this system constitutes a promising candidate in order to attempt an independent determination of the Hubble parameter  $H_0$ .

Browne *et al* (1993) have recently obtained a spectrum of this gravitational lens system ( $r \simeq 20$ ) with the William Herschel telescope. They report a redshift of 0.6847 for the lensing galaxy (late type spiral?) and a possible redshift  $z = 0.94$  for the source (see also the spectroscopic investigation of this system by O'Dea *et al* (1992)).

#### 8.4. Giant luminous arcs and arclets

We shall now describe a final class of lensing phenomena consisting of the fascinating optical giant luminous arcs and arclets. The most spectacular cases of giant arcs occur (see figure 22(h)) when some part of an extended source (e.g. a distant galaxy) covers one of the cusps of the diamond-shaped caustic associated with a cluster of galaxies as deflector (see figure 22(g)). Various other types of arc are also observed corresponding to the cases when the distant source covers different parts of the caustic. By definition, arclets are elongated images having an axis ratio larger than about 3:1, usually distributed perpendicularly to their radius vector pointing towards the centre of the deflecting mass distribution. They are usually the result of weak gravitational lensing caused by an asymmetric distribution of matter around the image position, giving rise to a shear term.

The first giant luminous arcs (angular extent  $\simeq 20''$ , angular width  $\leq 0.5''$ ) were discovered serendipitously in 1981 by Hoag, and quite independently in 1986 by Soucail and Fort and by Lynds and Petrosian plus their collaborators, to lie in the centres of rich clusters of galaxies (mass  $\simeq 10^{14} M_\odot$ ). As suggested by Paczyński (1987), the measurement of several arc redshifts has confirmed that they result from the gravitational lens distortions of distant background galaxies by rich foreground clusters acting as lenses (cf figures 24(t)–(u)). Up to now, about 20 giant arcs, whose surface brightness is only about one-tenth of the sky brightness, have been identified in rich clusters; half of them have a measured redshift which, in all cases, is larger than that of the cluster. Two well known examples of giant luminous arcs are presented below.

**Abell 370:** The A370 arc (see figure 24(t)) has been found to be the gravitationally lensed image(s) of a background source at a redshift  $z_s = 0.72$  (Soucail *et al* 1987, Lynds and Petrosian 1986, 1989). This source is most probably a nearly edge-on spiral galaxy, lensed by a rich foreground cluster at  $z_l = 0.37$ .

**Cl2244 – 02:** The core of the cluster Cl2244-02 seems to be dominated by galaxies that belong to two clumps. The detected arc (full angular extent  $\simeq 110^\circ$ , see figure 24(u)) consists of the gravitationally lensed image(s) of a background source (Lynds and Petrosian 1986, 1989), which is probably a star-forming galaxy at a redshift  $z = 2.238$ . This is one of the most distant regular galaxies that has been observed and it clearly shows how gravitational lenses may be used as cosmic telescopes to detect very faint and distant galaxies.

We discuss in subsection 9.3 how the fitting of giant luminous arcs and of the more numerous faint arclets has led to a new way of determining the mass distribution in the lensing clusters.

A non-exhaustive list of arcs and arclets that have been reported in the literature is given in table 5. Review papers on the astrophysical use of giant luminous arcs and arclets have

been recently published by Blandford and Narayan (1992), Fort (1992), Tyson (1992) and Soucail and Mellier (1993).

## 9. Cosmological and astrophysical applications

### 9.1. Determination of the Hubble parameter $H_0$

We shall now address one of the most interesting cosmological applications of gravitational lensing: the determination of the Hubble parameter  $H_0$  via the measurement of the time delay  $\Delta t$  between the observed light curves of multiply imaged QSOs. We discuss hereafter the wavefront method for the case of an axially symmetric lens (Refsdal 1964a, b, Chang and Refsdal 1976). An alternative way of calculating  $\Delta t$  was suggested by Cooke and Kantowski (1975); they showed that the time delay could be split into two parts: a geometrical time delay and a potential time delay. The equivalence of the two methods has been demonstrated by Borgeest (1983). A third independent method based on Fermat's principle has been developed by Schneider (1985, see also Blandford and Narayan 1986). The principle of the wavefront method for determining  $H_0$  can easily be understood by looking at figure 25 which shows wavefronts in a typical gravitational lens system. Close to the point source the wavefronts are spherical, however as they approach the deflector they are deformed because of curvature effects and time retardation and can, in many cases, self-intersect before reaching the observer. This self-intersection is connected with the formation of multiple images since each passage of the wavefront at the observer corresponds to an image in the direction perpendicular to the wavefront. Since all points located on a wavefront have identical propagation times, it is clear that the distance between the sections of the wavefront at the observer immediately gives the time delay between the corresponding images.

The main point is now that if the mass distribution of the lens and the redshifts of the source ( $z_s$ ) and of the lens ( $z_d$ ) are known, we may determine the distance ratio so that we can construct a wavefront diagram as indicated in figure 25. Only a scaling factor which determines the absolute distances in the system is unknown. It is thus obvious that a determination of the time delay, and thereby the distance between the wavefronts at the observer determines the scaling factor and all the distances in the system, for instance also the values of  $D_{od}$  and  $D_{os}$ . For small redshift values, these distances are given by the Hubble law

$$D_{od} = cz_d H_0^{-1} \quad D_{os} = cz_s H_0^{-1} \quad (9.1)$$

so that  $H_0$  can be determined. For large redshifts, Hubble's law must be modified; this requires a significant correction factor in equation (9.1) that depends on the cosmological model. However, because the calculation of  $\Delta t$  presented hereafter involves a distance ratio (cf equation (9.3)), the final correction factor which should be included in expression (9.7) for  $H_0$  is usually found to be less than 10–20% (see Refsdal 1966a, Kayser and Refsdal 1983).

We present now a simple application of the wavefront method for the case of an axially symmetric lens. The wavefronts from a distant, doubly imaged quasar are shown in figure 26 (we assume that the third image (C) is too faint to be seen). Since the wavefronts cross each other at the symmetry point E, they must represent the same light propagation time and for an observer O located at a distance  $x$  from the symmetry axis, the time delay must be equal to the distance between the wavefronts at the observer divided by the velocity of light ( $c$ ). Noting that  $\theta_{AB}$  is very small, we thus obtain from simple triangle geometry

$$\Delta t = t_B - t_A \simeq \theta_{AB} x c^{-1} \quad (9.2)$$

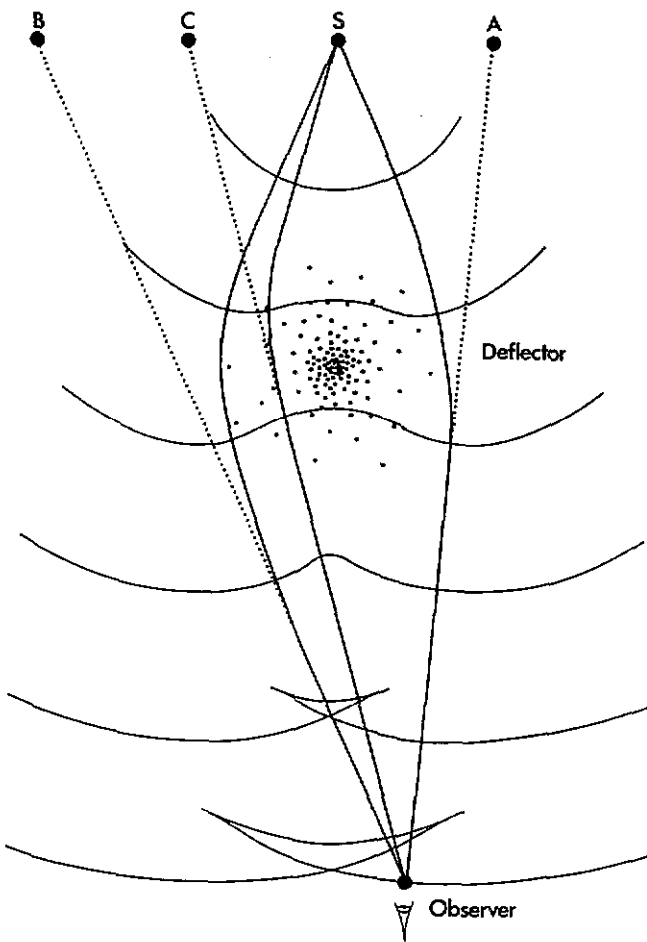


Figure 25. Deformation of a wavefront originating from a point source ( $S$ ) as it passes the deflector.

where  $t_A$  and  $t_B$  denote the propagation times along the two trajectories. Furthermore, we easily find that

$$\theta_S = x D_{\text{ds}} / (D_{\text{od}} D_{\text{os}}). \quad (9.3)$$

Assuming a deflection law of the type

$$\hat{\alpha} \propto |\xi|^{(\epsilon-1)} \quad (9.4)$$

for  $\xi_A \geq |\xi| \geq |\xi_B|$ , we find a simple relation between  $\theta_A$ ,  $\theta_B$  and  $\theta_S$

$$\theta_S = (\theta_A + \theta_B)(2 - \epsilon)/2, \quad (9.5)$$

where we note that  $\xi_B$  and  $\theta_B$  are chosen negative. It is very simple to derive equation (9.5) for the case  $\epsilon = 1$  (SIS lens, see equation (6.15)), and it is also accurate for  $\epsilon = 0$  (point mass lens, see equation (6.9)) and  $\epsilon \rightarrow 2$ . For intermediate values of  $\epsilon$  this equation is not exact; it is, however, accurate enough for the purpose of our discussion. On the basis of these

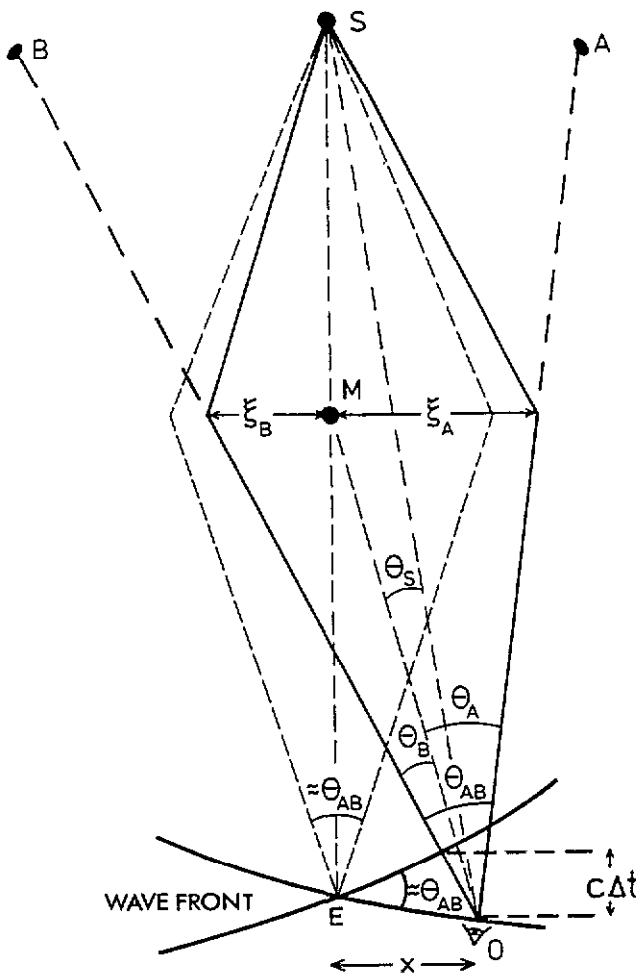


**Figure 26.** The wavefront method is here applied to the case of two selected light rays for the determination of the time delay (cf images A and B in the previous figure).

equations and with the help of the Hubble relation, we can easily derive an expression for  $H_0$  or, equivalently, for the Hubble age  $\tau_0$  of our universe in terms of observable quantities

$$\tau_0 = H_0^{-1} = \frac{2(z_s - z_d)\Delta t}{z_d z_s \theta_{AB}(\theta_A + \theta_B)(2 - \epsilon)} \quad (9.6)$$

which we see can be expressed as a dimensionless number that, with the exception of  $\epsilon$ , only depends on observable dimensionless quantities times  $\Delta t$ . For the case of the double quasar 0957+561 A and B (see section 8), we know the redshifts  $z_d = 0.36$  and  $z_s = 1.41$ , as well as the observed positions  $\theta_A = 5.1''$  and  $\theta_B = -1.04''$ , from which we derive

$$H_0 = 140(2 - \epsilon) \left( \frac{1 \text{ y}}{\Delta t} \right) \text{ km s}^{-1} \text{ Mpc}^{-1}. \quad (9.7)$$

The present best estimate of  $\Delta t$ , based on optical data collected over more than 10 y, is 1.14 y (Vanderriest *et al.* 1992, Kayser 1993, Schild and Thompson 1993); a value close

to 1.45 y can, however, not yet be totally excluded (Press *et al* 1992a, b). As more data accumulate, one may be confident that an accurate value of  $\Delta t$  will be obtained. The main difficulty is then obviously to determine the value of  $\epsilon$ . In particular, for the double quasar, this is very difficult since, in addition to the central galaxy, the surrounding cluster also acts as a lens, thus rendering the value of  $\epsilon$  very uncertain. As Rhee (1991) succeeded in determining independently the galaxy mass from the measurement of its radial velocity dispersion, the relative importance of the galaxy and cluster to the lensing could be estimated more accurately. Values of the Hubble parameter in the range  $30\text{--}80 \text{ km s}^{-1} \text{ Mpc}^{-1}$  then seemed possible, in reasonable agreement with results obtained from classical methods. Those values were derived by means of more sophisticated modelling, including a non-symmetric lens and all relevant observational data such as the brightness ratio of the two lensed images as well as radio data (Falco *et al* 1991a).

Very recently, Bernstein *et al* (1993) have reported the detection of luminous arcs surrounding 0957+561, making it possible to better constrain the mass parameters of the lensing cluster. This has very interesting consequences: it does not seem possible any longer to model this gravitational lens system with just a single lens plane. If one tries to do that, the value of the Hubble parameter is rather small ( $H_0 \leq 32 \text{ km s}^{-1} \text{ Mpc}^{-1}$ ). On the basis of recent redshift measurements, a second cluster at  $z_d \simeq 0.5$  has been identified and this could possibly correspond to a second deflector located at a distinct redshift. The modelling of such a system with two lens planes may lead to a more realistic value of  $H_0 (> 40 \text{ km s}^{-1} \text{ Mpc}^{-1})$ . The uncertainties are, however, still large and there probably exist other cleaner gravitational lens systems (for instance 0142 – 100, 0218+357, 1104 – 1805, 1115+080) which might lead, in the near future, to a more accurate determination of  $H_0$ .

### *9.2. Determination of the mass of the lensing galaxy from a multiply imaged quasar*

Since the observed separation ( $\simeq 2\alpha_0$ ) between multiply lensed images scales as  $MH_0$  (see section 6.1.1) and making use of the simple relation between the time delay  $\Delta t$  and  $H_0$  (see equation (9.7)), one may determine the mass  $M$  of the galaxy deflector, located within an angular radius  $\theta_{AB}/2$ , from the direct measurement of the time delay  $\Delta t$ , irrespective of the Hubble constant. A more detailed examination shows that this mass determination is also independent of the presence of the cluster and of the cosmological model (Borgeest 1986). For the case of 0957+561, Borgeest has derived the lens mass to be  $M = (0.8 \pm 0.1)10^{12}(\Delta t/1 \text{ y})M_\odot$ .

### *9.3. Determination of the mass of the lensing cluster from arcs and arclets*

The arcs and arclets described in section 8.4 offer exciting possibilities for determining the mass and the mass distribution of the lensing cluster. A rough and very simple analysis can be made for systems with a single arc. Indeed, such an arc can be considered as part of an Einstein ring so that the mass inside the ring can be estimated from equation (6.6). Typically, the angular radius of an arc is  $\simeq 20''$ , corresponding to about  $10^{14}M_\odot$ . This results in the determination of a mass to luminosity ratio of about 100, supporting the claim that dark matter is the principal constituent ( $\geq 90\%$ ) of galaxy clusters.

One may wonder why luminous arcs are not seen in pairs as one would expect by the breaking up of an Einstein ring. The reason is that only a slight deviation from axial symmetry usually transforms the second arc into a ‘normal’ image which may be difficult to detect, compare figure 22(h).

Additional information on the distribution of dark matter may be obtained from the large number of arclets seen behind a galaxy cluster. These arclets are very faint blue galaxies

which are distorted due to the shear term caused by the cluster. By means of very deep CCD imaging, Tyson (1988) has found that there is some 300 000 of these galaxies per square degree all over the sky. Due to this large number, the intrinsic distortion can be 'averaged out' and a distortion pattern which traces the gravitational field of the foreground cluster up to large distances from its centre can be determined (Tyson 1992). It is generally found that the dark matter is more centrally peaked than the distribution of red light of the galaxy cluster (see Hammer *et al* (1993) and Soucail and Mellier (1993)) and than the matter traced by the x-ray emitting plasma (Petrosian and Saraniti 1993). A big challenge for the future is to obtain the redshifts of the faint blue galaxies and arclets which are necessary for detailed modelling of these systems. This will be greatly facilitated with the use of the new generation of very large telescopes. More accurate values for the mass distribution in the universe will then result. This field of research is full of promise and should bring soon further results of great astrophysical and cosmological importance.

#### *9.4. Micro-lensing*

**9.4.1. Generalities.** We come now to another interesting aspect of lensing phenomena, the so-called micro-lensing due to individual stars or compact objects having a similar or even a lower mass, usually located in a galaxy which acts as a macro-gravitational lens. This was first discussed by Chang and Refsdal (1979) and further developed by Young (1981), Gott (1981) and Paczyński (1986a; see Kayser 1992, Stabell 1993 and Wambsganss 1993 for recent reviews). Since the angular sizes of quasars are smaller than, or comparable with, the Einstein ring of a star located at cosmological distances, this can lead to a splitting-up of each QSO macro-image into several micro-images, with typical angular separations of some micro-arcsec (see figure 27).

Of course, these micro-images are not resolvable with techniques available to-day; however, the integrated luminosity observed for all those micro-images will vary with time due to the relative transverse motions between the source, the star field and the observer. It is therefore an important and very interesting phenomenon. A simple way of visualizing the effects of micro-lensing is by the so-called ray plot diagram (Kayser *et al* 1986, Schneider and Weiss 1987), which consists in the mapping of a regular grid of points in the deflector plane onto the observer plane (source plane). One can easily show that, apart from a scaling factor, the ray plots in the observer plane are identical to those in the source plane. An example of such a diagram, constructed by a straightforward ray shooting (inverse ray shooting), is shown in figure 28 where the randomly distributed stars, here all with the same mass  $M$ , correspond to an optical depth for micro-lensing  $\tau = 0.4$ . This means that the Einstein rings of the stars cover a fraction 0.4 of the sky and that the smoothed-out surface mass density of the stars is  $0.4\Sigma_c$ .

If the source is point-like, the flux of the amplified macro-image under consideration is directly proportional to the density of points in a ray plot. For extended sources with a constant surface brightness, the flux is simply proportional to the number of points covered by the source. For sources with non-uniform surface brightness, the points in the ray plot diagram must be appropriately weighted.

We see that the same diamond-shaped caustic structures appear in the ray plot as in the optical gravitational lens experiment (see figure 22). In the case shown here, however, the diamond-shaped caustics are caused by a disturbance from the neighbouring stars. If we neglect the motions of the deflecting stars relative to one another, the corresponding ray plot will not change with time. However, due to the relative transverse motion between the source, the star field and the observer, the source will move across the ray plot, causing a variation in its brightness. It thus becomes clear that light variations caused by micro-lensing

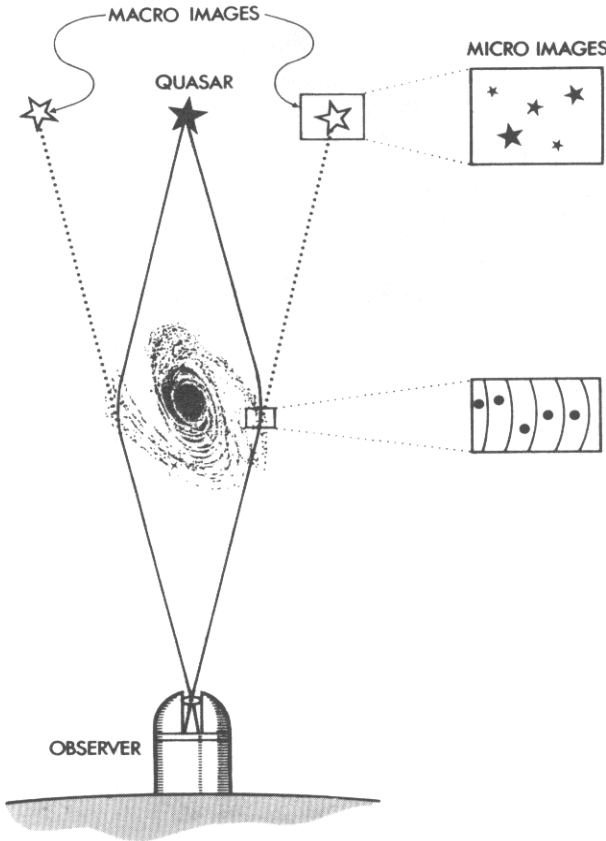


**Figure 27.** Splitting of a macro-image into several micro-images due to gravitational lensing by individual stars.

are greater and faster for small sources than for large ones, as clearly seen in figure 28. These light curves were constructed by moving sources with different sizes along the middle track indicated in the ray plot. The length unit in the ray plot diagram was chosen to be the radius of the Einstein ring, projected into the source plane, which for cosmological distances is typically  $x'_E = (D_{os}/D_{od})\xi_E \simeq 0.01\sqrt{M/M_\odot}$  pc, corresponding to a timescale of

$$t'_E = x'_E / V' \simeq 20 \text{ yr} \sqrt{M/M_\odot} (600 \text{ km s}^{-1} / V') \quad (9.8)$$

where  $V'$  is the effective transverse velocity in the source plane; compare with equation (6.25).

Since micro-lensing variability occurs independently for the different macro-images, this effect may complicate the determination of the time delay from the observed photometric light curves (see the case of Q0957+561 A and B in section 8). Also, when modelling macro-lensed images, one must consider with caution the observed flux ratios of compact sources. Note, however, that the observed positions and the true time delays of the macro-lensed images are very little affected by micro-lensing.

Gravitational lenses are basically achromatic but since the amplification factor due to micro-lensing depends on the source size, indirect chromatic effects may result if the source size depends on wavelength. In particular, the continuum source and the (much larger) broad emission line region of quasars may be differently amplified, causing differences between

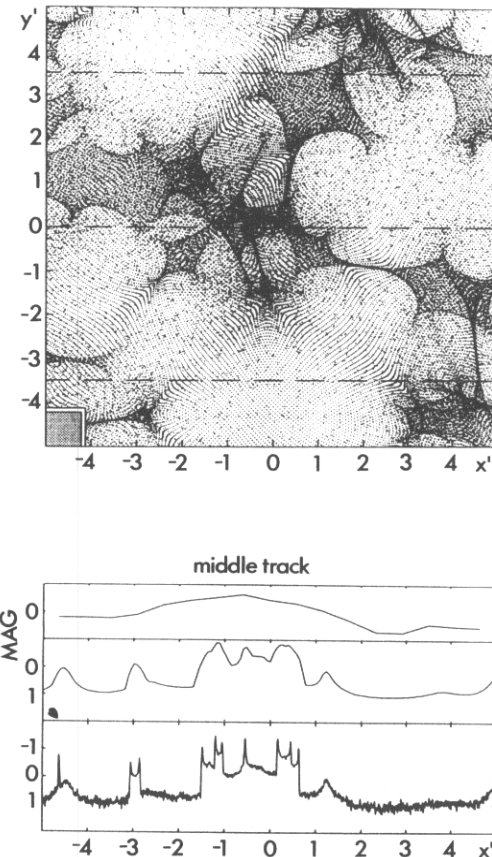


**Figure 28.** Ray plot diagram (top) for an optical depth  $\tau = 0.4$  and corresponding light curves (bottom) for three different sources with radii  $\simeq x'_E$ ,  $0.1x'_E$  and  $0.01x'_E$ , respectively. The simulated light curves correspond to motions of the source along the middle track drawn in the ray plot diagram. One unit along the  $x'$  and  $y'$  axes corresponds to  $x'_E$ , the radius of the Einstein ring projected onto the source plane.

the equivalent widths of emission lines observed in the spectra of the macro-images. Even small differences in the (emission or absorption) line profiles may occur (see the cases of 2237+0305 and 1413+117 in subsection 8.1.2). Such observations can be used as diagnostics of the geometry and kinematics of the broad line regions.

One might expect that we should often see lensing effects produced by stars in our own galaxy, because the angular size of their Einstein rings are larger than those of stars in a distant galaxy. But even if we add up the solid angles covered by the Einstein rings of all the stars in our galaxy, it comes out to only a minute fraction of the sky ( $\simeq 10^{-6}$ , see section 7.1). So it is extremely unlikely that a star in our galaxy could act as a lens for a distant quasar.

Even in our neighbouring galaxies, the total solid angle of the Einstein rings for all the stars covers only a small fraction of the total area of the galaxy. But the chances increase with distance. Indeed, the ratio between the solid angle due to all the star's Einstein rings to the solid angle of the galaxy containing these stars increases in proportion to its distance from us, out to about half the distance to the source (cf equation (6.6)). Therefore, the fractional area covered by the Einstein rings of all the stars also increases with the distance

of the deflector, out to half the source distance.

There is one important exception to the rule that stars in a nearby galaxy are not good candidates for micro-lensing. That is when we have already identified a galaxy that produces multiple images of a quasar by macro-lensing. In such cases, we know that a large amount of mass is located between the macro-images. Indeed, it is easy to show that the average surface mass density between the macro-lensed images is about  $\Sigma_c$  (see equation (6.5)) and that the Einstein rings of the individual stars fill up the whole area between the macro-images when all the matter is in stars; we may therefore reasonably expect a large optical depth for micro-lensing. Only if a very small fraction of the lensing mass is in the form of compact objects or if the mass distribution is strongly concentrated towards the centre of the macro-lens, should we expect a small optical depth for such systems.

There are even reasons why a small distance to a galaxy is favourable for discovering micro-lensing, knowing that this galaxy is acting as a macro-lens. For example, the apparent motion of the stars across the sky would be faster for a nearby galaxy, so that brightness variations of the micro-lensed images should be faster. Also, the angular size of the Einstein ring of a star would be larger, allowing larger background sources to show strong micro-lensing. For these reasons, the multiply lensed quasar Q2237+0305, composed of four lensed images surrounding the nucleus of a deflecting galaxy at a redshift of only 0.039, was chosen some years ago as the best bet for detecting micro-lensing effects. As already described in section 8, these effects were subsequently detected. Photometric monitoring of multiply imaged quasars is therefore a very promising way to obtain information on dark matter in distant galaxies. We should learn soon from such studies whether dark matter is in the form of large clumps, compact enough to produce micro-lensing effects, or in the form of much more uniformly distributed material.

**9.4.2. High amplification events (HAEs).** The so-called high amplification events (HAEs) which occur when the source (or observer) crosses a caustic are of special interest. For compact sources, one gets typical asymmetric peaks in the light curve of the relevant macro-image (see figure 28). We saw in our optical gravitational lens experiment that the number of micro-images then changes by two. Thus an HAE resembles an eclipse phenomenon and the timescale  $\delta t$  for the steep rise (or decline) of the light curve is simply given by

$$\delta t \simeq 2R_s/V'_N \quad (9.9)$$

where  $V'_N$  is the component of  $V'$  along the normal to the caustic and  $R_s$  the radius of the source. By analysing the light curve observed during an HAE, it is even possible to retrieve the intrinsic one-dimensional brightness profile of the source following a method similar to that used for stellar eclipsing binaries (Grieger *et al.* 1988). However, in contrast to a normal eclipse, we must take into account the increasing amplification  $\mu$  of the merging micro-images as the corresponding source element approaches the caustic ( $\mu \propto d^{-1/2}$ , where  $d$  is the distance to the caustic; this is a generic property of caustics). The results of numerical simulations have shown that the one-dimensional luminosity profile can usually be retrieved for a source whose radius is typically less than one-tenth of the projected Einstein radius, corresponding to a few light days for solar mass stars at cosmological distances (Grieger *et al.* 1988). We shall see now how it is possible to infer independently the value of  $V'_N$  such that  $R_s$  can be determined.

**9.4.3. The parallax effect.** We have just seen that micro-lensing causes flux gradients in the observer plane, so that a brightness difference

$$\delta m = \text{grad}(m)\delta r \quad (9.10)$$

is observed by two observers located at a distance  $\delta r$  from each other. This effect is often referred to as the parallax effect (Grieger *et al* 1986). Values of  $\text{grad}(m)$  are typically between  $10^{-4}$  and  $10^{-3} \text{ AU}^{-1}$  (1 astronomical unit = 1 AU  $\simeq 1.5 \times 10^{13} \text{ cm}$ , but during HAEs values up to  $10^{-2} \text{ AU}^{-1}$  may be reached (assuming that  $R_s \simeq 10^{-3} \text{ pc}$  and  $M \simeq M_\odot$ ). For two observers (1 and 2) located some AU apart, it should then be possible to determine the time lag  $\delta t_{1,2}$  between the photometric light curves recorded during an HAE and thereby obtain information on the velocity  $V_N$  (perpendicular component to the local caustic tangent) by which the caustic is sweeping through the solar system (see figure 29). Neglecting the 'small' velocity of the observers relative to the Sun and the very small curvature of the caustic, we get

$$V_N = r_{1,2} \sin(\beta) / \delta t_{1,2} \leq r_{1,2} / \delta t_{1,2} \quad (9.11)$$

where  $r_{1,2}$  represents the projected distance between the observers into the observer plane (perpendicular to the line-of-sight) and  $\beta$  is the angle between the line connecting the two observers and the caustic. Since  $\beta$  is not known, we obtain an upper limit on  $V_N$ . In the presence of a third observer, a second time lag may be derived and it then becomes possible to obtain a precise value for  $V_N$ . Taking into account the redshifts of the source and of the lens and assuming a cosmological model, we can determine  $V'_N$  (in the source plane) and thereby  $R_s$  from equation (9.9). We note that such velocity determinations have a great value in themselves since they should also allow one to probe deviations from the Hubble flow. Assuming  $V_N$  to be about  $600 \text{ km s}^{-1}$ , we note that this corresponds to approximately the distance to Saturn in one month; one would therefore expect a time lag of about one month between a terrestrial observer and an observer located close to Saturn.

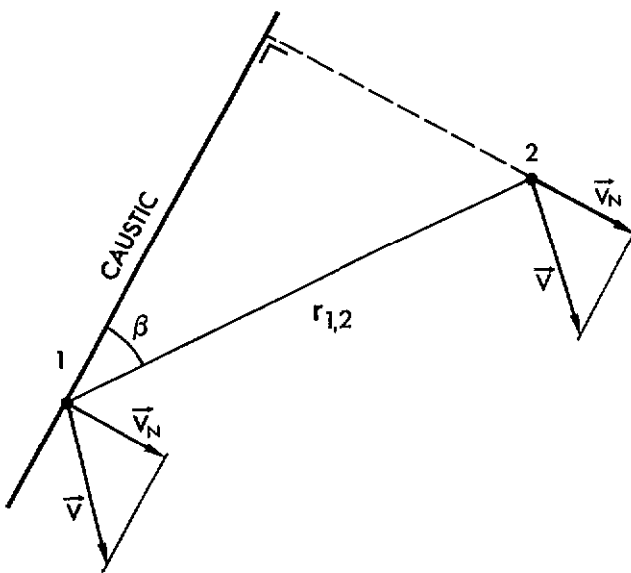


Figure 29. Parallax effect between two observers during the crossing of a caustic (HAE). The observer positions and velocities are projected into the observer plane.

From the known micro-lensing variability ( $\simeq 0.1 \text{ mag/month}$ ) reported for the A and B images in the Einstein cross (Q2237+0305, see section 8), it is clear that simultaneous

observations of this system from the Earth and with an even modest space observatory passing near Saturn should allow one to measure the time lag  $\delta t$ .

An interesting point in connection with the measurement of a time lag is that it would immediately prove that we are dealing with micro-lensing variability and not with intrinsic variations since the latter ones would only produce extremely small time lags which can easily be corrected for. This is particularly important for sources with only one macro-image since then the distinction between the two types of variability is very difficult to establish by other means.

Considering baselines of the order of 100 AU or even larger, we expect that most distant quasars should show small brightness differences. Observations of a large number of quasars would then provide very valuable information on the mass distribution in the universe (masses between  $\simeq 0.001M_\odot$  and  $\simeq 100M_\odot$ ). One should note that the space observatories needed to achieve these goals could be mostly dedicated to other scientific projects but that the applications suggested here would represent by-products of great astrophysical importance.

**9.4.4. Search for dark matter: compact lenses.** Various types of lens observation can provide us with information on dark matter in the universe. This is a field which is still in its infancy, but with a great promise for the future.

As already discussed in section 7, the frequency of multiply imaged sources (e.g. quasars) depends on the cosmological density parameter  $\Omega_L$  of compact objects. Let us, however, note that an amplification bias may strongly influence the results derived from flux-limited samples of quasars (cf subsection 7.2). Since the highest angular resolution achievable today is slightly below  $10^{-3}''$ (VLBI), compact masses down to  $10^4M_\odot$  can, in principle, be searched for at cosmological distances (see equation (6.6)).

Another way of searching for compact objects in the universe with masses in the range  $10^{-5}$ – $10^2M_\odot$  is based upon the detection of micro-lensing effects which produce characteristic light variations of distant compact sources (e.g. quasars). Particularly promising are the multiply (macro-) imaged quasars whose lensing galaxy should have a large optical depth for micro-lensing effects. We expect that important information on the nature of dark matter in these galaxies will be obtained. For single isolated quasars, it is, however, more difficult to distinguish micro-lensing variability from intrinsic light variations and, therefore, parallax observations of light curves for a large number of quasars over many years would be very useful in order to set reasonable limits on  $\Omega_L$  (see subsection 9.4.3). As already mentioned, instantaneous parallax observations of quasars with a large baseline ( $\simeq 100$  AU) would also offer very exciting possibilities to ‘detect’ compact masses in the range given above.

**9.4.5. Search for dark matter in the galaxy halo.** As first suggested by Paczyński (1986b), gravitational lensing effects of putative massive astrophysical compact halo objects (hereafter MACHOS) on stars in the Large and Small Magellanic Clouds (LMC and SMC) should lead to HAEs as observed from the ground. Assuming that the dark halo of our galaxy mainly consists of MACHOS in the mass range  $10^{-8}$ – $10^{-1}M_\odot$  (including brown dwarf and planet candidates), such micro-lensing effects should be readily detectable by inspection of millions of stars in the LMC, with a timescale of hours to years (because the instantaneous probability of amplification is of the order of  $10^{-6}$ ). Such searches for micro-lensing effects are based on the expected achromaticity of the light amplification and on its expected time dependence. There are presently two direct imagery projects of LMC and SMC stars dedicated to a search for MACHOS: the Americano-Australian MACHO project carried out in Australia (see Alcock *et al* 1992) and the French EROS project at ESO (La Silla) see Vidal-Madjar *et al* (1993).

Paczyński (1991) and Mao and Paczyński (1991) have also proposed searching for micro-lensing effects of galactic bulge stars in Baade's windows by galactic disk stars, binaries and possible planetary systems. This is further discussed by Paczyński (1992), Udalski *et al* (1993a) and Szymański *et al* (1993) who describe their Optical Gravitational Lens Experiment (OGLE) consisting in direct observations of the galactic bulge stars with a large CCD camera from the Las Campinas observatory (Chile).

## 10. General conclusions

We have seen in this article that the existence of gravitational lenses and their possible use as astrophysical and cosmological tools had been anticipated well before their discovery. This is probably one of the reasons why since 1979 studies of 'gravitational lensing effects' have expanded so rapidly: more than 1000 scientific papers have been written on the subject, among which one book in Russian (Bliokh and Minakhov 1989) and one in English (Schneider *et al* 1992).

Just as for atmospheric lensing, the physics of gravitational lensing is straightforward: elementary optical experiments allow one to simulate most of the image properties seen from distant sources that are gravitationally lensed. For certain types of deflecting mass distribution, it is even possible to handle all these interesting problems with simple analytical expressions. The present authors are therefore very much convinced that this field of research constitutes an excellent discipline for popular science diffusion as well as science teaching at the undergraduate level.

It is remarkable that for any given pair of light source and compact deflecting object in the universe, there exists a two-dimensional caustic of light, and that an observer located very near to it will actually see the distant source subject to gravitational lensing effects. The former one will actually see the distant source amplified and usually also multiply imaged. This simple example helps in understanding how our vision of the distant universe may result from a complex convolution of an unknown background population of light sources (e.g. quasars, etc) by an unknown network of caustics (induced by intervening stars, galaxies, clusters, etc). Furthermore, this network of caustics changes with time because of the relative motion between sources, deflectors and the observer. In this context, we have pointed out in the present article how important it is to take into account the amplification bias correction factor when estimating the frequency of multiply imaged distant quasars or when setting an upper limit on the cosmological density of compact objects in the universe. We have also mentioned that the observed excess of galaxies found in the close neighbourhood of bright quasars could essentially be due to this amplification bias effect. There is no doubt that much more work related to quantifying the importance of gravitational lensing effects on our view of the distant universe will be carried out during the coming years.

From the numerous detailed observational and theoretical investigations that have been made in the recent past for the several tens of known gravitational lenses (multiply imaged quasars, radio and optical rings, giant luminous arcs and arclets), we have learned how important it was to obtain deep multi-wavelength (optical, radio, x-ray, etc) direct imagery and, if possible, two-dimensional spectroscopic observations of these systems with an angular resolution as high as possible (speckle imaging, adaptive optics) in order to constrain at best the (luminous and dark) matter distribution in the lens as well as the physical structure (size of the continuum and of the emission-line regions, radio jet, etc) of the source that is being lensed. It is clear that gravitational lens systems will constitute prime targets for observations with the next generation of very large ground-based telescopes and space instruments. Let us also remember that gravitational lens systems consist by themselves of

natural telescopes, allowing one to detect galaxies which are otherwise too faint and too distant.

Many efforts should also be made in the future to monitor in good conditions (transparency, seeing, etc) multiply imaged distant sources known to be photometrically variable. We recall that there exists the possibility of determining the value of the Hubble parameter  $H_0$  from the direct measurement of the time delay  $\Delta t$  between the light curves of multiply imaged extragalactic objects. Current astrophysical and cosmological projects would therefore greatly benefit from the possible use of a telescope (2–4 m in size) fully dedicated to the photometric monitoring of known lensed distant sources. Furthermore, the detections of high amplification events (HAEs) or parallax effects due to micro-lensing would also offer the possibility of probing the nature of dark matter in our and external galaxies, the structure and the size of quasars, etc. We conclude that gravitational lenses do indeed offer very promising prospects of a better understanding of the content and geometry of our universe as a whole.

### Acknowledgments

We should like to address our thanks to M-C Angonin, J F Claeskens, R Stabell and Ch Vanderriest for their comments on the first version of this article and to P Schneider for all his suggestions as a referee. Our great thanks also go to E Janssen (ESO) for the preparation of all diagrams illustrating this article, to H Zodet and H-H Heyer (ESO) for the very good quality of photographs they have produced and to F Hammer, J Hjorth, J Lehár, G Lelièvre, R McMahon, A Patnaik, A Smette, G Soucail, Ch Vanderriest and the NRAO for providing us with colour slides or photographs of gravitational lenses presented in figure 24. Both authors wish to express their great appreciation to their wives for their infinite understanding and patience with them. SR (JS) would like to acknowledge the help received from Dr R Schroeder (S Ballon) during the construction of the point-mass (spiral galaxy) optical lens at the Hamburg (ESO) Observatory. Most of this research was made while JS was visiting the ESO (Garching bei München, Germany), during the period September 1992–February 1993. JS wishes to thank all ESO staff, and in particular, P Shaver, for the very good working conditions and atmosphere during that time. Part of this research has also been supported by the German Research Council (DFG), the Belgian National Research Science Foundation (FNRS) and ARC 90/94 ‘Actions de recherche concertée de la Communauté Française de Belgique’.

#### *Notes added in proof.*

**2345+007** (see subsection 8.2): Reanalysing the distortion pattern of the background galaxies in the field of the multiple oso images 2345+007 A and B, Bonnet *et al* (1993) report good evidence for the detection of shear effects (including arc(let)s) compatible with weak lensing due to a foreground dark massive halo. Tyson (1994, private communication) has detected galaxy members of a high redshift cluster ( $z \geq 1$ ) that are most likely responsible for the formation of the macro-lensed images of 2345+007.

**1131+0456** (see subsection 8.3): Using the 10 m Keck telescope, Larkin *et al* (1994) have very distinctly detected in the K band the infrared counterparts of the compact radio components observed for the gravitational lens system MG1131+0456. The colours observed for the lensed object strongly suggest that the source is either a very reddened quasar or an intrinsically very red one.

**Search for dark matter in the galaxy halo** (see subsection 9.4.5): During last Autumn (September–October 1993), the three teams (EROS, MACHO and OGLE) involved in the search for micro-lensing events from distant background stars by foreground compact galactic objects have reported four possible detections (Alcock *et al* 1993, Aubourg *et al* 1993, Udalski *et al* 1993b). All four detected photometric events (two reported by EROS, one

by MACHO and also one by OGLE) turn out to be very similar to those expected on theoretical grounds. The corresponding photometric light curves first show no photometric variations during most of the data taking; then a sudden but similar rise in brightness ( $\Delta m \geq 0.9$ ) is seen at two different wavelengths (in the B and R bands in this case) followed by a decrease in brightness down to the same light levels as before the events. The most probable lens mass that is inferred from the duration of these candidate micro-lensing events is near  $0.1M_{\odot}$ . The number of events observed so far is consistent with the number expected if the halo is dominated by compact objects with masses in the range  $0.01-1.0M_{\odot}$ . These compact lenses could either be large Jupiter-like objects and/or brown dwarfs and/or M dwarfs and/or any other unknown type of more exotic objects (cf mini black holes, etc). Because of the absence of detection of micro-lensing events with smaller light amplitudes (e.g. with  $\Delta m \approx 0.4-0.9$  mag), it cannot however be excluded at the moment that a new type of variable star mimics the candidate micro-lensing events. More observations are urgently needed to confirm the micro-lensing hypothesis and the first possible detection of compact dark matter in the halo and/or in the disk of our Galaxy.

**The parallax effect** (see subsection 9.4.3): For the type of events described above, the parallax effect offers interesting possibilities. Since the flux gradient  $\text{grad}(m)$  is here much larger than for the case of lensed quasars (we easily estimate values of  $\text{grad}(m)$  up to 1 mag/AU), a space observatory at a distance of only a few hundredths of an AU could observe a significant difference in luminosity. This estimate is based on a maximum in the observed time variability  $m$  of about 0.01 mag/h and an assumed effective transverse velocity of about  $200 \text{ km s}^{-1}$ . Such measurements would of course constitute a definite proof that we are observing a lensed star and not a variable star. Furthermore, the two lightcurves will provide independent determinations of  $V$  and  $X_E$  (see Refsdal 1966a,b). Since the uncertainty in  $V$  causes the largest uncertainty in  $M$  when we have only one observed lightcurve, this means that the parallax effect will also provide us with a much better estimate of the lens mass.

## References

- Adam G, Bacon R, Courtès G, Georgelin Y, Monnet G and Pécontal E 1989 *Astron. Astrophys.* **208** L15  
 Alcock C, Axelrod T S, Bennett D P, Cook K H and Park H-S *et al* 1992 *Gravitational Lenses (Lecture Notes in Physics 406)* (Berlin: Springer) p 156  
 Alcock C *et al* 1993 *Nature* **365** 621  
 Altieri B and Giraud E 1991 *The Messenger* **63** 65  
 Angonin M C, Remy M, Surdej J and Vanderriest C 1990 *Astron. Astrophys.* **233** L5  
 Angonin M C and Soucail G 1992 *Gravitational Lenses (Lecture Notes in Physics 406)* (Berlin: Springer) p 362  
 Angonin-Willaime M-C, Vanderriest C, Hammer F and Magain P 1993a *Astron. Astrophys.* in press  
 Angonin-Willaime M C, Vanderriest C and Hartmer F 1993b in preparation  
 Annis J T 1992 *Astrophys. J.* **391** L17  
 Annis J T and Luppino G A 1993 *Astrophys. J. Lett.* **407** L69  
 Arnould P, Remy M, Gosset E, Hainault O, Hutsemékers D, Magain P, Smette A, Surdej J and Van Drom E 1993  
*Proc. 31st Liège Int. Astrophysical Coll. 'Gravitational Lenses in the Universe'* ed J Surdej *et al* p 169  
 Aubourg E *et al* 1993 *Nature* **365** 623  
 Bahcall J N, Maoz D, Schneider D P, Yanny B and Doxsey R 1992a *Astrophys. J. Lett.* **392** L1  
 Bahcall J N, Hartig G F, Jannuzi B T, Maoz D and Schneider D P 1992b *Astrophys. J. Lett.* **400** L51  
 Barnothy J M 1965 *Astron. J.* **70** 666  
 Bernstein G M, Tyson J A and Kochanek C S 1993 *Astron. J.* **105** 816  
 Beskin G M and Oknyanskij V L 1992 *Gravitational Lenses (Lecture Notes in Physics 406)* (Berlin: Springer) p 67  
 Blandford R and Narayan R 1986 *Astrophys. J.* **310** 568  
 ——— 1992 *Ann. Rev. Astron. Astrophys.* **30** 311  
 Bliokh P V and Minakov A A 1989 *Gravitational Lensing* in Russian  
 Bonnet H, Fort B, Kneib J-P, Soucail G and Mellier Y 1993 *Astron. Astrophys. Lett.* at press  
 Borgeest U 1983 *Astron. Astrophys.* **128** 162  
 ——— 1986 *Astrophys. J.* **309** 467  
 Bourassa R R and Kantowski R 1975 *Astrophys. J.* **195** 13  
 Bourassa R R, Kantowski R and Norton T D 1973 *Astrophys. J.* **185** 747  
 Browne I W A, Patnaik A R, Walsh D and Wilkinson P N 1993 *31st Liège Int. Astrophysics Coll. 'Gravitational Lenses in the Universe'* ed J Surdej *et al* p 331  
 Burke W L 1981 *Astrophys. J.* **244** L1  
 Canizares C R 1982 *Astrophys. J.* **263** 508  
 Chang K and Refsdal S 1976 *Colloques Int. du CNRS* **263** 369  
 ——— 1979 *Nature* **282** 561

- Chen G H and Hewitt J N 1993 *Proc. Sub-Arcsec Radio Astronomy (Manchester, July 1992)* in press
- Christian C A, Crabtree D and Waddell P 1987 *Astrophys. J.* **312** 45
- Chwolson O 1924 *Astr. Nach.* **221** 329
- Claeskens J F, Collette P and Surdej J 1994 in preparation
- Conner S R, Léhár J and Burke B F 1992 *Astrophys. J. Lett.* **387** L61
- Cooke J H and Kantowski R 1975 *Astrophys. J.* **195** L11
- Corrigan R T et al 1991 *Astron. J.* **102** 34
- Crane P et al 1991 *Astrophys. J.* **369** L59
- Daulie G, Hainaut O, Hutsemékers D, Magain P, Remy M, Smette A, Surdej J and Van Drom E 1993 *Proc. 31st Liège Int. Astrophysical Coll. 'Gravitational Lenses in the Universe'* ed J Surdej et al p 181
- De Robertis M M and Yee H K C 1988 *Astrophys. J.* **332** L49
- 1992 *Gravitational Lenses (Lecture Notes in Physics 406)* (Berlin: Springer) p 117
- Djorgovski S et al 1992 *Mon. Not. R. Astron. Soc.* **257** 240
- Djorgovski S and Spinrad H 1984 *Astrophys. J.* **282** L1
- Duncan R C 1991 *Astrophys. J.* **375** L41
- Dyer C C and Roeder R C 1972 *Astrophys. J.* **174** L115
- Dyson F W, Eddington A S and Davidson C R 1920 *Mem. R. Astron. Soc.* **62** 291
- Eddington A S 1920 *Space, Time and Gravitation* (Cambridge: Cambridge University Press)
- Einstein A 1915 *Sitzungber. Preuß. Akad. Wissenschaft. ersten Halbband*, p 831
- Einstein A 1936 *Science* **84** 506
- Etherington I M H 1933 *Phil. Mag.* **15** 761
- Falco E E 1992 *Gravitational Lenses (Lecture Notes in Physics 406)* (Berlin: Springer) p 50
- Falco E E, Shapiro I I and Krolik J H 1990 *Gravitational Lensing (Lecture Notes in Physics 360)* (Berlin: Springer) p 96
- Falco E E, Gorenstein M V and Shapiro I I 1991a *Astrophys. J.* **372** 364
- Falco E E, Wambsganss J and Schneider P 1991b *Mon. Not. R. Astron. Soc.* **251** 698
- Filippenko A V 1989 *Astrophys. J.* **338** L49
- Foltz C B, Hewett P C, Webster R L and Lewis G F 1992 *Astrophys. J.* **386** L43
- Foltz C B, Weymann R J, Roeser H J and Chaffee F H 1984 *Astrophys. J.* **281** L1
- Fomalont E B and Sramek R A 1975a *Astrophys. J.* **199** 749
- 1975b *Phys. Rev. Lett.* **36** 1475
- Fort B 1992 *Gravitational Lenses (Lecture Notes in Physics 406)* (Berlin: Springer) p 267
- Fort B, Le Fèvre O, Hammer F and Cailloux M 1992 *Astrophys. J. Lett.* **399** L125
- Foy R, Bonneau D and Blazit A 1985 *Astron. Astrophys.* **149** L13
- Fukugita M and Turner E L 1991 *Mon. Not. R. Astron. Soc.* **253** 99
- Garrett M A, Walsh D and Carswell R F 1992a *Gravitational Lenses (Lecture Notes in Physics 406)* (Berlin: Springer) p 122
- 1992b *Mon. Not. R. Astron. Soc.* **254** 27p
- Garrett M A et al 1993a *Conf. Sub-arcsecond in Astronomy* in press
- Garrett M A, Patnaik A R, Muxlow T W B, Wilkinson P N and Walsh D 1993b *Sub-Arcsec Radio Astronomy Conf.* ed R Booth and R J Davis (Cambridge: Cambridge University Press) in press
- Giraud E 1988 *Astrophys. J.* **334** L69
- Gott J R 1981 *Astrophys. J.* **243** 140
- Grieger B, Kayser R and Refsdal S 1986 *Nature* **324** 126
- 1988 *Astron. Astrophys.* **194** 54
- Hammer F et al 1993 *31st Liège Int. Astrophysics Coll. 'Gravitational Lenses in the Universe'* ed J Surdej et al p 609
- Hammer F and Le Fèvre O 1990 *Astrophys. J.* **357** 38
- Hammer F, Le Fèvre O, Angonin M C, Meylan G, Smette A and Surdej J 1991 *Astron. Astrophys.* **250** L5
- Hazard C, McMahon R G and Sargent W L W 1986 *Nature* **322** 38
- Heflin M B, Gorenstein M V, Lawrence C R and Burke B F 1991 *Astrophys. J.* **378** 519
- Henry J P and Heasley J N 1986 *Nature* **321** 139
- Hewett P C, Webster R L, Harding M E, Jedrzejewski R I, Foltz C B, Chaffee F H, Irwin M J and Le Fèvre O 1989 *Astrophys. J.* **346** L61
- Hewitt J N 1986 *PhD Thesis* MIT
- Hewitt J N, Burke B F, Turner E L, Schneider D P, Lawrence C R, Langston G I and Brody J P 1989 *Gravitational Lenses (Lecture Notes in Physics 330)* (Berlin: Springer) p 147
- Hewitt J N, Turner E L, Lawrence C R, Schneider D P and Brody J P 1992 *Astron. J.* **104** 968

- Hewitt J N, Turner E L, Lawrence C R, Schneider D P, Gunn J E, Bennett C L, Burke B F, Mahoney J H, Langston G I, Schmidt M, Oke J B and Hoessel J G 1987 *Astrophys. J.* **321** 706
- Hewitt J N, Turner E L, Schneider D P, Burke B F, Langston G I, Lawrence C R 1988 *Nature* **333** 537
- Hoag A 1981 *Bull. Am. Astron. Soc.* **13** 799
- Huchra J *et al* 1985 *Astron. J.* **90** 691
- Irwin M J, Webster R L, Hewett P C, Corrigan R T and Jedrzejewski R I 1989 *Astron. J.* **98** 1989
- Jauncey D L *et al* 1991 *Nature* **352** 132
- Jauncey D L *et al* 1992 *Gravitational Lenses (Lecture Notes in Physics 406)* (Berlin: Springer) p 333
- Jones C, Stern C, Falco E E, Forman W, David L, Shapiro I and Fabian A C 1993 *Preprint 3510* Harvard-Smithsonian CfA
- Kassinola A and Kovner I 1992 *Astrophys. J.* **388** 33
- Kassinola A, Kovner I and Blandford R D 1991 *Astrophys. J.* **381** 6
- Katz C A and Hewitt J N 1993 *Astrophys. J.* **409** L9
- Kayser R 1992 *Gravitational Lenses (Lecture Notes in Physics 406)* (Berlin: Springer) p 143
- 1993 *Proc. 31st Liège Int. Astrophysical Coll. 'Gravitational Lenses in the Universe'* ed J Surdej *et al* p 5
- Kayser R and Refsdal S 1983 *Astron. Astrophys.* **128** 156
- 1989 *Nature* **338** 745
- Kayser R, Refsdal S and Stabell R 1986 *Astron. Astrophys.* **166** 36
- Kayser R, Surdej J, Condon J J, Hazard C, Kellermann K I, Magain P, Remy M and Smette A 1990 *Astrophys. J.* **364** 15
- Klimov Y G 1963 *Sov. Phys. Doklady* **8** 119
- Kochanek C S 1991a *Astrophys. J.* **382** 58
- 1991b *Astrophys. J.* **373** 354
- 1993 *Astrophys. J.* in press
- Kochanek C S, Blandford R D, Lawrence C R and Narayan R 1989 *Mon. Not. R. Astron. Soc.* **238** 43
- Kochanek C and Narayan R 1992 *Astrophys. J.* **401** 461
- Koo D C 1987 *Large Scale Motions in the Universe* ed V G Rubin and G V Coyne (Princeton, NJ: Princeton University Press) p 513
- Langston G I, Fischer J and Aspin C 1991 *Astron. J.* **102** 1253
- Langston G I, Schneider D P, Conner S, Carilli C L, Lehár J, Burke B F, Turner E L, Gunn J E, Hewitt J N and Schmidt M 1989 *Astron. J.* **97** 1283
- Larkin J E *et al* 1994 *Astrophys. J. Lett.* in press
- Lavery R J and Henry J P 1988 *Astrophys. J.* **329** L21
- Lawrence C R, Neugebauer G and Matthews K 1993 *Astron. J.* **105** 17
- Lawrence C R, Neugebauer G, Weir N, Matthews K and Patnaik A R 1992 *Mon. Not. R. Astron. Soc.* **259** 5P
- Lawrence C R, Schneider D P, Schmidt M, Bennett C L, Hewitt J N, Burke B F, Turner E L and Gunn J E 1984 *Science* **233** 46
- Le Fèvre O and Hammer F 1988 *Astrophys. J.* **333** L37
- Le Fèvre O, Hammer F, Nottale L and Mathez G 1987 *Nature* **326** 268
- Lehár J, Hewitt J N, Roberts D H and Burke B F 1992 *Astrophys. J.* **384** 453
- Lehár J, Langston G I, Silber A, Lawrence C R and Burke B F 1993 *Astron. J.* **105** 847
- Lelièvre G, Nieto J-L and Salmon D 1988 *Astron. Astrophys.* **200** 301
- Liebes S 1964 *Phys. Rev. B* **133** 835
- Link F 1937 *Bullet. Astron.* **10** 73
- Lodge O J 1919 *Nature* **104** 354
- Luppino G A and Gioia I M 1992 *Astron. Astrophys.* **265** L9
- Lynds R and Petrosian V 1986 *Bull. Am. Astron. Soc.* **18** 1014
- 1989 *Astrophys. J.* **336** 1
- Magain P, Surdej J, Swings J-P, Borgeest U, Kayser R, Kühr H, Refsdal S and Remy M 1988 *Nature* **334** 325
- Magain P, Hutsemékers D, Surdej J and Van Drom E 1992a *Gravitational Lenses (Lecture Notes in Physics 406)* (Berlin: Springer) p 88
- Magain P, Surdej J, Vanderriest C, Pirenne B and Hutsemékers D 1992b *Astron. Astrophys.* **253** L13
- Mao S and Paczyński B 1991 *Astrophys. J.* **374** L37
- Maoz D, Bahcall J N, Schneider D P, Doxsey R, Bahcall N A, Filippenko A V, Goss W M, Lahav O and Yanny B 1992 *Astrophys. J.* **386** L1
- Mathez G, Fort B, Mellier Y, Picat J-P and Soucail G 1992 *Astron. Astrophys.* **256** 343
- McMahon R, Irwin M, Hazard C and Corrigan R 1992 *Gemini* **36** 1
- Mellier Y, Fort B, Soucail G, Mathez G and Cailloux M 1991 *Astrophys. J.* **380** 334
- Mellier Y, Fort B and Kneib J-P 1993 *Astrophys. J.* **407** 33

- Melnick J, Altieri B, Gopal-Krishna and Giraud E 1993 *Astron. Astrophys.* **271** L5  
 Meylan G and Djorgovski S 1989 *Astrophys. J.* **338** L1  
 Nadeau D, Yee H K C, Forrest W J, Garnett J D, Ninkov Z and Pipher J L 1991 *Astrophys. J.* **376** 430  
 Nair S, Narasimha D and Rao A P 1993 *Astrophys. J.* **407** 46  
 Narasimha D and Chitre S M 1989 *Astron. J.* **97** 327  
 Narayan R 1989 *Astrophys. J.* **339** L53  
 ——— 1991 *Astrophys. J.* **378** L5  
 Nemiroff R J 1991 *Comm. Astrophys.* **15** 139  
 Newton I 1704 *Optics* 2nd edn, query 1  
 Nieto J L, Roques S, Llebaria A, Vanderriest Ch, Lelièvre G, Di Serego Alighieri S, Macchetto F D and Perryman M A C 1988 *Astrophys. J.* **325** 644  
 O'Dea C P, Baum S A, Stanghellini C, Dey A, Van Breugel W, Deustua S and Smith E 1992 *Astron. J.* **104** 1320  
 Paczyński B 1986a *Astrophys. J.* **301** 503  
 ——— 1986b *Astrophys. J.* **304** 1  
 ——— 1987 *Nature* **325** 572  
 ——— 1991 *Astrophys. J.* **371** L63  
 ——— 1992 *Gravitational Lenses (Lecture Notes in Physics 406)* (Berlin: Springer) p 163  
 Patnaik A R, Browne I W A, Walsh D, Chaffee F H and Foltz C B 1992a *Mon. Not. R. Astron. Soc.* **259** 1P  
 Patnaik A R, Browne I W A, King L J, Muxlow T W B, Walsh D and Wilkinson P N 1992b *Mon. Not. R. Astron. Soc.* in press  
 Patnaik A R, Browne I W A, King L J, Muxlow T W B, Walsh D and Wilkinson P N 1992c *Gravitational Lenses (Lecture Notes in Physics 406)* (Berlin: Springer) p 140  
 Patnaik A, Browne I, King L, Muxlow T, Walsh D and Wilkinson P 1993 *Sub-Arcsec Radio Astronomy Conf.* ed R Booth and R J Davis (Cambridge: Cambridge University Press) in press  
 Pello-Descayre R, Soucail G, Sanahuja B, Mathez G and Ojero E 1988 *Astron. Astrophys.* **190** L11  
 Pello R, Le Borgne J F, Soucail G, Mellier Y and Sanahuja B 1991 *Astrophys. J.* **366** 405  
 Pello R, Le Borgne J F, Sanahuja B, Mathez G and Fort B 1992 *Astron. Astrophys.* **266** 6  
 Petrosian V and Saraniti D W 1993 *Bull. Am. Astr. Soc.* **25** 838  
 Pirenne B, Surdej J and Magain P 1992 *ST-ECF Newsletter* **17** 22  
 Pospieszalska-Surdej A, Surdej J and Véron P 1993 *Proc. 31st Liège Int. Astrophysical Coll. 'Gravitational Lenses in the Universe'* ed J Surdej et al p 671  
 Press W H and Gunn J E 1973 *Astrophys. J.* **185** 397  
 Press W H, Rybicki G B and Hewitt J N 1992a *Astrophys. J.* **385** 404  
 ——— 1992b *Astrophys. J.* **385** 416  
 Racine R 1991 *Astron. J.* **102** 454  
 ——— 1992 *Astrophys. J. Lett.* **395** L65  
 Rao A P and Subrahmanyam R 1988 *Mon. Not. R. Astron. Soc.* **231** 229  
 Rauch K P and Blandford R D 1991 *Astrophys. J. Lett.* **381** L39  
 Refsdal S 1964a *Mon. Not. R. Astron. Soc.* **128** 295  
 ——— 1964b *Mon. Not. R. Astron. Soc.* **128** 307  
 ——— 1965 *Proc. Int. Conf. on Relativistic Theories of Gravitation (London)*  
 ——— 1966a *Mon. Not. R. Astron. Soc.* **132** 101  
 ——— 1966b *Mon. Not. R. Astron. Soc.* **134** 315  
 ——— 1970 *Astrophys. J.* **159** 357  
 ——— 1992 *Gravitational Lenses (Lecture Notes in Physics 406)* (Berlin: Springer) p 61  
 Refsdal S and Stabell R 1993 *Astron. Astrophys.* **278** L5  
 Refsdal S and Surdej J 1992 *Highlights of Astronomy* **9** 3  
 Remy M, Surdej J, Smette A and Claeskens J F 1993 *Astron. Astrophys.* **278** L19  
 Remy M et al 1994 in preparation  
 Rhee G 1991 *Nature* **350** 211  
 Rix H-W, Schneider D P and Bahcall J N 1992 *Astron. J.* **104** 959  
 Roberts D, Lehár J, Hewitt J N and Burke B F 1991 *Nature* **352** 43  
 Robertson D S, Carter W E and Dillinger W H 1991 *Nature* **349** 768  
 Sanitt N 1971 *Nature* **234** 199  
 Sargent W L W, Filippenko A V, Steidel C C, Hazard C and McMahon R G 1986 *Nature* **322** 40  
 Saust A B 1991 *Astron. Astrophys.* **243** 33  
 Schechter P L and Moore C B 1993 *Astron. J.* **105** 1  
 Schild R E 1990 *Astron. J.* **100** 1771  
 Schild R E and Smith R C 1991 *Astron. J.* **101** 813

- Schild R and Thompson D J 1993 *Proc. 31st Liège Int. Astrophysical Coll. 'Gravitational Lenses in the Universe'* ed J Surdej *et al* p 415
- Schmidt M 1963 *Nature* **197** 1040
- Schneider D P, Gunn J E, Turner E L, Lawrence C R, Hewitt J N, Schmidt M and Burke B F 1986 *Astron. J.* **91** 991
- Schneider P 1985 *Astron. Astrophys.* **143** 413
- 1987a *Astron. Astrophys.* **179** 71
- 1987b *Astron. Astrophys.* **179** 80
- Schneider P and Weiss A 1987 *Astron. Astrophys.* **171** 49
- Schneider D P, Turner E L, Gunn J E, Hewitt J N, Schmidt M and Lawrence C R 1988 *Astron. J.* **95** 1619; 1988 *Astron. J.* **96** 1755
- Schneider P, Ehlers J and Falco E E 1992 *Gravitational Lensing* (Berlin: Springer)
- Shaklan S B and Hege E K 1986 *Astrophys. J.* **303** 605
- Smail J, Ellis R S, Fitchett M J, Norgaard-Nielsen H U, Hansen L and Jorgensen H J 1991 *Mon. Not. R. Astron. Soc.* **252** 19
- Smette A, Surdej J, Shaver P A, Foltz C B, Chaffee F H, Weymann R J, Williams R E and Magain P 1992 *Astrophys. J.* **389** 39
- Sol H, Vanderriest C, Lelièvre G, Pedersen H and Schneider J 1984 *Astron. Astrophys.* **132** 105
- Soldner J 1804 *Berliner Astron. Jahrb.* 161
- Soucail G, Fort B, Mellier Y and Picat J P 1987 *Astron. Astrophys.* **172** L14
- Soucail G and Mellier Y 1993 *Proc. 31st Liège Int. Astrophysical Coll. 'Gravitational Lenses in the Universe'* ed J Surdej *et al* p 595
- Soucail G, Arnaud M and Mathez G 1993 in preparation
- Sramek R A and Weedman D W 1978 *Astrophys. J.* **221** 468
- Stabell R 1993 *Proc. 31st Liège Int. Astrophysical Coll. 'Gravitational Lenses in the Universe'* ed J Surdej *et al* p 407
- Steidel C C and Sargent W L W 1990 *Astron. J.* **99** 1693
- 1991 *Astron. J.* **102** 1610
- Subrahmanyam R, Narasimha D, Pramesh Rao A and Swarup G 1990 *Mon. Not. R. Astron. Soc.* **246** 263
- Subrahmanyam R, Kesteven M J and te Lintel Hekkert P 1992 *Mon. Not. R. Astron. Soc.* **259** 63
- Surdej J, Magain P, Swings J-P, Borgeest U, Courvoisier T J-L, Kayser R, Kellermann K I, Kühr H and Refsdal S 1987 *Nature* **329** 695
- Surdej J *et al* 1992 *The Distribution of Matter in the Universe (Proc. 2nd DAEC Mtg)* ed G A Mamon and D Gerbal, p 97
- Surdej J, Claeskens J-F, Crampton D, Filippenko A V, Hutsemékers D, Magain P, Pirenne B, Vanderriest C and Yee H K C 1993a *Astron. J.* **105** 2064
- Surdej J, Remy M, Smette A, Claeskens J-F, Magain P, Refsdal S, Swings J-P and Véron M 1993b *Proc. 31st Liège Int. Astrophysical Coll. 'Gravitational Lenses in the Universe'* ed J Surdej *et al* p 153
- Szymański M *et al* 1993 *Proc. 31st Liège Int. Astrophysical Coll. 'Gravitational Lenses in the Universe'* ed J Surdej *et al* p 503
- Turner E L, Ostriker J P and Gott J R 1984 *Astrophys. J.* **284** 1
- Turner E L, Hillenbrand L A, Schneider D P, Hewitt J N and Burke B F 1988 *Astron. J.* **96** 1682
- Tyson A 1988 *Astron. J.* **96** 1
- 1992 *Physics Today* (June) p 24
- Tyson J A, Valdes F and Wenk R A 1990 *Astrophys. J.* **349** L1
- Udalski A, Szymański M, Kałużny J, Kubiak M and Mateo M 1993a *Acta Astron.* **43** 69
- Udalski A, Szymański M, Kałużny J, Kubiak M, Krzemieński W, Mateo M, Preston G W and Paczyński B 1993b *Acta Astron.*
- Van Drom E, Surdej J, Magain P, Hutsemékers D, Gosset E, Claeskens J-F, Shaver P and Melnick J 1993 *Proc. 31st Liège Int. Astrophysical Coll. 'Gravitational Lenses in the Universe'* ed J Surdej *et al* p 301
- Vanderriest C 1985 (*Lecture Notes in Physics* 212) (Berlin: Springer) p 265
- Vanderriest C, Gosset E, Remy M and Swings J-P 1992 *Gravitational Lenses (Lecture Notes in Physics* 406) (Berlin: Springer) p 107
- Vanderriest C, Schneider J, Herpe G, Chèvreton M, Moles M and Wlérick G 1989 *Astron. Astrophys.* **215** 1
- Vanderriest C, Wlérick G, Lelièvre G, Schneider J, Sol H, Horville D, Renard L and Servan B 1986 *Astron. Astrophys.* **158** L5
- Vidal-Madjar A 1993 *Proc. 31st Liège Int. Astrophysical Coll. 'Gravitational Lenses in the Universe'* ed J Surdej *et al* p 481
- Walsh D, Carswell R F and Weymann R J 1979 *Nature* **279** 381

- Wambsganss J 1992 *Gravitational Lenses* (*Lecture Notes in Physics 406*) (Berlin: Springer) p 183  
— 1993 *Proc. 31st Liège Int. Astrophysical Coll. 'Gravitational Lenses in the Universe'* ed J Surdej *et al* p 369  
Wambsganss J and Paczyński B 1991 *Astron. J.* **102** 864  
Wambsganss J, Paczyński B and Katz N 1990a *Astrophys. J.* **352** 407  
Wambsganss J, Paczyński B and Schneider P 1990b *Astrophys. J.* **358** L33  
Wampler E J, Baldwin J A, Burke W L, Robinson L B and Hazard C 1973 *Nature* **246** 203  
Weedmann D W, Weymann R J, Green R F and Heckmann T M 1982 *Astrophys. J.* **255** L5  
Weigelt G *et al* 1994 in preparation  
Weir N and Djorgovski S 1991a *Astron. J.* **101** 66  
— 1991b *Proc. 10th Int. Max. Entr. and Bayes. Meth. Work.*  
Weymann R J, Latham D, Angel J R P, Green R F, Liebert J W, Turnshek D A, Turnshek D E and Tyson J A 1980 *Nature* **285** 641  
Wilkinson P N 1990 *Space VLBI—The Missions and the Sc.* (*COSPAR, Hague*)  
Wisotzki L, Köler T, Kayser R and Reimers D 1993 *Proc. 31st Liège Int. Astrophysical Coll. 'Gravitational Lenses in the Universe'* ed J Surdej *et al* p 143  
Witt H J, Kayser R and Refsdal S 1993 *Astron. Astrophys.* **268** 501  
Yee H K C 1988 *Astron. J.* **95** 1331  
Yee H K C and De Robertis M M 1991 *Astrophys. J.* **381** 386  
Young P 1981 *Astrophys. J.* **244** 756  
Zel'dovich Ya B 1964 *Sov. Astron.* **8** 13  
Zwicky F 1937a *Phys. Rev. Lett.* **51** 290  
— 1937 *Phys. Rev. Lett.* **51** 679  
— 1957 *Morphological Astronomy* (Berlin: Springer)